Spring 5-2017

Design and Synthesis of Polymer Brush Surfaces with Complex Molecular Architectures and Morphologies

Wei Guo
University of Southern Mississippi

DESIGN AND SYNTHESIS OF POLYMER BRUSH SURFACES WITH COMPLEX MOLECULAR ARCHITECTURES AND MORPHOLOGIES

by

Wei Guo

A Dissertation
Submitted to the Graduate School
and the School of Polymers and High Performance Materials
at The University of Southern Mississippi
in Partial Fulfillment of the Requirements
for the Degree of Doctor of Philosophy

Approved:

_____
Dr. Derek L. Patton, Committee Chair
Associate Professor, Polymers and High Performance Materials

_____
Dr. Sarah E. Morgan, Committee Member
Professor, Polymers and High Performance Materials

_____
Dr. Robson F. Storey, Committee Member
Professor, Polymers and High Performance Materials

_____
Dr. Sergei Nazarenko, Committee Member
Professor, Polymers and High Performance Materials

_____
Dr. Yoan C. Simon, Committee Member
Assistant Professor, Polymers and High Performance Materials

_____
Dr. Jeffrey Wiggins
Director, School of Polymers and High Performance Materials

_____
Dr. Karen S. Coats
Dean of the Graduate School

May 2017

Published by the Graduate School

ABSTRACT

DESIGN AND SYNTHESIS OF POLYMER BRUSH SURFACES WITH COMPLEX MOLECULAR ARCHITECTURES AND MORPHOLOGIES

by Wei Guo

May 2017

The combination of surface-initiated polymerization (SIP) and postpolymerization modification (PPM) is a powerful technique for the fabrication of functional soft surfaces. Better understanding the influence of the aforementioned factors on the PPM effectiveness is valuable for fulfilling the potential of the PPM approach for the fabrication of functional soft surfaces. Specifically, by carefully balancing modification reactivity and limitation of mass transport, polymer brush with composition heterogeneity and gradient along the normal direction of the surface otherwise unattainable by methods of direct polymerization can be fabricated via the PPM approach which opens doors to new routes to polymer brush with complex functionality and morphology (i.e. buckling). This dissertation is focused on designing and synthesizing polymer brush surfaces with complex molecular architectures and morphologies with specific emphasis on improving the understanding of PPM effectiveness and the distribution of post-modification moieties on grafted polymer chains.

In the first study, microwave-assisted surface-initiated polymerization (μW-SIP) was developed and employed to demonstrate the synthesis of polymer brushes on silicon and quartz substrates. The μW-SIP approach shows significant enhancements in polymer brush thickness at reduced reaction times and monomer concentration.

In the second study, the postpolymerization modification of a poly(2-isocyanatoethyl methacrylate) (pNCOMA) brush surfaces with deuterated thiols of different sizes was studied and the depth profiles of the distribution of the modified brush were drawn using neutron reflectometry analysis. By applying a sequential PPM strategy, polymer brush with tapered block copolymer architectures was synthesized.

In the third study, a poly(styrene-alt-maleic anhydride) (pSMA) copolymer brush was synthesized in an effort to fabricate pendent polyfunctional thiols polymer brush for further thiol-ene modifications. Furthermore, the pSMA brush itself was found to be a stable and versatile platform for amine modification.

In the last study, a straightforward PPM approach, utilizing the knowledge gained in previous studies, to engineer ultrathin polymer brush surfaces with tunable wrinkled morphologies was demonstrated by creating a modulus mismatch between the top layer and bottom of the polymer brush via selectively crosslinking of the outer layer of pSMA brushes by balancing the rate of PPM and reactive molecule diffusion.

ACKNOWLEDGMENTS

First and foremost, I would like to thank my advisor, Dr. Derek L. Patton, for his guidance, encouragement and constant support throughout the years. I thank him for teaching me how to do research, how to write scientifically and how to present. I also thank him for helping me overcome many benchtop challenges - from my first surface-initiated polymerization to lab-made reaction cells. I appreciate that his office is always open for discussions and I thank him for being an understanding, approachable and considerate mentor

I would like to express my gratitude to the members of my committee – Dr. Sarah E. Morgan, Dr. Sergei I. Nazarenko, Dr. Yoan C. Simon, and Dr. Robson F. Storey. I thank them for the insightful suggestions from time to time. I appreciate all the great questions that I received at my defense. I thank Dr. Morgan for the help with ellipsometry. Also, I'd like to thank Dr. Daniel Savin and Dr. Marek Urban for all the help in the early 2010s – from chemicals to instruments to discussions. I truly wish they were here at the USM. I would like to acknowledge Dr. Gopinath Subramanian for the opportunity to collaborate on molecular dynamic simulation of polymer brushes.

Many thanks go to Dr. William L. Jarrett, Morgan group, Story group, McCormick group, Wiggins group, Savin group, Kyoungtae, Shahab and Lifeng for the help with urgently needed chemicals, supplies, and access to instruments. I would like to thank all the staff at the School of Polymers and High Performance Materials, in particularly, Dr. Bret Calhoun, Ms. Jody, Ms. Stephanie, Ms. Beverly and Ms. Candy for their assistance no matter what the circumstances.

I thank the past and present members of the Patton Research Group – Dr. Ryan Hensarling, Dr. Bradley Sparks, Dr. Austin Baranek, Matthew Jungman, Dr. Jananee Narayanan, Dr. Emily Hoff, Dr. Brian Donovan, Dr. Li Xiong, Yidan Guan, Dahlia Amato, Douglas Amato, Cassandra Reese, and Michelle Vekasy. As lab safety officer, I thank Dr. Jarrett, Dr. Lynn Landrum, Mrs. Martha Sparrow and everyone in the lab for helping me with my duty.

I would also thank everyone I have had the privilege to work with – Ryan, who pioneered the polymer brush research in the group, Li, Cassandra, Emily, Arthur, Brian, Austin, Brad, and Dr. Santosh Rahane. I thank Mitchell Woellner and William White for helping me with summer projects. I thank Jananee and Yidan for sharing lab space with me in many late nights. I thank Dr. Brooks Abel, Phil Pickett, Dr. Qi Wu, Dr. Lea Paslay, Dr. Sarah Exley, and Pradipta Das.for helpful discussions. I thank Dr. Bradley Lokitz and Dr. John Ankner of ORNL for the help with neutron reflectometry (NR). I thank Dr. Olga Ovchinnikova and Dr. Anton Ievlev of ORNL for the help with SIMS experiments. I thank Dr. Chris Stafford of NIST for insightful discussions about buckling instability. I thank my friends and colleagues at the polymer science department especially Yaling, Jianwei, Xiaonan, Xiaole, Dahlia, Doug, Jananee, Yidan, Qi, Bin, and Yingji for all the help and support during the years.

I would like to thank my best friend, Li, for your invaluable encouragement, inspiration, patience, support and the time you've shared with me in my life.

DEDICATION

To my Mom and to my wife, Li, for your endless love

To my daughter for her patience as she awaits the Birth

TABLE OF CONTENTS

LIST OF TABLES

LIST OF ILLUSTRATIONS

LIST OF SCHEMES

LIST OF ABBREVIATIONS

AFM	atomic force microscopy
AIBN	azobisisobutyronitrile
ATRP	atom transfer radical polymerization
ATR-FTIR	attenuated total reflection Fourier transform infrared spectroscopy
BMA	butyl methacrylate
CuAAC	copper catalyzed azide-alkyne cyclo addition
DBU	1,8-Diazabicyclo[5.4.0]undec-7-ene
DDT	dodecanethiol
DI	deionized
DLS	dynamic light scattering
DMA	N,N-dimethylacrylamide
DMAEMA	2-(dimethylamino)ethyl methacrylate
d_7-PPT	d_7-propanethiol
d_{25}-DDT	d_{25}-dodecanethiol
EDX	energy disperse X-ray
EMA	ethyl methacrylate
FFT	fast Fourier transform
FTIR	Fourier transform infrared spectroscopy
gATR-FTIR	grazing angle attenuated total reflection Fourier transform infrared spectroscopy

GPC	gel permeation chromatography
HEA	2-hydroxyethyl acrylate
HEMA	hydroxyethyl methacrylate
LbL	Layer-by-Layer
L-B	Langmuir-Blodgett
MMA	methyl methacrylate
M_n	number averaged molecular weight
MW	molecular weight
N_A	Avogadro number
NCO	Isocyanate
NCOMA	2-isocyanatoethyl methacrylate
NHS	N-Hydroxysuccinimide
NMP	nitroxide mediated polymerization
NPC	p-nitrophenyl chloroformate
NR	neutron reflectivity
PBS	phosphate-buffered saline
PEG	poly(ethylene glycol)
PEG-NH_2	amine-functionalized poly(ethylene glycol)
PDMS	polydimethylsiloxane
PMA	propyl methacrylate
PPM	postpolymerization modification
PPT	propanethiol
pBMA	poly(butyl methacrylate）

pDMA	poly(N,N-dimethylacrylamide)
pDMAEMA	poly(2-(dimethylamino)ethyl methacrylate)
PEGMA	poly(ethylene glycol) methacrylate
pEMA	poly(ethyl methacrylate)
pHEA	poly(2-hydroxyethyl acrylate)
pHEMA	poly(hydroxyethyl methacrylate)
pMMA	poly(methylmethacrylate)
pNCOMA	poly(2-Isocyanatoethyl methacrylate)
pPMA	poly(propyl methacrylate)
POSS	polyhedral oligomeric silsesquioxane
pPFPA	poly(pentafluorophenyl acrylate)
pSMA	poly(styrene-alt-maleic anhydride)
pSty	polystyrene
QCM	quartz crystal microbalance
QNM	quantitative nanomechanical property mapping
RAFT	reversible addition−fragmentation chain-transfer polymerization
RI	refractive indices
RMS	root-mean-squared
ROMP	ring opening metathesis polymerization
SAMs	self-assembled monolayers
SEM	scanning electron microscopy

SIMS	secondary ion mass spectroscopy
SIP	surface-initiated polymerization
SLD	scattering length density
SR	swelling ratio
Sty	styrene
TCEP	tris(2-carboxylethyl) phosphine hydrochloride
TEA	trimethylamine
TEM	transmission electron microscopy
TGA	thermogravimetric analysis
T_g	glass transition temperature
THF	tetrahydrofuran
ToF-SIMS	time of flight secondary ion mass spectroscopy
UV	ultraviolet
XPS	X-ray photoelectron spectroscopy
XRR	X-ray reflectivity
μCaP	microcapillary printing
μCP	microcontact printing
μW-SIP	microwave-assisted surface-initiated polymerization
2D	two-dimensional
3D	three-dimensional

CHAPTER I - INTRODUCTION

1.1 Functional Soft Surfaces

Coatings can improve the properties of objects by tuning the interaction of the underlying material with the adverse environmental conditions. Utilization of thin coatings for decoration and protection purposes has been known to mankind for a very long time. People discovered lacquer and applied it onto wooden surfaces in eastern China in Neolithic Ages (~5000 B.C.).[1-2]. The early Egyptians used beeswax, clay, and gelatin to produce varnishes, enamels and to waterproofed ships with coatings from pitch and balsam. In ancient Mediterranean and East Asia, lacquers were used for decoration and protection coatings of homes, ships, and mausoleums.[3-4] Today, solid surface modification with thin coatings has gained great interest as the range of coatings expands from decoration and protection to functional soft surfaces such as anti-corrosion,[5] adhesion,[6] lubrication,[7] colloid stabilization,[8] catalyst immobilization,[9] controlled wettability,[10] and many others.[11]

1.2 Methods of Thin Films Fabrication

Surface coating techniques can be categorized into two types – thin films that are physically attached to the substrates and thin films that are covalently bonded to the surfaces.[4] The methods that rely on physical interactions for film assembly include Langmuir–Blodgett (L-B) technique,[12] Layer-by-Layer (LbL),[13] spin coating, spray coating, dip coating, doctor blading, and many others.[14-15] In general, coating techniques that rely on physical interactions are simple to process but the films are less robust. An alternative approach to improve the long-term stability of coatings is to attach molecules and/or polymers covalently to the substrate. The self-assembled monolayer (SAM)

technique uses a small molecule with a reactive head group that reacts with a corresponding moiety on the surface (e.g., alkylphosphonic acid/metals, alkylthiolate/noble metals and organosilane/SiO_2) forming a covalently bonded single layer on the surface that contains desired functionality.[16-17] While SAMs are more robust due to covalent linkage, it has the disadvantage of low functionality as the surface reaction is self-limiting and the SAM films are very thin (less than 5 nm).[18]

1.3 Grafted Polymers, Polymer Brush and Surface-Initiated Polymerization

Polymers that are covalently bonded to surfaces (also known as grafted polymers) can be fabricated via grafting to, grafting through and grafting from approaches (shown in Scheme 1.1). Polymers can be directly grafted onto the surface – a process known as the 'grafting to' method – via an 'anchor' group.[4, 19-20] Another approach, referred to as the 'grafting through' approach, uses SAMs of monomer or polymerizable groups that will participate in a solution initiated polymerization process.[21-22]

For both methods, the bottleneck step is the 'grafting to' process of polymers or macromolecular radicals onto the surface. The 'grafting to' process is self-limiting due to thermodynamic and kinetic reasons. First of all, the attachment of chains onto a surface already covered with polymers can be thermodynamically unfavorable. At high grafting densities, the surface-grafted polymers are in an extended conformation due to strong intermolecular segment–segment interactions. Any chain in solution which is to be grafted to the surface must change from a random coil conformation to an extended conformation at the surface. The only energy compensation for the entropy loss during the conformation change is the formation of one covalent linkage between the polymer and the surface. When the grafting density is high the entropy penalty can be great

enough to inhibit any new chain attachment to the surface. Kinetics is another factor that disfavors the 'grafting to' process. As the grafting density increases, the polymer concentration in the regions near the substrate quickly becomes higher than the polymer concentration in solution. Any additional polymers to be tethered to the surface would have to overcome the concentration gradient. This diffusion barrier significantly slows down the rate of the 'grafting to' process and would occur at low grafting density conditions and result in low film thickness. Both theoretical and experimental studies have shown that it would take thousands or millions years to add a few more chains onto a surface after the surface is covered by grafted coils. [23-24]

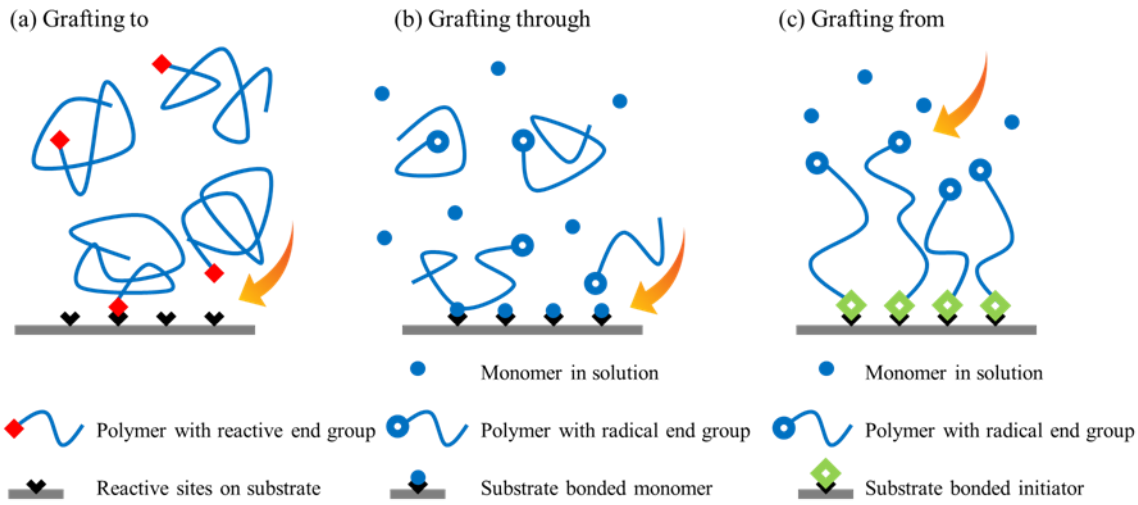

Scheme 1.1 Schematic illustration of (a) grafting to, (b) grafting through and (c) grafting from approach.

To overcome the intrinsic limitation of 'grafting to/through' methods and to achieve higher thickness, 'grafting from' or surface-initiated polymerization (SIP) approach has been developed. The 'grafting from' method starts with immobilization of an initiator onto a surface (forms a SAMs layer) followed by direct polymerization of

polymer chains from surface attached initiators[19-20] and is capable of achieving much higher grafting density and film thickness (greater than 100 nm).[25]

As one of the most effective and versatile pathways towards surfaces with desired physicochemical properties, SIP allows control over grafting density, brush thickness and functionality.[26-27] At low grafting density, surface-tethered polymer chains exhibit random coil conformation which is often referred as 'mushroom regime' as shown in Scheme 1.2. When the grafting density is high, the surface-bound chains are forced to stretched away from the surface and adopt the 'polymer brush' conformation due to strong segment-segment interactions and the polymer brush thickness, h, scales to 1/3 order of grafting density, σ.[4, 19, 28] Grafted polymers with low grafting density or in the 'mushroom regime' can be fabricated by the 'grafting to/through' approaches. Grafted polymers with high grafting density or in the 'brush regime' require the 'grafting from' method.

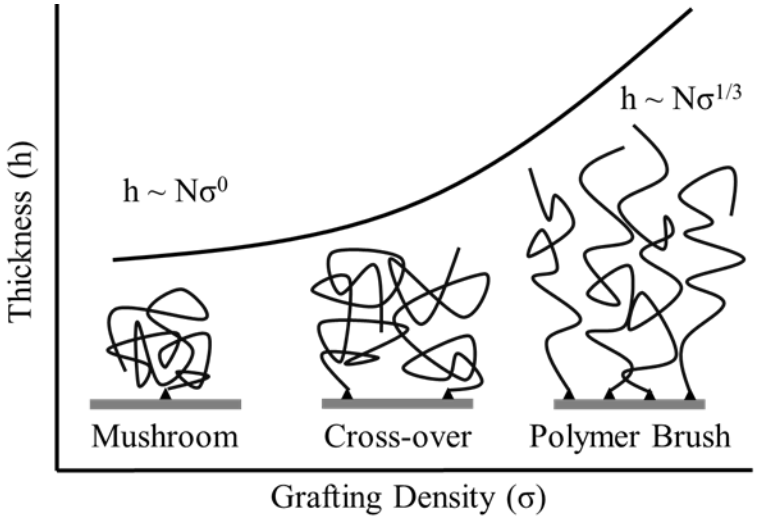

Scheme 1.2 Schematic illustration of the conformations of polymer grafted on surfaces in which h represents thickness, N represents the degree of polymerization and σ represents grafting density of grafted polymers.

Polymer brushes can be synthesized on a number of substrates/surfaces including silicon,[29] quartz,[29] glass,[30] stainless steel,[29, 31] Al,[32-33] Ti,[29, 34-35] Ni,[35] gold,[29, 36] cellulose,[37] and polymers.[30, 38-41] Other than flat substrates, polymer brushes can be grown from microchannels,[39, 42] membranes,[32, 37] AFM probes (silicon nitride),[43] nanoparticles (e.g. SiO_2,[44-45] Fe_3O_4,[46] Fe_2O_3,[47] TiO_2,[48] and clay[49]), graphene,[50] carbon nanotubes,[51] carbon fibers,[52] deformable materials,[41, 53] and layer-by-layer (LbL) films.[54] Other than the SAM technique, macromolecular initiators[38, 40-41, 51] are also used for the SIP process. Polymer brush surfaces can be synthesized via anionic polymerization,[55] cationic polymerization[56] ring opening metathesis polymerization (ROMP)[57-58] and radical polymerization techniques (thermal-initiated/photo-initiated free radical polymerization,[4, 26, 59] NMP,[60] ATRP,[61-64] and RAFT[65]). Using surface-initiated ATRP, block copolymer brushes have also been prepared.[63-64]

1.4 Physical Properties of Polymer Brush

Compared to sub-10 nm films prepared by SAMs and/or grafting to/through approaches, the higher thickness of polymer brush greatly enhances the functionality of the surfaces which benefits applications such as membranes and biosensors.[66-67] Applications that rely on the chemical functionality of polymer brush surfaces are summarized in a number of literature.[59, 68-70] Compared to solution cast polymeric ultrathin films, polymer brush films have a number of unique properties: (1) greater stability due to covalent linkages between polymer chains and the substrate; (2) increased effective T_g due to stronger interfacial energy (γ) between polymers and the substrate; (3) stronger elastic modulus in the vertical direction of the surface due to extended polymer chain conformation.

The glass transition temperature (T_g) of spin coated ultrathin films (below 80 nm) is lower than the bulk T_g with low interfacial energy (γ) between the film and substrate.[71-72] The effective T_g and elastic modulus of polymer brush (under dry and/or glassy state) are found to be consistently higher than that of spin-coated films of equivalent thicknesses owing to the anisotropic structure of extended chains. This feature of increased T_g and modulus of polymer brush has found applications in wear resistance surfaces,[73] lithography and millipede data storage technology in semiconductor industry.[74-75] For spin coated films the deviation in the T_g from the bulk value increases with decreasing film thickness. For polymer brush, the T_g increases sharply with decrease of brush thickness within the range of 50 nm predominately due to the restricted mobility of tethered polymer chains as shown by Scheme 1.3.[76-78]

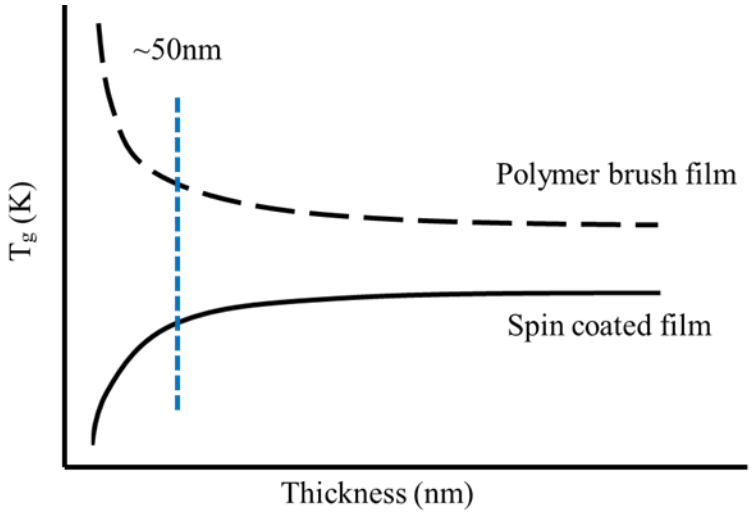

Scheme 1.3 Schematic illustration of the relation between the glass transition temperature and the film thickness of polymer brush and spin coated films.

The estimation of shear modulus of polymer brush under molten state was first proposed by Fredrickson *et al.*[79] and compared well with measurement by Fujii *et al.* who found that monodispersed brushes show much smaller shear modulus than brushes with

polydispersed molecular weight.[80] Nalam *et al.* observed shear moduli of swelling polymer brushes decrease with improving solvent quality.[81] Domack *et al.* reported that shear modulus of swelling polymer brush could be much lower than the shear modulus of a polymer solution of equivalent segmental density.[82] Similarly, Espinosa-Marzal *et al.*[83] and Sui *et al.*[84] found that the elastic moduli of swelling polymer brush decrease with improving solvent quality and swelling ratio. Polymer brush surfaces with low shear modulus have found applications in the field of friction reduction and lubrication.[73, 85-86]

1.5 Characterization of Polymer Brushes

Characterization of ultrathin polymer brush is challenging yet important to the understand the chemical and physical properties.[59] The thickness of ultrathin films can be directly measured by atomic force microscopy (AFM) scratch test which involves removal of soft film materials from rigid substrates.[87] Ellipsometry, on the other hand, is the most convenient and widely used non-destructive method for SAMs and polymer brush thickness measurement.[62] Ellipsometry directly measures the complex reflectance ratio ρ (via amplitude component Ψ and the phase difference Δ) of a beam of laser passing through thin film samples. The film thickness can be calculated using a multilayer model, based on Fresnel equations, with given refractive index (RI) values of each layer. Ellipsometry can also be used to back calculate RI of an ultrathin film with known thickness values.[88] X-ray reflectivity (XRR)[63-64, 89] and neutron reflectivity (NR) [90-92] can also be used to determine film thickness. For polymer brush grafted on particles, transmission electron microscopy (TEM)[93] and dynamic light scattering (DLS)[94] are the techniques to deduce polymer brush thickness. Thermogravimetric

analysis (TGA) has been used to determine the weight percentage of polymer brush on brush coated nanoparticles.[94]

Grafting density, σ, is an important parameter of a polymer brush. In theory, σ can be calculated based on the film thickness (h), mass density (ρ) and molecular weight (M) of degrafted polymer brush previously tethered on the substrate, as shown by the following equation, in which N_A is the Avogadro number.[20, 95]

$$\sigma = \frac{h\rho N_A}{M_n} \qquad \text{Equation 1}$$

In practice, a sacrificial initiator was added to the polymerization solution and the number average molecular weight of the solution-borne polymer (measured by GPC) was used as M_n.[96] In Equation 1, the mass density (ρ) of polymer brush was usually assumed to be equivalent to that of bulk polymer or, if the density of polymer is not available, monomer.

A number of microscopic techniques have been used to study the morphology of polymer brush surfaces, including optical microscopy,[97-99] fluorescence microscopy,[100] [101] scanning electron microscopy (SEM) and AFM,[99, 102] ranging from sub-millimeter to sub-micron sized domains. AFM and photo profilometer are capable of providing images with 3D information and surface roughness values.[103]

Mechanical properties (modulus[104] and adhesion[105]) and phase separation of ultrathin polymer brush can be characterized using AFM. Stafford and other researchers have developed methods using surface buckling behavior to characterize mechanical properties of a PDMS tethered polymer brush.[53]

Attenuated total reflection Fourier transform infrared spectroscopy (ATR-FTIR) is suited for the characterization of the chemical component of ultrathin polymer brush.[106]

Depth profiling (and mapping analysis) of the through thickness chemical composition of polymer brush can be achieved by X-ray photoelectron spectroscopy (XPS),[64, 89, 107] time of flight secondary ion mass spectroscopy (ToF-SIMS)[108] and NR.[90-92] Elemental distribution of polymer brush surfaces can be characterized using SEM energy disperse X-ray (EDX).[31, 109]

Wetting behavior of polymer brushes can be characterized using contact angle goniometer. Surface free energy of samples can be obtained using two probe liquids (usually DI water and hexadecane) according to the Fowkes two component model.[110]

Quartz crystal microbalance (QCM) is a technique that measures the mass per unit area based on the change in frequency of a quartz crystal resonator and it has been used to monitor conformational changes of polymer brush upon swelling.[111-112] Ellipsometry with a liquid cell can also be used to monitor the swelling of polymer brush (Also see Chapter V).[113]

1.6 Postpolymerization Modification (PPM) of Polymer Brush

Many applications of polymer brush surfaces depend on the functionality carried by the polymer chains tethered on the substrate.

Unfortunately, direct polymerization of monomers bearing desired functionality is not always applicable, due to chemistry (e.g. thiols and alkenes groups versus radical polymerization), physical (steric hindrance) and/or economic reasons. Post-polymerization modification (PPM) is a better approach which involves SIP of monomers containing polymerization-inert functional groups followed by subsequent conversion of the functional moiety groups into desired functionality.[114]

Postmodification of polymer brushes, in a lot of cases, involves addition of small molecules onto the already stretched polymer chains, thus requiring efficient chemistries to overcome the entropic penalty to achieve high conversion. 'Click chemistries' and other highly efficient reactions such as copper catalyzed azide-alkyne cycloaddition (CuAAC),[115-117] amine-active ester reactions (N-Hydroxysuccinimide/NHS[67, 118] and pentafluorophenol[119]), epoxy ring opening reactions,[120-122] Diels-Alder cycloadditions,[123-130] nitroxide photo-click reaction[131] and thiol-based reactions[132] (alkenes,[129-130, 133-136] alkynes,[98, 134, 137] isocyanates,[99] epoxy,[138] and halogens[139-141]) have been used for the SIP-PPM approach. Polymer brush surfaces with multiple functional groups can also be synthesized using the SIP-PPM approach via sequential modifications[142] or orthogonal chemistries.[98, 143-146] Surfaces with complex morphology and compositionally controlled patterned domains can be achieved via the combination of polymer brushes with patterning techniques including photomasking,[98, 100-101] microcontact printing (μCP),[97, 102] microcapillary printing (μCaP),[99, 145] lithography,[100] and techniques relying on surface buckling instability.[145, 147]

1.7 Effectiveness of PPM

Upon postmodification, the polymer brush thickness changes due to the change of molecular mass of the repeating unit. Murada *et al.* first studied the relationship between the polymer brush thickness change and molecular mass and found that, by assuming constant grafting density and mass density before and after modification, the brush thickness is proportional to the molar masses, as is expressed in the following equation,

$$\frac{T_2}{T_1} = \frac{M_2}{M_1} \qquad \text{Equation 2}$$

where T_1 and T_2 are the polymer brush thicknesses, and M_1 and M_2 are the molar mass of the repeating unit of the polymer brush before and after modification, respectively.[67]

For PPM involving addition of reactive moieties onto polymer brush, by assuming good solvent conditions, the number of reactive molecules in solution is orders of magnitudes larger than the number of potential reactive sites on the polymer brush resulting in pseudo first order kinetics. Arnold *et al.* reported that pseudo first order kinetics fits well with the aminolysis of an active ester pendent brush.[119] In some cases, due to diffusion limitation, PPM of polymer brush do not always follow the pseudo first order model. Upon exposure to the PPM solution, the outskirt of the polymer brush will first be modified by the free reactive molecules. The increased molar mass of the repeating units will force the polymer chains into a more stretched conformation leading to increased film thickness. Together this makes the mass transfer of reactive molecules in the solution to the regions of polymer brush close to the substrate more difficult, rendering a reduced if not diminished observed reaction rate. Orski *et al.* reported the kinetics of PPM of a CuAAC polymer brush exhibiting a diffusion limited region with much lower reaction rate at higher conversion.[148]

The diffusion limitation may negatively affect the effectiveness of the PPM process in terms of overall conversion, depth of penetration and homogeneity of the modified brush. Factors of high film thickness, grafting density, chain stiffness, size or molecular weight of the modifier and poor solvent quality reduce the PPM efficacy and penetration depths while increasing compositional heterogeneity of the modified polymer brush as shown by Scheme 1.4. Schuh *et al.* reported the penetration depth of amine-functionalized poly(ethylene glycol) (PEG-NH_2) within an active ester pendent polymer

brush.[149] The authors discovered that while the molecular weight of the incoming molecules have a strong influence on the extent of the PPM the brush thickness and grafting density have only a weak effect on the PPM process. Schüwer *et al.* studied the PPM process and the distribution of small molecular modifies on p-nitrophenyl chloroformate (NPC) pre-activated poly(hydroxyethyl methacrylate) (pHEMA) brushes.[91] Using neutron reflectometry the authors showed that the PPM of a pre-activated polymer brush depends on both the size of the incoming modifier, polymer brush thickness and the grafting density in that smaller molecules penetrate deeper into the polymer brush and polymer brushes with high thickness and grafting density led to significant amount of functional groups in the inner part of polymer brushes remain unreacted after PPM. Alswieleh *et al.* demonstrated spatially controlled crosslinking within a brush surface via solvent quality; crosslinking in good solvent provided homogeneous crosslinked brush throughout the brush, whereas in poor solvent resulted in crosslinking primarily in the surface region of the brush[150]. Polymer brush with heterogeneity along the normal axis, although are not favorable in some applications, provides a new route towards polymer brushes with complex architectures otherwise unattainable by methods of direct polymerization as will be discussed in Chapter V.

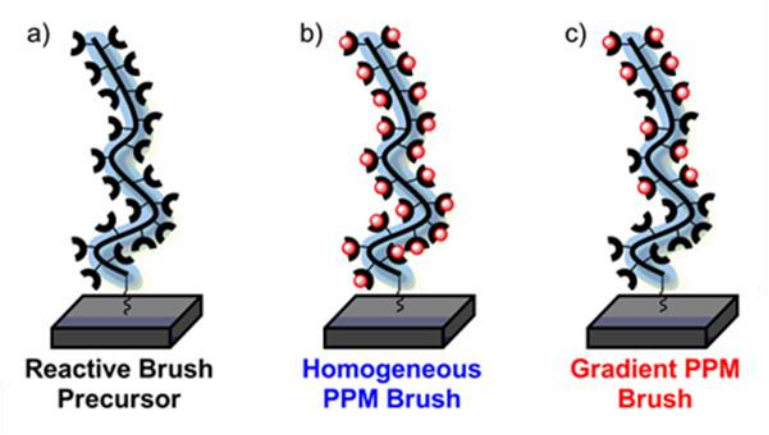

Scheme 1.4 Illustration of (a) reactive polymer brush before modification, (b) homogeneously post modified polymer brush and (c) post modified polymer brush with functionality gradient along the normal direction of the substrate.

1.8 Surfaces with Buckling Instability

Buckling instabilities (creasing, wrinkling, and folding) are a very common phenomenon in nature. Contrary to traditional mindset of viewing surface buckling as a nuisance to be avoided[151], recent advancements in technology have focused on exploiting strain-induced wrinkling of thin films as a powerful approach to define the shape, morphology, and function of surfaces with ordered or disordered patterns at multiple length scales.[152] Surfaces with buckling instabilities have found applications in the fields of advanced adhesion,[153-156] tunable wettability,[157-158] antifouling,[159-160] particle assembly,[161-162] stem cell growth and differentiation,[163] ultrasensitive pressure sensor,[164] and stretchable electronics,[165-168] among many others.[151, 169-170] Buckling with orientation particularly finds application in microlens arrays,[171] diffraction gratings,[172-173] microcontact printing,[174] maskless lithography,[175] and open-channel microfluidics.[176] Stafford and other researchers developed a method using surface buckling to measure thin film properties including elastic modulus,[177-179] residue stress,[180] and relaxation[181].

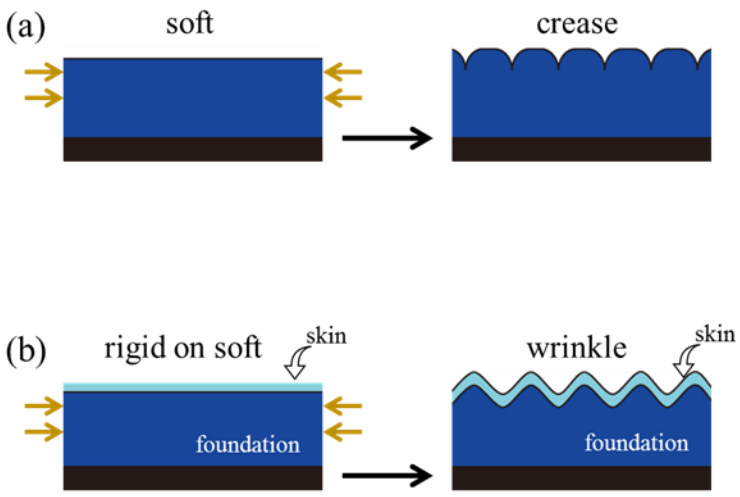

Scheme 1.5 Schematic illustration of in-plane compression induced (a) crease and (b) wrinkling.

Creasing instabilities are the result of a large compressive strain in a soft, elastic material,[151, 182] as shown by Scheme 1.5a. As a comparison, the principles of wrinkling instability have been illustrated using rigid-on-soft models,[151-152] as shown by Scheme 1.5b. Consider a model with a thin film thickness h, width w, and with elastic moduli of the top and bottom layers represented as E_s and E_f, respectively. The Poisson ratio of the top 'skin' and 'foundation' materials are v_s and v_f, respectively. By neglecting any interfacial shear stress, the in-plane compressive force expression is given by Equation 3.[152]

$$F = E_s \left[\left(\frac{\pi}{\lambda}\right)^2 \frac{wh^3}{3\left(1-v_s^2\right)} + \frac{\lambda}{\pi} \frac{E_f w}{4\left(1-v_f^2\right)E_s} \right] \quad \text{Equation 3}$$

in which λ represents the scale of a sinusoidal deflection or the wrinkle wavelength. Buckling instability occurs when the in-plane compressive force is greater than a critical value F_c at which $(dF/d\lambda) = 0$ is obtained. The wrinkle wavelength at this critical point is λ_c, as shown in the Equation 4.[152]

$$\lambda_c = 2\pi h \left[\frac{\left(1-v_f^2\right)E_s}{3\left(1-v_s^2\right)E_f}\right]^{1/3} \qquad \text{Equation 4}$$

Cerda and Mahadevan developed a simplified theory to describe the wrinkling scale (λ) and amplitude (A) using Equations 5 and 6,[183]

$$\lambda \sim \left(\frac{B}{K}\right)^{1/4} \qquad \text{Equation 5}$$

$$A \sim \lambda \left(\frac{\Delta}{w}\right)^{1/2} \qquad \text{Equation 6}$$

where (B/K) represents the relative stiffness of the top layer and bottom layer, and (Δ/w) represents the imposed compressive strain. For films on flat substrates, the scaling law in Equation 5 reduces to $\lambda \sim \left(E_s/E_f\right)^{1/3}$, in agreement with Equation 4.

1.9 Synthesis of Polymeric Films with Buckling Instability

Polymeric films with buckling instabilities can be engineered based on layered, homogeneous, and gradient systems.[152, 169] In the bilayer system composed of a high modulus thin film bonded to a semi-infinite, low modulus substrate, surface wrinkling can occur from in-plane compression with the wrinkle wavelength dictated by the thickness of the top film and the film/substrate modulus ratio, whereas the wrinkle amplitude is related to applied strain. Researchers have created buckling surfaces based on thin film structures using methods including metal deposition,[172] UV/ozone oxidation,[184] photo-induced crosslinking,[185-186] and surface-grafting techniques;[53] however, these methods have focused primarily on the fabrication of thin films on elastomeric substrates with micro-scale morphologies. Relatively few studies have induced buckling instabilities in ultrathin (i.e. <100 nm) polymer films attached to rigid substrates.[185, 187]

Recently, Brooks *et al.* combined active ester modification and μCP techniques to fabricate nanoscale creases in polymer brush surfaces on silicon substrates.[147] The PPM process increased the molecular weight of the brush resulting in osmotic swelling normal to the substrate surface. Confinement of the swollen brush during the μCP process resulted in a critical in-plane stress, which was relieved via formation of creases. Furthermore, control of crease morphology was demonstrated by changing the stamping pressure. However, the prerequisite of mechanical confinement to induce the buckling instability may limit the process to substrates with simple 2D geometries.

1.10 Summary and Research Overview

The combination of surface-initiated polymerization and postpolymerization modification (SIP-PPM) is a powerful technique for the fabrication of functional soft surfaces. The effectiveness of the PPM of polymer brush is governed by factors such as brush thickness, grafting density, size of free reactive moieties and reaction conditions. Better understanding the influence of the aforementioned factors on the PPM effectiveness is valuable for fulfilling the potential of the PPM approach for the fabrication of functional soft surfaces. Specifically, by carefully balancing modification reactivity and limitation of mass transport, PPM with heterogeneity and functionality gradients opens doors to new routes for the design and synthesis of polymer brushes with complex functionality and morphologies (i.e. buckling) otherwise unattainable by methods of direct polymerization.

This dissertation is focused on designing and synthesizing polymer brush surfaces with complex molecular architectures and morphologies with specific emphasis on

improving the understanding of PPM effectiveness and the distribution of post-modification moieties on grafted polymer chains.

In Chapter II, microwave-assisted surface-initiated polymerization (μW-SIP) was developed and employed to demonstrate the synthesis of polymer brushes on silicon and quartz substrates. The μW-SIP approach shows significant enhancements in polymer brush thickness at reduced reaction times and monomer concentration.

In Chapter III, the postpolymerization modification of a poly(2-isocyanatoethyl methacrylate) (pNCOMA) brush surfaces with two deuterated thiols of different sizes was studied and the depth profiles of the distribution of deuterated thiourethane alkyl moieties within the polymer brush was drawn using neutron reflectometry analysis. By applying a sequential PPM strategy, a polymer brush with tapered block copolymer architectures was synthesized.

In Chapter IV, a poly(styrene-alt-maleic anhydride) (pSMA) copolymer brush was synthesized in an effort to fabricate a polymer brush surface containing pendent polyfunctional thiols for further thiol-ene modifications via a two-step modification. Furthermore, the pSMA brush itself was found to be a stable and versatile platform for amine modifications.

In Chapter V, a straightforward PPM approach, utilizing the knowledge gained in Chapter III and IV, to engineer ultrathin polymer brush surfaces with tunable wrinkled morphologies was demonstrated by creating a modulus mismatch between the top layer and bottom of the polymer brush via selectively crosslinking of the outer layer of pSMA brushes by balancing the rate of PPM and reactive molecule diffusion.

1.11 References

1. Stark, M. T., *Archaeology of Asia*. Wiley: 2008; p 130.
2. Xia, J. R.; Lin, J. H.; Xu, Y. L.; Chen, Q. H., On the UV-Induced Polymeric Behavior of Chinese Lacquer. *Acs Appl Mater Inter* **2011,** *3* (2), 482-489.
3. Langhals, H.; Bathelt, D., The restoration of the largest archaelogical discovery-a chemical problem: Conservation of the polychromy of the Chinese terracotta army in Lintong. *Angew Chem Int Edit* **2003,** *42* (46), 5676-5681.
4. Rühe, J., Polymer Brushes: On the Way to Tailor-Made Surfaces. In *Polymer Brushes*, Wiley: 2006; pp 1-31.
5. Caldona, E. B.; de Leon, A. C. C.; Thomas, P. G.; Naylor Iii, D. F.; Pajarito, B. B.; Advincula, R. C., Superhydrophobic rubber-modified polybenzoxazine/SiO2 nanocomposite coating with anti-corrosion, anti-ice, and superoleophilicity properties. *Industrial & Engineering Chemistry Research* **2017**.
6. Brubaker, C. E.; Messersmith, P. B., The Present and Future of Biologically Inspired Adhesive Interfaces and Materials. *Langmuir* **2012,** *28* (4), 2200-2205.
7. Kobayashi, M.; Terayama, Y.; Ishikawa, T.; Terada, M.; Soejima, H.; Murakami, D.; Takahara, A., Applications of Surface Initiated ATRP to the Preparation of Polyelectrolyte Brushes for Antifouling, Adhesion Control, Friction Control. In *Progress in Controlled Radical Polymerization: Materials and Applications*, American Chemical Society: 2012; Vol. 1101, pp 183-195.
8. Napper, D. H., *Polymeric stabilization of colloidal dispersions*. Academic Press: London, 1983.
9. Bergbreiter, D. E., Chemically Modified Surfaces in Catalysis. In *Chemically Modified Surfaces in Catalysis and Electrocatalysis*, AMERICAN CHEMICAL SOCIETY: 1982; Vol. 192, pp 1-8.
10. Anastasiadis, S. H., Development of Functional Polymer Surfaces with Controlled Wettability. *Langmuir* **2013,** *29* (30), 9277-9290.
11. Zarras, P.; Wood, T.; Richey, B.; Benicewicz, B. C., Overview of Coatings for Advanced Applications. In *New Developments in Coatings Technology*, American Chemical Society: 2007; Vol. 962, pp 1-5.
12. Moehwald, H.; Brezesinski, G., From Langmuir Monolayers to Multilayer Films. *Langmuir* **2016,** *32* (41), 10445-10458.
13. Decher, G.; Schlenoff, J. B., *Multilayer Thin Films: Sequential Assembly of Nanocomposite Materials*. Wiley: 2006.
14. Halperin, A.; Tirrell, M.; Lodge, T. P., Tethered chains in polymer microstructures. In *Macromolecules: Synthesis, Order and Advanced Properties*, Springer Berlin Heidelberg: Berlin, Heidelberg, 1992; pp 31-71.
15. Jones, R. A. L.; Richards, R. W., *Polymers at Surfaces and Interfaces*. Cambridge University Press: 1999.
16. Samanta, D.; Sarkar, A., Immobilization of bio-macromolecules on self-assembled monolayers: methods and sensor applications. *Chemical Society Reviews* **2011,** *40* (5), 2567-2592.
17. Ulman, A., Formation and Structure of Self-Assembled Monolayers. *Chemical Reviews* **1996,** *96* (4), 1533-1554.

18. Ulman, A., *An Introduction to Ultrathin Organic Films: From Langmuir--Blodgett to Self--Assembly*. Elsevier Science: 2013.
19. Minko, S., Grafting on Solid Surfaces: "Grafting to" and "Grafting from" Methods. In *Polymer Surfaces and Interfaces: Characterization, Modification, and Applications*, Stamm, M., Ed. Springer Berlin Heidelberg: Berlin, Heidelberg, 2008; pp 215-234.
20. Zhao, B.; Brittain, W. J., Polymer brushes: surface-immobilized macromolecules. *Progress in Polymer Science* **2000,** *25* (5), 677-710.
21. Henze, M.; Madge, D.; Prucker, O.; Ruhe, J., "Grafting Through": Mechanistic Aspects of Radical Polymerization Reactions with Surface-Attached Monomers. *Macromolecules* **2014,** *47* (9), 2929-2937.
22. Sejoubsari, R. M.; Martinez, A. P.; Kutes, Y.; Wang, Z. L.; Dobrynin, A. V.; Adamson, D. H., "Grafting-Through": Growing Polymer Brushes by Supplying Monomers through the Surface. *Macromolecules* **2016,** *49* (7), 2477-2483.
23. Kopf, A.; Baschnagel, J.; Wittmer, J.; Binder, K., On the Adsorption Process in Polymer Brushes: A Monte Carlo Study. *Macromolecules* **1996,** *29* (5), 1433-1441.
24. Zajac, R.; Chakrabarti, A., Irreversible polymer adsorption from semidilute and moderately dense solutions. *Physical Review E* **1995,** *52* (6), 6536-6549.
25. Prucker, O.; Christian, S.; Bock, H.; Ruhe, J.; Frank, C. W.; Knoll, W., On the glass transition in ultrathin polymer films of different molecular architecture. *Macromol Chem Physic* **1998,** *199* (7), 1435-1444.
26. Prucker, O.; Rühe, J., Polymer Layers through Self-Assembled Monolayers of Initiators. *Langmuir* **1998,** *14* (24), 6893-6898.
27. Hensarling, R. M.; Patton, D. L., CHAPTER 12 Surface Engineering with Thiol-click Chemistry. In *Thiol-X Chemistries in Polymer and Materials Science*, The Royal Society of Chemistry: 2013; pp 259-285.
28. Milner, S. T., Polymer Brushes. *Science* **1991,** *251* (4996), 905.
29. Liu, J.; Ye, Q.; Yu, B.; Wang, X.; Zhou, F., Contact printing a biomimetic catecholic monolayer on a variety of surfaces and derivation reaction. *Chemical Communications* **2012,** *48* (3), 398-400.
30. Welch, M. E.; Ober, C. K., Characterization of Polymer Brush Membranes via HF Etch Liftoff Technique. *ACS Macro Letters* **2013,** *2* (3), 241-245.
31. Friis, J. E.; Brøns, K.; Salmi, Z.; Shimizu, K.; Subbiahdoss, G.; Holm, A. H.; Santos, O.; Pedersen, S. U.; Meyer, R. L.; Daasbjerg, K.; Iruthayaraj, J., Hydrophilic Polymer Brush Layers on Stainless Steel Using Multilayered ATRP Initiator Layer. *Acs Appl Mater Inter* **2016,** *8* (44), 30616-30627.
32. Bruening, M. L.; Dotzauer, D. M.; Jain, P.; Ouyang, L.; Baker, G. L., Creation of Functional Membranes Using Polyelectrolyte Multilayers and Polymer Brushes. *Langmuir* **2008,** *24* (15), 7663-7673.
33. Sugnaux, C.; Lavanant, L.; Klok, H.-A., Aqueous Fabrication of pH-Gated, Polymer-Brush-Modified Alumina Hybrid Membranes. *Langmuir* **2013,** *29* (24), 7325-7333.
34. Fan, X.; Lin, L.; Messersmith, P. B., Cell Fouling Resistance of Polymer Brushes Grafted from Ti Substrates by Surface-Initiated Polymerization: Effect of Ethylene Glycol Side Chain Length. *Biomacromolecules* **2006,** *7* (8), 2443-2448.

35. Fan, X.; Lin, L.; Dalsin, J. L.; Messersmith, P. B., Biomimetic Anchor for Surface-Initiated Polymerization from Metal Substrates. *Journal of the American Chemical Society* **2005,** *127* (45), 15843-15847.
36. Rastogi, A.; Nad, S.; Tanaka, M.; Mota, N. D.; Tague, M.; Baird, B. A.; Abruña, H. D.; Ober, C. K., Preventing Nonspecific Adsorption on Polymer Brush Covered Gold Electrodes Using a Modified ATRP Initiator. *Biomacromolecules* **2009,** *10* (10), 2750-2758.
37. Keating, J. J.; Imbrogno, J.; Belfort, G., Polymer Brushes for Membrane Separations: A Review. *Acs Appl Mater Inter* **2016,** *8* (42), 28383-28399.
38. Zhao, H.; Zhu, B.; Luo, S.-C.; Lin, H.-A.; Nakao, A.; Yamashita, Y.; Yu, H.-h., Controlled Protein Absorption and Cell Adhesion on Polymer-Brush-Grafted Poly(3,4-ethylenedioxythiophene) Films. *Acs Appl Mater Inter* **2013,** *5* (11), 4536-4543.
39. Fortin, N.; Klok, H.-A., Glucose Monitoring Using a Polymer Brush Modified Polypropylene Hollow Fiber-based Hydraulic Flow Sensor. *Acs Appl Mater Inter* **2015,** *7* (8), 4631-4640.
40. Coad, B. R.; Bilgic, T.; Klok, H.-A., Polymer Brush Gradients Grafted from Plasma-Polymerized Surfaces. *Langmuir* **2014,** *30* (28), 8357-8365.
41. Dokukin, M. E.; Kuroki, H.; Minko, S.; Sokolov, I., AFM Study of Polymer Brush Grafted to Deformable Surfaces: Quantitative Properties of the Brush and Substrate Mechanics. *Macromolecules* **2017,** *50* (1), 275-282.
42. Lanotte, L.; Guido, S.; Misbah, C.; Peyla, P.; Bureau, L., Flow Reduction in Microchannels Coated with a Polymer Brush. *Langmuir* **2012,** *28* (38), 13758-13764.
43. Gabriel, S.; Jérôme, C.; Jérôme, R.; Fustin, C.-A.; Pallandre, A.; Plain, J.; Jonas, A. M.; Duwez, A.-S., One-Step Polymer Grafting from Silicon Nitride SPM Probes: From Isolated Chains to Brush Regime. *Journal of the American Chemical Society* **2007,** *129* (27), 8410-8411.
44. Choi, J.; Hore, M. J. A.; Clarke, N.; Winey, K. I.; Composto, R. J., Nanoparticle Brush Architecture Controls Polymer Diffusion in Nanocomposites. *Macromolecules* **2014,** *47* (7), 2404-2410.
45. Prucker, O.; Rühe, J., Mechanism of Radical Chain Polymerizations Initiated by Azo Compounds Covalently Bound to the Surface of Spherical Particles. *Macromolecules* **1998,** *31* (3), 602-613.
46. Dolatkhah, A.; Wilson, L. D., Magnetite/Polymer Brush Nanocomposites with Switchable Uptake Behavior Toward Methylene Blue. *Acs Appl Mater Inter* **2016,** *8* (8), 5595-5607.
47. Huang, Y.; Sasano, T.; Tsujii, Y.; Ohno, K., Well-Defined Polymer-Brush-Coated Rod-Shaped Particles: Synthesis and Formation of Liquid Crystals. *Macromolecules* **2016,** *49* (22), 8430-8439.
48. Fan, X.; Lin, L.; Messersmith, P. B., Surface-initiated polymerization from TiO2 nanoparticle surfaces through a biomimetic initiator: A new route toward polymer–matrix nanocomposites. *Composites Science and Technology* **2006,** *66* (9), 1198-1204.
49. Fan, X.; Xia, C.; Fulghum, T.; Park, M.-K.; Locklin, J.; Advincula, R. C., Polymer Brushes Grafted from Clay Nanoparticles Adsorbed on a Planar Substrate by Free Radical Surface-Initiated Polymerization. *Langmuir* **2003,** *19* (3), 916-923.

50. Steenackers, M.; Gigler, A. M.; Zhang, N.; Deubel, F.; Seifert, M.; Hess, L. H.; Lim, C. H. Y. X.; Loh, K. P.; Garrido, J. A.; Jordan, R.; Stutzmann, M.; Sharp, I. D., Polymer Brushes on Graphene. *Journal of the American Chemical Society* **2011,** *133* (27), 10490-10498.
51. Zhang, Y.; He, H.; Gao, C., Clickable Macroinitiator Strategy to Build Amphiphilic Polymer Brushes on Carbon Nanotubes. *Macromolecules* **2008,** *41* (24), 9581-9594.
52. Li, L.; Lukehart, C. M., Synthesis of Hydrophobic and Hydrophilic Graphitic Carbon Nanofiber Polymer Brushes. *Chemistry of Materials* **2006,** *18* (1), 94-99.
53. Huang, H.; Chung, J. Y.; Nolte, A. J.; Stafford, C. M., Characterizing polymer brushes via surface wrinkling. *Chemistry of Materials* **2007,** *19* (26), 6555-6560.
54. Estillore, N. C.; Advincula, R. C., Stimuli-Responsive Binary Mixed Polymer Brushes and Free-Standing Films by LbL-SIP. *Langmuir* **2011,** *27* (10), 5997-6008.
55. Zhou, Q.; Nakamura, Y.; Inaoka, S.; Park, M.-k.; Wang, Y.; Fan, X.; Mays, J.; Advincula, R., Surface-Iniatiated Anionic Polymerization: Tethered Polymer Brushes on Silicate Flat Surfaces. In *Polymer Nanocomposites*, American Chemical Society: 2001; Vol. 804, pp 39-55.
56. Jordan, R.; Ulman, A., Surface Initiated Living Cationic Polymerization of 2-Oxazolines. *Journal of the American Chemical Society* **1998,** *120* (2), 243-247.
57. Haque, H. A.; Kakehi, S.; Hara, M.; Nagano, S.; Seki, T., High-Density Liquid-Crystalline Azobenzene Polymer Brush Attained by Surface-Initiated Ring-Opening Metathesis Polymerization. *Langmuir* **2013,** *29* (25), 7571-7575.
58. Jiang, G.; Ponnapati, R.; Pernites, R.; Felipe, M. J.; Advincula, R., Surface-Initiated Ring-Opening Metathesis Polymerization (SI-ROMP): Synthesis and Electropolymerization of Terthiophene-Functionalized Olefin Peripheral Dendrons. *Macromolecules* **2010,** *43* (24), 10262-10274.
59. Barbey, R.; Lavanant, L.; Paripovic, D.; Schüwer, N.; Sugnaux, C.; Tugulu, S.; Klok, H.-A., Polymer Brushes via Surface-Initiated Controlled Radical Polymerization: Synthesis, Characterization, Properties, and Applications. *Chemical Reviews* **2009,** *109* (11), 5437-5527.
60. Roling, O.; Mardyukov, A.; Krings, J. A.; Studer, A.; Ravoo, B. J., Polymer Brushes Exhibiting Versatile Supramolecular Interactions Grown by Nitroxide-Mediated Polymerization and Structured via Microcontact Chemistry. *Macromolecules* **2014,** *47* (7), 2411-2419.
61. Hui, C. M.; Pietrasik, J.; Schmitt, M.; Mahoney, C.; Choi, J.; Bockstaller, M. R.; Matyjaszewski, K., Surface-Initiated Polymerization as an Enabling Tool for Multifunctional (Nano-)Engineered Hybrid Materials. *Chemistry of Materials* **2014,** *26* (1), 745-762.
62. Pyun, J.; Kowalewski, T.; Matyjaszewski, K., Synthesis of Polymer Brushes Using Atom Transfer Radical Polymerization. *Macromolecular Rapid Communications* **2003,** *24* (18), 1043-1059.
63. Yu, K.; Wang, H.; Xue, L.; Han, Y., Stimuli-Responsive Polyelectrolyte Block Copolymer Brushes Synthesized from the Si Wafer via Atom-Transfer Radical Polymerization. *Langmuir* **2007,** *23* (3), 1443-1452.

64. Yu, K.; Wang, H.; Han, Y., Motion of Integrated CdS Nanoparticles by Phase Separation of Block Copolymer Brushes. *Langmuir* **2007,** *23* (17), 8957-8964.
65. Baum, M.; Brittain, W. J., Synthesis of Polymer Brushes on Silicate Substrates via Reversible Addition Fragmentation Chain Transfer Technique. *Macromolecules* **2002,** *35* (3), 610-615.
66. Senaratne, W.; Andruzzi, L.; Ober, C. K., Self-Assembled Monolayers and Polymer Brushes in Biotechnology: Current Applications and Future Perspectives. *Biomacromolecules* **2005,** *6* (5), 2427-2448.
67. Murata, H.; Prucker, O.; Ruhe, J., Synthesis of functionalized polymer monolayers from active ester brushes. *Macromolecules* **2007,** *40* (15), 5497-5503.
68. Jain, P.; Baker, G. L.; Bruening, M. L., Applications of Polymer Brushes in Protein Analysis and Purification. *Annu Rev Anal Chem* **2009,** *2*, 387-408.
69. Ayres, N., Polymer brushes: Applications in biomaterials and nanotechnology. *Polym Chem-Uk* **2010,** *1* (6), 769-777.
70. Azzaroni, O., Polymer brushes here, there, and everywhere: Recent advances in their practical applications and emerging opportunities in multiple research fields. *J Polym Sci Pol Chem* **2012,** *50* (16), 3225-3258.
71. Tsui, O. K. C.; Russell, T. P.; Hawker, C. J., Effect of Interfacial Interactions on the Glass Transition of Polymer Thin Films. *Macromolecules* **2001,** *34* (16), 5535-5539.
72. Fryer, D. S.; Peters, R. D.; Kim, E. J.; Tomaszewski, J. E.; de Pablo, J. J.; Nealey, P. F.; White, C. C.; Wu, W.-l., Dependence of the Glass Transition Temperature of Polymer Films on Interfacial Energy and Thickness. *Macromolecules* **2001,** *34* (16), 5627-5634.
73. Sakata, H.; Kobayashi, M.; Otsuka, H.; Takahara, A., Tribological Properties of Poly(methyl methacrylate) Brushes Prepared by Surface-Initiated Atom Transfer Radical Polymerization. *Polym J* **2005,** *37* (10), 767-775.
74. Baljon, A. R. C.; Van Weert, M. H. M.; DeGraaff, R. B.; Khare, R., Glass Transition Behavior of Polymer Films of Nanoscopic Dimensions. *Macromolecules* **2005,** *38* (6), 2391-2399.
75. Vettiger, P.; Cross, G.; Despont, M.; Drechsler, U.; Durig, U.; Gotsmann, B.; Haberle, W.; Lantz, M. A.; Rothuizen, H. E.; Stutz, R.; Binnig, G. K., The "millipede" - nanotechnology entering data storage. *IEEE Transactions on Nanotechnology* **2002,** *1* (1), 39-55.
76. Urayama, K.; Yamamoto, S.; Tsujii, Y.; Fukuda, T.; Neher, D., Elastic Properties of Well-Defined, High-Density Poly(methyl methacrylate) Brushes Studied by Electromechanical Interferometry. *Macromolecules* **2002,** *35* (25), 9459-9465.
77. Higaki, Y.; Okazaki, R.; Takahara, A., Semirigid Biobased Polymer Brush: Poly(α-methylene-γ-butyrolactone) Brushes. *ACS Macro Letters* **2012,** *1* (9), 1124-1127.
78. Yamamoto, S.; Tsujii, Y.; Fukuda, T., Glass Transition Temperatures of High-Density Poly(methyl methacrylate) Brushes. *Macromolecules* **2002,** *35* (16), 6077-6079.
79. Fredrickson, G. H.; Ajdari, A.; Leibler, L.; Carton, J. P., Surface modes and deformation energy of a molten polymer brush. *Macromolecules* **1992,** *25* (11), 2882-2889.
80. Fujii, Y.; Yang, Z.; Clough, A.; Tsui, O. K. C., Shear Modulus of a Polymer Brush. *Macromolecules* **2010,** *43* (9), 4310-4313.

81. Nalam, P. C.; Daikhin, L.; Espinosa-Marzal, R. M.; Clasohm, J.; Urbakh, M.; Spencer, N. D., Two-Fluid Model for the Interpretation of Quartz Crystal Microbalance Response: Tuning Properties of Polymer Brushes with Solvent Mixtures. *The Journal of Physical Chemistry C* **2013,** *117* (9), 4533-4543.
82. Domack, A.; Prucker, O.; Rühe, J.; Johannsmann, D., Swelling of a polymer brush probed with a quartz crystal resonator. *Physical Review E* **1997,** *56* (1), 680-689.
83. Espinosa-Marzal, R. M.; Nalam, P. C.; Bolisetty, S.; Spencer, N. D., Impact of solvation on equilibrium conformation of polymer brushes in solvent mixtures. *Soft Matter* **2013,** *9* (15), 4045-4057.
84. Sui, X.; Zapotoczny, S.; Benetti, E. M.; Schon, P.; Vancso, G. J., Characterization and molecular engineering of surface-grafted polymer brushes across the length scales by atomic force microscopy. *Journal of Materials Chemistry* **2010,** *20* (24), 4981-4993.
85. Raviv, U.; Giasson, S.; Kampf, N.; Gohy, J.-F.; Jerome, R.; Klein, J., Lubrication by charged polymers. *Nature* **2003,** *425* (6954), 163-165.
86. Klein, J.; Kumacheva, E.; Mahalu, D.; Perahia, D.; Fetters, L. J., Reduction of frictional forces between solid surfaces bearing polymer brushes. *Nature* **1994,** *370* (6491), 634-636.
87. Guo, W.; Hensarling, R. M.; LeBlanc, A. L.; Hoff, E. A.; Baranek, A. D.; Patton, D. L., Rapid Synthesis of Polymer Brush Surfaces via Microwave-Assisted Surface-Initiated Radical Polymerization. *Macromolecular Rapid Communications* **2012,** *33* (9), 863-868.
88. McCrackin, F. L.; Passaglia, E.; Stromberg, R. R.; Steinberg, H. L., Measurement of the thickness and refractive index of very thin films and the optical properties of surfaces by ellipsometry. *J Res Natl Inst Stan* **2001,** *106* (3), 589-603.
89. Barbey, R.; Laporte, V.; Alnabulsi, S.; Klok, H.-A., Postpolymerization Modification of Poly(glycidyl methacrylate) Brushes: An XPS Depth-Profiling Study. *Macromolecules* **2013,** *46* (15), 6151-6158.
90. Yim, H.; Kent, M. S.; Mendez, S.; Balamurugan, S. S.; Balamurugan, S.; Lopez, G. P.; Satija, S., Temperature-Dependent Conformational Change of PNIPAM Grafted Chains at High Surface Density in Water. *Macromolecules* **2004,** *37* (5), 1994-1997.
91. Schüwer, N.; Geue, T.; Hinestrosa, J. P.; Klok, H.-A., Neutron Reflectivity Study on the Postpolymerization Modification of Poly(2-hydroxyethyl methacrylate) Brushes. *Macromolecules* **2011,** *44*, 6868-6874.
92. Zhang, J.; Nylander, T.; Campbell, R. A.; Rennie, A. R.; Zauscher, S.; Linse, P., Novel evaluation method of neutron reflectivity data applied to stimulus-responsive polymer brushes. *Soft Matter* **2008,** *4* (3), 500-509.
93. Dey, T., Polymer-coated magnetic nanoparticles: Surface modification and end-functionalization. *J Nanosci Nanotechno* **2006,** *6* (8), 2479-2483.
94. Chen, X.; Randall, D. P.; Perruchot, C.; Watts, J. F.; Patten, T. E.; von Werne, T.; Armes, S. P., Synthesis and aqueous solution properties of polyelectrolyte-grafted silica particles prepared by surface-initiated atom transfer radical polymerization. *Journal of Colloid and Interface Science* **2003,** *257* (1), 56-64.
95. Prucker, O.; Rühe, J., Synthesis of Poly(styrene) Monolayers Attached to High Surface Area Silica Gels through Self-Assembled Monolayers of Azo Initiators. *Macromolecules* **1998,** *31* (3), 592-601.

96. Marutani, E.; Yamamoto, S.; Ninjbadgar, T.; Tsujii, Y.; Fukuda, T.; Takano, M., Surface-initiated atom transfer radical polymerization of methyl methacrylate on magnetite nanoparticles. *Polymer* **2004,** *45* (7), 2231-2235.
97. Azzaroni, O.; Zheng, Z.; Yang, Z.; Huck, W. T. S., Polyelectrolyte Brushes as Efficient Ultrathin Platforms for Site-Selective Copper Electroless Deposition. *Langmuir* **2006,** *22* (16), 6730-6733.
98. Hensarling, R. M.; Doughty, V. A.; Chan, J. W.; Patton, D. L., "Clicking" Polymer Brushes with Thiol-yne Chemistry: Indoors and Out. *J Am Chem Soc* **2009,** *131* (41), 14673-+.
99. Hensarling, R. M.; Rahane, S. B.; LeBlanc, A. P.; Sparks, B. J.; White, E. M.; Locklin, J.; Patton, D. L., Thiol-isocyanate "click" reactions: rapid development of functional polymeric surfaces. *Polym Chem-Uk* **2011,** *2* (1), 88-90.
100. Dong, R.; Krishnan, S.; Baird, B. A.; Lindau, M.; Ober, C. K., Patterned Biofunctional Poly(acrylic acid) Brushes on Silicon Surfaces. *Biomacromolecules* **2007,** *8* (10), 3082-3092.
101. Hensarling, R. M.; Hoff, E. A.; LeBlanc, A. P.; Guo, W.; Rahane, S. B.; Patton, D. L., Photocaged pendent thiol polymer brush surfaces for postpolymerization modifications via thiol-click chemistry. *Journal of Polymer Science Part A: Polymer Chemistry* **2013,** *51* (5), 1079-1090.
102. Zhou, F.; Zheng, Z.; Yu, B.; Liu, W.; Huck, W. T. S., Multicomponent Polymer Brushes. *Journal of the American Chemical Society* **2006,** *128* (50), 16253-16258.
103. Liu, C.; Lee, J.; Ma, J.; Elimelech, M., Antifouling Thin-Film Composite Membranes by Controlled Architecture of Zwitterionic Polymer Brush Layer. *Environmental Science & Technology* **2017**.
104. Julthongpiput, D.; LeMieux, M.; Tsukruk, V. V., Micromechanical properties of glassy and rubbery polymer brush layers as probed by atomic force microscopy. *Polymer* **2003,** *44* (16), 4557-4562.
105. Jones, D. M.; Smith, J. R.; Huck, W. T. S.; Alexander, C., Variable Adhesion of Micropatterned Thermoresponsive Polymer Brushes: AFM Investigations of Poly(N-isopropylacrylamide) Brushes Prepared by Surface-Initiated Polymerizations. *Advanced Materials* **2002,** *14* (16), 1130-1134.
106. Yamamoto, S.; Ejaz, M.; Tsujii, Y.; Fukuda, T., Surface Interaction Forces of Well-Defined, High-Density Polymer Brushes Studied by Atomic Force Microscopy. 2. Effect of Graft Density. *Macromolecules* **2000,** *33* (15), 5608-5612.
107. LeMieux, M. C.; Peleshanko, S.; Anderson, K. D.; Tsukruk, V. V., Adaptive Nanomechanical Response of Stratified Polymer Brush Structures. *Langmuir* **2007,** *23* (1), 265-273.
108. Kim, Y.-P.; Lee, B. S.; Kim, E.; Choi, I. S.; Moon, D. W.; Lee, T. G.; Kim, H.-S., Activity-Based Assay of Matrix Metalloproteinase on Nonbiofouling Surfaces Using Time-of-Flight Secondary Ion Mass Spectrometry. *Analytical Chemistry* **2008,** *80* (13), 5094-5102.
109. Paripovic, D.; Klok, H.-A., Polymer Brush Guided Formation of Thin Gold and Palladium/Gold Bimetallic Films. *Acs Appl Mater Inter* **2011,** *3* (3), 910-917.
110. Fowkes, F. M., ATTRACTIVE FORCES AT INTERFACES. *Industrial & Engineering Chemistry* **1964,** *56* (12), 40-52.

111. Jhon, Y. K.; Bhat, R. R.; Jeong, C.; Rojas, O. J.; Szleifer, I.; Genzer, J., Salt-Induced Depression of Lower Critical Solution Temperature in a Surface-Grafted Neutral Thermoresponsive Polymer. *Macromolecular Rapid Communications* **2006,** *27* (9), 697-701.
112. Moya, S. E.; Azzaroni, O.; Kelby, T.; Donath, E.; Huck, W. T. S., Explanation for the Apparent Absence of Collapse of Polyelectrolyte Brushes in the Presence of Bulky Ions. *The Journal of Physical Chemistry B* **2007,** *111* (25), 7034-7040.
113. Willott, J. D.; Murdoch, T. J.; Humphreys, B. A.; Edmondson, S.; Webber, G. B.; Wanless, E. J., Critical Salt Effects in the Swelling Behavior of a Weak Polybasic Brush. *Langmuir* **2014,** *30* (7), 1827-1836.
114. Galvin, C. J.; Genzer, J., Applications of surface-grafted macromolecules derived from post-polymerization modification reactions. *Prog Polym Sci* **2012,** *37* (7), 871-906.
115. Kolb, H. C.; Finn, M. G.; Sharpless, K. B., Click chemistry: Diverse chemical function from a few good reactions. *Angew Chem Int Edit* **2001,** *40* (11), 2004-+.
116. Wang, C.; Wu, J. A.; Xu, Z. K., High-Density Glycosylation of Polymer Membrane Surfaces by Click Chemistry for Carbohydrate-Protein Recognition. *Macromol Rapid Comm* **2010,** *31* (12), 1078-1082.
117. Zhang, S.; Vi, T.; Luo, K.; Koberstein, J. T., Kinetics of Polymer Interfacial Reactions: Polymer Brush Formation by Click Reactions of Alkyne End-Functional Polymers with AzideFunctional Substrates. *Macromolecules* **2016,** *49* (15), 5461-5474.
118. Orski, S. V.; Fries, K. H.; Sheppard, G. R.; Locklin, J., High Density Scaffolding of Functional Polymer Brushes: Surface Initiated Atom Transfer Radical Polymerization of Active Esters. *Langmuir* **2010,** *26* (3), 2136-2143.
119. Arnold, R. M.; Sheppard, G. R.; Locklin, J., Comparative Aminolysis Kinetics of Different Active Ester Polymer Brush Platforms in Postpolymerization Modification with Primary and Aromatic Amines. *Macromolecules* **2012,** *45* (13), 5444-5450.
120. Lokitz, B. S.; Messman, J. M.; Hinestrosa, J. P.; Alonzo, J.; Verduzco, R.; Brown, R. H.; Osa, M.; Ankner, J. F.; Kilbey, S. M., Dilute Solution Properties and Surface Attachment of RAFT Polymerized 2-Vinyl-4,4-dimethyl Azlactone (VDMA). *Macromolecules* **2009,** *42* (22), 9018-9026.
121. Barbey, R.; Klok, H. A., Room Temperature, Aqueous Post-Polymerization Modification of Glycidyl Methacrylate-Containing Polymer Brushes Prepared via Surface-Initiated Atom Transfer Radical Polymerization. *Langmuir* **2010,** *26* (23), 18219-18230.
122. Soto-Cantu, E.; Lokitz, B. S.; Hinestrosa, J. P.; Deodhar, C.; Messman, J. M.; Ankner, J. F.; Kilbey, S. M., Versatility of Alkyne-Modified Poly(Glycidyl Methacrylate) Layers for Click Reactions. *Langmuir* **2011,** *27* (10), 5986-5996.
123. Sun, X. L.; Stabler, C. L.; Cazalis, C. S.; Chaikof, E. L., Carbohydrate and protein immobilization onto solid surfaces by sequential Diels-Alder and azide-alkyne cycloadditions. *Bioconjugate Chem* **2006,** *17* (1), 52-57.
124. Dirlam, P. T.; Strange, G. A.; Orlicki, J. A.; Wetzel, E. D.; Costanzo, P. J., Controlling Surface Energy and Wetability with Diels-Alder Chemistry. *Langmuir* **2010,** *26* (6), 3942-3948.
125. Arumugam, S.; Popik, V. V., Patterned Surface Derivatization Using Diels-Alder Photoclick Reaction. *J Am Chem Soc* **2011,** *133* (39), 15730-15736.

126. Tasdelen, M. A., Diels-Alder "click" reactions: recent applications in polymer and material science. *Polym Chem-Uk* **2011,** *2* (10), 2133-2145.
127. Arumugam, S.; Orski, S. V.; Locklin, J.; Popik, V. V., Photoreactive Polymer Brushes for High-Density Patterned Surface Derivatization Using a Diels-Alder Photoclick Reaction. *J Am Chem Soc* **2012,** *134* (1), 179-182.
128. Pauloehrl, T.; Delaittre, G.; Winkler, V.; Welle, A.; Bruns, M.; Borner, H. G.; Greiner, A. M.; Bastmeyer, M.; Barner-Kowollik, C., Adding Spatial Control to Click Chemistry: Phototriggered Diels-Alder Surface (Bio)functionalization at Ambient Temperature. *Angew Chem Int Edit* **2012,** *51* (4), 1071-1074.
129. Gevrek, T. N.; Bilgic, T.; Klok, H. A.; Sanyal, A., Maleimide-Functionalized Thiol Reactive Copolymer Brushes: Fabrication and Post-Polymerization Modification. *Macromolecules* **2014,** *47* (22), 7842-7851.
130. Dubner, M.; Gevrek, T. N.; Sanyal, A.; Spencer, N. D.; Padeste, C., Fabrication of Thiol-Ene "Clickable" Copolymer-Brush Nanostructures on Polymeric Substrates via Extreme Ultraviolet Interference Lithography. *Acs Appl Mater Inter* **2015,** *7* (21), 11337-11345.
131. Mardyukov, A.; Li, Y.; Dickschat, A.; Schafer, A. H.; Studer, A., Chemical Modification of Polymer Brushes via Nitroxide Photoclick Trapping. *Langmuir* **2013,** *29* (21), 6369-6376.
132. Arumugam, S.; Popik, V. V., Attach, Remove, or Replace: Reversible Surface Functionalization Using Thiol-Quinone Methide Photoclick Chemistry. *J Am Chem Soc* **2012,** *134* (20), 8408-8411.
133. Jonkheijm, P.; Weinrich, D.; Koehn, M.; Engelkamp, H.; Christianen, P. C. M.; Kuhlmann, J.; Maan, J. C.; Nuesse, D.; Schroeder, H.; Wacker, R.; Breinbauer, R.; Niemeyer, C. M.; Waldmann, H., Photochemical surface patterning by the thiol-ene reaction. *Angew Chem Int Edit* **2008,** *47* (23), 4421-4424.
134. Wendeln, C.; Rinnen, S.; Schulz, C.; Arlinghaus, H. F.; Ravoo, B. J., Photochemical Microcontact Printing by Thiol-Ene and Thiol-Yne Click Chemistry. *Langmuir* **2010,** *26* (20), 15966-15971.
135. Cai, T.; Wang, R.; Neoh, K. G.; Kang, E. T., Functional poly(vinylidene fluoride) copolymer membranes via surface-initiated thiol-ene click reactions. *Polym Chem-Uk* **2011,** *2* (8), 1849-1858.
136. Madaan, N.; Terry, A.; Harb, J.; Davis, R. C.; Schlaad, H.; Linford, M. R., Thiol-Ene-Thiol Photofunctionalization of Thiolated Monolayers with Polybutadiene and Functional Thiols, Including Thiolated DNA. *J Phys Chem C* **2011,** *115* (46), 22931-22938.
137. Wang, C.; Ren, P. F.; Huang, X. J.; Wu, J. A.; Xu, Z. K., Surface glycosylation of polymer membrane by thiol-yne click chemistry for affinity adsorption of lectin. *Chem Commun* **2011,** *47* (13), 3930-3932.
138. Gadwal, I.; Rao, J. Y.; Baettig, J.; Khan, A., Functionalized Molecular Bottlebrushes. *Macromolecules* **2014,** *47* (1), 35-40.
139. Rosen, B. M.; Lligadas, G.; Hahn, C.; Percec, V., Synthesis of Dendrimers Through Divergent Iterative Thio-Bromo "Click" Chemistry. *J Polym Sci Pol Chem* **2009,** *47* (15), 3931-3939.

140. Rosen, B. M.; Lligadas, G.; Hahn, C.; Percec, V., Synthesis of Dendritic Macromolecules Through Divergent Iterative Thio-Bromo "Click" Chemistry and SET-LRP. *J Polym Sci Pol Chem* **2009,** *47* (15), 3940-3948.
141. Xu, J. T.; Tao, L.; Boyer, C.; Lowe, A. B.; Davis, T. P., Combining Thio-Bromo "Click" Chemistry and RAFT Polymerization: A Powerful Tool for Preparing Functionalized Multiblock and Hyperbranched Polymers. *Macromolecules* **2010,** *43* (1), 20-24.
142. Chapman, P.; Ducker, R. E.; Hurley, C. R.; Hobbs, J. K.; Leggett, G. J., Fabrication of Two-Component, Brush-on-Brush Topographical Microstructures by Combination of Atom-Transfer Radical Polymerization with Polymer End-Functionalization and Photopatterning. *Langmuir* **2015,** *31* (21), 5935-5944.
143. Rahane, S. B.; Hensarling, R. M.; Sparks, B. J.; Stafford, C. M.; Patton, D. L., Synthesis of multifunctional polymer brush surfaces via sequential and orthogonal thiol-click reactions. *J Mater Chem* **2012,** *22* (3), 932-943.
144. Arnold, R. M.; Huddleston, N. E.; Locklin, J., Utilizing click chemistry to design functional interfaces through post-polymerization modification. *Journal of Materials Chemistry* **2012,** *22* (37), 19357-19365.
145. Brooks, K.; Yatvin, J.; McNitt, C. D.; Reese, R. A.; Jung, C.; Popik, V. V.; Locklin, J., Multifunctional Surface Manipulation Using Orthogonal Click Chemistry. *Langmuir* **2016,** *32* (26), 6600-6605.
146. Arnold, R. M.; Locklin, J., Self-Sorting Click Reactions That Generate Spatially Controlled Chemical Functionality on Surfaces. *Langmuir* **2013,** *29* (19), 5920-5926.
147. Brooks, K.; Razavi, M. J.; Wang, X.; Locklin, J., Nanoscale Surface Creasing Induced by Post-polymerization Modificatio. *ACS Nano* **2015,** *9* (11), 10961–10969.
148. Orski, S. V.; Sheppard, G. R.; Arumugam, S.; Arnold, R. M.; Popik, V. V.; Locklin, J., Rate Determination of Azide Click Reactions onto Alkyne Polymer Brush Scaffolds: A Comparison of Conventional and Catalyst-Free Cycloadditions for Tunable Surface Modification. *Langmuir* **2012,** *28* (41), 14693-14702.
149. Schuh, C.; Rühe, J., Penetration of Polymer Brushes by Chemical Nonidentical Free Polymers. *Macromolecules* **2011,** *44* (9), 3502-3510.
150. Alswieleh, A. M.; Cheng, N.; Leggett, G. J.; Armes, S. P., Spatial control over cross-linking dictates the pH-responsive behavior of poly(2-(tert-butylamino)ethyl methacrylate) brushes. *Langmuir* **2014,** *30* (5), 1391-400.
151. Chen, D.; Yoon, J.; Chandra, D.; Crosby, A. J.; Hayward, R. C., Stimuli-responsive buckling mechanics of polymer films. *Journal of Polymer Science Part B: Polymer Physics* **2014,** *52* (22), 1441-1461.
152. Genzer, J.; Groenewold, J., Soft matter with hard skin: From skin wrinkles to templating and material characterization. *Soft Matter* **2006,** *2* (4), 310-323.
153. Chan, E. P.; Smith, E. J.; Hayward, R. C.; Crosby, A. J., Surface wrinkles for smart adhesion. *Advanced Materials* **2008,** *20* (4), 711-+.
154. Davis, C. S.; Crosby, A. J., Mechanics of wrinkled surface adhesion. *Soft Matter* **2011,** *7* (11), 5373-5381.
155. Davis, C. S.; Martina, D.; Creton, C.; Lindner, A.; Crosby, A. J., Enhanced Adhesion of Elastic Materials to Small-Scale Wrinkles. *Langmuir* **2012,** *28* (42), 14899-14908.

156. Jeong, H. E.; Kwak, M. K.; Suh, K. Y., Stretchable, Adhesion-Tunable Dry Adhesive by Surface Wrinkling. *Langmuir* **2010,** *26* (4), 2223-2226.
157. Li, Y. Y.; Dai, S. X.; John, J.; Carter, K. R., Superhydrophobic Surfaces from Hierarchically Structured Wrinkled Polymers. *Acs Appl Mater Inter* **2013,** *5* (21), 11066-11073.
158. Zhang, Z. Q.; Zhang, T.; Zhang, Y. W.; Kim, K. S.; Gao, H. J., Strain-Controlled Switching of Hierarchically Wrinkled Surfaces between Superhydrophobicity and Superhydrophilicity. *Langmuir* **2012,** *28* (5), 2753-2760.
159. Efimenko, K.; Finlay, J.; Callow, M. E.; Callow, J. A.; Genzer, J., Development and Testing of Hierarchically Wrinkled Coatings for Marine Antifouling. *Acs Appl Mater Inter* **2009,** *1* (5), 1031-1040.
160. Hoipkemeier-Wilson, L.; Schumacher, J. F.; Carman, M. L.; Gibson, A. L.; Feinberg, A. W.; Callow, M. E.; Finlay, J. A.; Callow, J. A.; Brennan, A. B., Antifouling Potential of Lubricious, Micro-engineered, PDMS Elastomers against Zoospores of the Green Fouling Alga Ulva (Enteromorpha). *Biofouling* **2004,** *20* (1), 53-63.
161. Muller, M.; Karg, M.; Fortini, A.; Hellweg, T.; Fery, A., Wrinkle-assisted linear assembly of hard-core/soft-shell particles: impact of the soft shell on the local structure. *Nanoscale* **2012,** *4* (7), 2491-2499.
162. Efimenko, K.; Rackaitis, M.; Manias, E.; Vaziri, A.; Mahadevan, L.; Genzer, J., Nested self-similar wrinkling patterns in skins. *Nat Mater* **2005,** *4* (4), 293-297.
163. Guvendiren, M.; Burdick, J. A., The control of stem cell morphology and differentiation by hydrogel surface wrinkles. *Biomaterials* **2010,** *31* (25), 6511-6518.
164. Gao, N.; Zhang, X.; Liao, S.; Jia, H.; Wang, Y., Polymer Swelling Induced Conductive Wrinkles for an Ultrasensitive Pressure Sensor. *ACS Macro Letters* **2016**, 823-827.
165. Wagner, S.; Lacour, S. P.; Jones, J.; Hsu, P. H. I.; Sturm, J. C.; Li, T.; Suo, Z. G., Electronic skin: architecture and components. *Physica E* **2004,** *25* (2-3), 326-334.
166. Khang, D. Y.; Jiang, H. Q.; Huang, Y.; Rogers, J. A., A stretchable form of single-crystal silicon for high-performance electronics on rubber substrates. *Science* **2006,** *311* (5758), 208-212.
167. Watanabe, M.; Shirai, H.; Hirai, T., Wrinkled polypyrrole electrode for electroactive polymer actuators. *J Appl Phys* **2002,** *92* (8), 4631-4637.
168. Lacour, S. P.; Wagner, S.; Huang, Z. Y.; Suo, Z., Stretchable gold conductors on elastomeric substrates. *Appl Phys Lett* **2003,** *82* (15), 2404-2406.
169. Rodríguez-Hernández, J., Wrinkled interfaces: Taking advantage of surface instabilities to pattern polymer surfaces. *Progress in Polymer Science* **2015,** *42*, 1-41.
170. Yang, S.; Khare, K.; Lin, P.-C., Harnessing Surface Wrinkle Patterns in Soft Matter. *Advanced Functional Materials* **2010,** *20* (16), 2550-2564.
171. Chan, E. P.; Crosby, A. J., Fabricating microlens arrays by surface wrinkling. *Advanced Materials* **2006,** *18* (24), 3238-+.
172. Bowden, N.; Brittain, S.; Evans, A. G.; Hutchinson, J. W.; Whitesides, G. M., Spontaneous formation of ordered structures in thin films of metals supported on an elastomeric polymer. *Nature* **1998,** *393* (6681), 146-149.
173. Harrison, C.; Stafford, C. M.; Zhang, W.; Karim, A., Sinusoidal phase grating created by a tunably buckled surface. *Appl Phys Lett* **2004,** *85* (18), 4016-4018.

174. Meitl, M. A.; Zhu, Z. T.; Kumar, V.; Lee, K. J.; Feng, X.; Huang, Y. Y.; Adesida, I.; Nuzzo, R. G.; Rogers, J. A., Transfer printing by kinetic control of adhesion to an elastomeric stamp. *Nat Mater* **2006,** *5* (1), 33-38.
175. Pretzl, M.; Schweikart, A.; Hanske, C.; Chiche, A.; Zettl, U.; Horn, A.; Boker, A.; Fery, A., A Lithography-Free Pathway for Chemical Microstructuring of Macromolecules from Aqueous Solution Based on Wrinkling. *Langmuir* **2008,** *24* (22), 12748-12753.
176. Khare, K.; Zhou, J. H.; Yang, S., Tunable Open-Channel Microfluidics on Soft Poly(dimethylsiloxane) (PDMS) Substrates with Sinusoidal Grooves. *Langmuir* **2009,** *25* (21), 12794-12799.
177. Stafford, C. M.; Harrison, C.; Beers, K. L.; Karim, A.; Amis, E. J.; Vanlandingham, M. R.; Kim, H. C.; Volksen, W.; Miller, R. D.; Simonyi, E. E., A buckling-based metrology for measuring the elastic moduli of polymeric thin films. *Nat Mater* **2004,** *3* (8), 545-550.
178. Stafford, C. M.; Vogt, B. D.; Harrison, C.; Julthongpiput, D.; Huang, R., Elastic moduli of ultrathin amorphous polymer films. *Macromolecules* **2006,** *39* (15), 5095-5099.
179. Chung, J. Y.; Nolte, A. J.; Stafford, C. M., Surface Wrinkling: A Versatile Platform for Measuring Thin-Film Properties. *Advanced Materials* **2011,** *23* (3), 349-368.
180. Chung, J. Y.; Chastek, T. Q.; Fasolka, M. J.; Ro, H. W.; Stafford, C. M., Quantifying Residual Stress in Nanoscale Thin Polymer Films via Surface Wrinkling. *Acs Nano* **2009,** *3* (4), 844-852.
181. Chan, E. P.; Kundu, S.; Lin, Q. H.; Stafford, C. M., Quantifying the Stress Relaxation Modulus of Polymer Thin Films via Thermal Wrinkling. *Acs Appl Mater Inter* **2011,** *3* (2), 331-338.
182. Wu, Z. G.; Bouklas, N.; Huang, R., Swell-induced surface instability of hydrogel layers with material properties varying in thickness direction. *Int J Solids Struct* **2013,** *50* (3-4), 578-587.
183. Cerda, E.; Mahadevan, L., Geometry and physics of wrinkling. *Phys Rev Lett* **2003,** *90* (7), 074302.
184. Bowden, N.; Huck, W. T. S.; Paul, K. E.; Whitesides, G. M., The controlled formation of ordered, sinusoidal structures by plasma oxidation of an elastomeric polymer. *Appl Phys Lett* **1999,** *75* (17), 2557.
185. Chandra, D.; Crosby, A. J., Self-wrinkling of UV-cured polymer films. *Adv Mater* **2011,** *23* (30), 3441-5.
186. Guvendiren, M.; Burdick, J. A.; Yang, S., Solvent induced transition from wrinkles to creases in thin film gels with depth-wise crosslinking gradients. *Soft Matter* **2010,** *6* (22), 5795.
187. Singamaneni, S.; McConney, M. E.; Tsukruk, V. V., Spontaneous self-folding in confined ultrathin polymer gels. *Adv Mater* **2010,** *22* (11), 1263-8.
188. Kappe, C. O., Controlled microwave heating in modern organic synthesis. *Angew. Chem. Int. Ed.* **2004,** *43* (46), 6250-6284.
189. Ebner, C.; Bodner, T.; Stelzer, F.; Wiesbrock, F., One decade of microwave-assisted polymerizations: Quo vadis? *Macromolecular Rapid Comm.* **2011,** *32* (3), 254-288.

190. Hoogenboom, R.; Schubert, U. S., Microwave-assisted polymer synthesis: Recent developments in a rapidly expanding field of research. *Macromol. Rapid Commun.* **2007,** *28* (4), 368-386.
191. Kempe, K.; Becer, C.; Schubert, U., Microwave-Assisted Polymerizations: Recent Status and Future Perspectives. *Macromolecules* **2011,** *44* (15), 5825-5842.
192. Zhu, J.; Zhu, X.; Zhang, Z.; Cheng, Z., Reversible addition–fragmentation chain transfer polymerization of styrene under microwave irradiation. *J. Polym. Sci., Part A: Polym. Chem.* **2006,** *44* (23), 6810-6816.
193. Brown, S. L.; Rayner, C. M.; Perrier, S., Microwave-Accelerated RAFT Polymerization of Polar Monomers. *Macromol. Rapid Commun.* **2007,** *28* (4), 478-483.
194. Brown, S. L.; Rayner, C. M.; Graham, S.; Cooper, A.; Rannard, S.; Perrier, S., Ultra-fast microwave enhanced reversible addition-fragmentation chain transfer (RAFT) polymerization: monomers to polymers in minutes. *Chem. Commun.* **2007,** (21), 2145-2147.
195. Roy, D.; Sumerlin, B. S., Block copolymerization of vinyl ester monomers via RAFT/MADIX under microwave irradiation. *Polymer* **2011,** *52* (14), 3038-3045.
196. Roy, D.; Ullah, A.; Sumerlin, B. S., Rapid Block Copolymer Synthesis by Microwave-Assisted RAFT Polymerization. *Macromolecules* **2009,** *42* (20), 7701-7708.
197. Chen, G.; Zhu, X.; Cheng, Z.; Lu, J.; Chen, J., Controlled/'living' radical polymerization of methyl methacrylate with p-TsCl/CuBr/BPY initiating system under microwave irradiation. *Polym. Int.* **2004,** *53* (4), 357-363.
198. Zhang, H.; Schubert, U. S., Monomode Microwave-Assisted Atom Transfer Radical Polymerization. *Macromol. Rapid Commun.* **2004,** *25* (13), 1225-1230.
199. Kwak, Y.; Mathers, R. T.; Matyjaszewski, K., Critical Evaluation of the Microwave Effect on Radical (Co)Polymerizations. *Macromol Rapid Comm* **2012,** *33* (1), 80-86.
200. Boukherroub, R.; Petit, A.; Loupy, A.; Chazalviel, J.-N.; Ozanam, F., Microwave-Assisted Chemical Functionalization of Hydrogen-Terminated Porous Silicon Surfaces. *J. Phys. Chem. B* **2003,** *107* (48), 13459-13462.
201. Liu, X.; Han, H.-M.; Liu, H.-B.; Xiao, S. J., Enhanced protein loading on a planar Si(111)–H surface with second generation NTA. *Surface Sci.* **2010,** *604* (15-16), 1315-1319.
202. Petit, A.; Delmotte, M.; Loupy, A.; Chazalviel, J.; Ozanam, F.; Boukherroub, R., Microwave Effects on Chemical Functionalization of Hydrogen-Terminated Porous Silicon Nanostructures. *J. Phys. Chem. C* **2008,** *112* (42), 16622-16628.
203. Haensch, C.; Erdmenger, T.; Fijten, M.; Hoeppener, S.; Schubert, U. S., Fast Surface Modification by Microwave Assisted Click Reactions on Silicon Substrates. *Langmuir* **2009,** *25* (14), 8019-8024.
204. Liu, X.; Zheng, H. N.; Ma, Y. Z.; Yan, Q.; Xiao, S. J., Microwave irradiated click reactions on silicon surfaces via derivertization of covalently grafted poly(PEGMA) brushes. *J. Colloid Interf. Sci.* **2011,** *358* (1), 116-122.
205. Jhaveri, S. B.; Carter, K., Disubstituted polyacetylene brushes grown via surface-directed tungsten-catalyzed polymerization. *Langmuir* **2007,** *23* (16), 8288-8290.
206. Jhaveri, S.; Peterson, J.; Carter, K., Poly(9,9-dihexylfluorene) layers grown via surface-directed Ni(0) condensation polymerization. *Langmuir* **2009,** *25* (16), 9552-9556.

207. Ofir, Y.; Moran, I. W.; Subramani, C.; Carter, K. R.; Rotello, V. M., Nanoimprint lithography for functional three-dimensional patterns. *Adv. Mater.* **2010,** *22* (32), 3608-3614.
208. Barbey, R.; Lavanant, L.; Paripovic, D.; Schüwer, N.; Sugnaux, C.; Tugulu, S.; Klok, H.-A., Polymer Brushes via Surface-Initiated Controlled Radical Polymerization: Synthesis, Characterization, Properties, and Applications. *Chem. Rev.* **2009,** *109* (11), 5437-5527.
209. Ayres, N., Polymer brushes: Applications in biomaterials and nanotechnology. *Polym. Chem.* **2010,** *1* (6), 769-777.
210. Patton, D. L.; Page, K. A.; Xu, C.; Genson, K. L.; Fasolka, M. J.; Beers, K. L., Measurement of reactivity ratios in surface-initiated radical copolymerization. *Macromolecules* **2007,** *40* (17), 6017-6020.
211. Thompson, K.; Booske, J.; Gianchandani, Y.; Cooper, R., Electromagnetic annealing for the 100 nm technology node. *IEEE Elec. Dev. Lett.* **2002,** *23* (3), 127-129.
212. Murata, H.; Prucker, O.; Rühe, J., Synthesis of Functionalized Polymer Monolayers from Active Ester Brushes. *Macromolecules* **2007,** *40* (15), 5497-5503.

CHAPTER II - RAPID SYNTHESIS OF POLYMER BRUSH SURFACES VIA MICROWAVE ASSISTED SURFACE-INITIATED RADICAL POLYMERIZATION

2.1 Introduction

The use of microwave irradiation for the rapid and highly efficient synthesis of organic and inorganic materials has attracted considerable attention in recent years[1]. Improved yields, reduced reaction times, and decreased side reactions are just a few of the salient features of microwave-assisted small molecule synthesis in comparison with conventional heating. These features have also resulted in a growing interest in microwave-assisted polymerizations of all mechanistic types including step-growth, ring-opening and conventional/controlled radical polymerizations[2-4]. Significant enhancements in polymerization rate and/or polydispersity have been reported in some polymerizations[5-9], whereas in others no appreciable acceleration was observed[10-11] highlighting the complex interplay between experimental parameters (e.g. temperature and polarity) and microwave equipment. A recent report from Kwak et al.[12] showed that with more precise temperature control during microwave-assisted conventional radical polymerizations, minimal effects of microwave irradiation on polymerization rate, initiator decomposition, and comonomer reactivity could be observed. Irrespective of the driving force for reaction enhancements (e.g. actual versus apparent temperature or "microwave effect"), microwave-assisted polymerization has been demonstrated as a viable approach for the rapid synthesis of a variety of polymeric materials, including the preparation of block copolymers[8-9].

Microwave-assisted surface reactions, on the other hand, have received much less attention. The relatively few examples reported in literature include hydrosilylation of

silicon hydride surfaces[13-15] and copper-catalyzed 1,3-dipolar cycloaddition of alkynes with azide-modified surfaces (or vice versa) [16-17]. To our knowledge, the only examples of microwave-assisted surface-initiated polymerization (μW-SIP) were provided by Carter and coworkers[18-19] for the preparation of conjugated polymer-modified surfaces; however, in these initial reports, no comparison was made with surface-initiated polymerization (SIP) via conventional heating. More recently, Carter's group reported μW-SIP of polyfluorene grafted surfaces with dramatic decreases in reaction time under microwave irradiation at 163 °C in comparison with conventional SIP; however, these improvements were in comparison with conventional heating (80 °C) at less than half the microwave reaction temperature[20]. Regardless, these examples demonstrate the potential utility of μW-SIP as an efficient route to synthesize functional polymer thin films and justify a continued exploration of this approach.

To date, we are unaware of any reported examples of the synthesis of polymer brush surfaces via radical-mediated μW-SIP. Radical-mediated SIP is one of the most effective and versatile methods for tailoring the physicochemical properties of surfaces[21-22]. Despite the advantageous characteristics of polymer brush surfaces, the radical-mediated SIP process can often be time-consuming and require large quantities/high concentration of monomer to completely submerge the substrate and achieve acceptable reaction rates. Hence, any process that can significantly reduce the reaction time and/or monomer concentration required for SIP would be beneficial in the preparation of polymer brush surfaces. Herein, we demonstrate the use of microwave-assisted surface-initiated radical polymerization for the rapid synthesis of polymer brush surfaces on two-dimensional substrates. μW-SIP is carried out at constant temperature and microwave

power allowing comparison with conventional SIP carried out in an oil bath at the same effective solution temperature. We show μW-SIP enables significant enhancements in brush thickness at reduced reaction times for a range of monomer types (i.e. acrylamides, acrylates, methacrylates, and styrene). The effects of reaction time, monomer concentration, and microwave power on film thickness are explored.

2.2 Experimental Section

2.2.1 Materials

All reagents and solvents were obtained at the highest purity available from Aldrich Chemical Company or Fisher Scientific and used without further purification unless otherwise specified. All monomers were purified by passing through a short column of activated alumina to remove inhibitor prior to use. After purification, monomers were stored at -20 °C and warmed to room temperature directly before use. The asymmetric trichlorosilyl-functionalized azo initiator was prepared according to a previously reported protocol.[23] Silicon wafers were purchased from University Wafer and glass slides (75 mm × 25 mm × 1 mm) were purchased from Fisher Scientific.

2.2.2 Instrumentation and Characterization

Ellipsometry measurements were carried out using a Gartner Scientific Corporation LSE ellipsometer with a 632.8 nm laser at 70° from the normal. The following refractive indices were used for thickness calculations: 3.89 for silicon, 1.46 for silicon oxide, 1.43 for initiator, 1.44 for N,N'-dimethylacrylamide (DMA), 1.45 for 2-hydroxylethyl acrylate (HEA), 1.44 for 2-(dimethylamino)ethyl methacrylate (DMAEMA), 1.49 for methyl methacrylate (MMA), and 1.59 for styrene (Sty). Grazing angle attenuated total reflection FTIR (gATR-FTIR) analysis was carried out using a

ThermoScientific FTIR instrument (Nicolet 8700) equipped with a VariGATR™ accessory (grazing angle 65°, germanium crystal; Harrick Scientific). Spectra were collected with a resolution of 4 cm^{-1} by accumulating a minimum of 128 scans per sample. All spectra were collected while purging the VariGATR™ attachment and FTIR instrument with N_2 gas along the infrared beam path to minimize the peaks corresponding to atmospheric moisture and CO_2. Spectra were analyzed and processed using Omnic software. A Varian Mercury Plus 200MHz NMR spectrometer operating at a frequency of 200.13 MHz with VNMR 6.1C software was used for proton analysis. Atomic force microscopy was performed using a Bruker Icon in contact mode to measure film thickness on glass substrates. A small scratch was made on the film in order to use the bare glass or silicon substrate as a reference height. The samples were scanned with SNL-10 silicon nitride probes (Bruker AFM Probes) with a spring constant of 0.24 – 0.35 N/m.

2.2.3 Functionalization of Silicon Wafer

Silicon and glass wafers were cut into appropriate sized pieces (12 mm × 10 mm) and subsequently sonicated twice for 5 min each in DI water, acetone, and ethanol. Wafers were then dried under a stream of N_2 and exposed to UV-ozone for 45 min. The substrates were stored in a 120 °C oven before functionalization. Substrates (two wafers oriented back-to-back, polished side out) were transferred into dry, septum-sealed test tubes containing a toluene solution of AIBN-trichlorosilane (4 mmol, 13 mL) and triethylamine (0.2 mL). Substrates were allowed to react for 45 min and were then rinsed and sonicated in toluene and dried under a stream of N_2. If not used immediately, initiator substrates were stored in the dark at -20 °C in toluene. The average initiator thickness

was 4.9 nm which indicates the formation of a multilayer. The thickness of the initiator was found to have minimal effect on the observed brush growth.

2.2.4 Microwave-Assisted Surface-Initiated Polymerization

All μW-SIP reactions were carried out in a mono-mode microwave reactor (CEM Corporation Discover S-Class) with a calibrated infrared temperature sensor in constant power mode with simultaneous cooling to maintain the desired temperature. In some cases (particularly for polar solvents and monomers), it was necessary to pass the cooling gas through coiled copper tubing immersed in an ice bath to adequately control the temperature of the reaction. The apparent solution temperature measured outside the reaction vial was compared with the actual solution temperature inside the vial using a thermocouple inserted through the rubber septum of the sealed vial. Microwave irradiation had to be paused to get a stable temperature reading from the metal thermocouple. Monomers investigated include N, N-dimethylacrylamide (DMA), 2-hydroxyethyl acrylate (HEA), 2-(dimethylamino)ethyl methacrylate (DMAEMA), methyl methacrylate (MMA) and styrene (Sty). All reactions were carried out in benzene with the exception of HEA, which was carried out in water. All surface-initiated polymerizations under both microwave and conventional heating were carried out in 10 mL microwave vials provided by CEM. The reaction volume was kept constant at 1.2 mL, which was sufficient to completely immerse the substrates in the monomer solution, for both microwave and conventional heating conditions. After adding the monomer solution and initiator-coated substrate in the CEM microwave vial the polymerization container was capped and sealed. The monomer solution was then degassed by purging N_2 for 20 min before placed in the microwave synthesis unit. Upon exposing to the

microwave radiation, the temperature increases. The approximate ramp time to reach the temperature set point varied between 30 – 90 s depending on the polarity of the reaction mixture. Reaction times reported do not include the initial ramp time. After radiation, the CEM reaction vial was cooled down to room temperature by the cooling gas before it was removed from the microwave synthesis unit. The sample substrate was taken out of the polymerization solution and was extensively sonicated and rinsed in a good solvent to remove any physically absorbed polymer from the surface followed by drying with nitrogen. This washing process was continued until no change in brush thickness could be measured by an ellipsometer.

2.2.5 Microwave-Assisted Surface-Initiated Polymerization Conditions for DMA

For DMA, thickness versus concentration plot was obtained by doing polymerization in N_2 purged DMA/benzene solutions with the concentration of 0.81 mol/L, 1.62 mol/L, 3.23 mol/L, 4.85 mol/L, and 6.47 mol/L at 65 °C for 10 min with radiation power set at 50 W. Thickness versus reaction time plot was obtained by performing polymerization in degassed DMA/benzene solution (4.85 mol/L) and irradiating at 50 W at 65 °C for 2 min, 10 min and 20 min. Thickness versus power plot was collected in degassed DMA/benzene solution (4.85 mol/L) and then irradiating at 50 W, 100 W, 150 W and 200 W at 65 °C for 10 min.

2.2.6 Microwave-Assisted Surface-Initiated Polymerization Conditions for DMAEMA

For DMAEMA, thickness versus concentration plot was obtained polymerizing in N_2 purged DMAEMA/benzene solutions with the concentration of 1.19 mol/L, 2.98 mol/L, 4.75 mol/L, and 5.93 mol/L at 65 °C for 10 min with radiation power set at 50 W.

Thickness versus reaction time plot was similarly obtained by immersing the substrates in degassed DMAEMA/benzene solution (2.98 mol/L) and irradiating at 50 W at 65 °C for 2 min, 10 min and 20 min. Thickness versus power plot was obtained by doing polymerization in degassed DMAEMA/benzene solution (2.98 mol/L) and then irradiating at 50 W, 100 W, 150 W and 250 W at 65 °C for 10 min.

2.2.7 Microwave-Assisted Surface-Initiated Polymerization Conditions for HEA

For HEA, thickness versus concentration plot was obtained by polymerizing in N_2 purged HEA/H_2O solutions with the concentration of 0.013 mol/L, 0.033 mol/L, 0.066 mol/L and 0.100 mol/L at 65 °C for 10 min with radiation power set at 25 W. Thickness versus reaction time plot was similarly obtained by polymerization using degassed HEA/H2O solution (0.066 mol/L) and irradiating at 10 W at 65 °C for 2 min, 6 min, 10 min, 13 min and 16 min. Thickness versus power plot was obtained by immersing the substrates in degassed HEA/H_2O solution (0.066 mol/L) and then irradiating at 10 W, 15 W, 20 W and 25 W at 65 °C for 10 min.

2.2.8 Conventional Surface-Initiated Polymerization in an Oil Bath

Conventional SIP using an oil bath was carried out in the same type of CEM microwave vials. In a typical polymerization, an initiator-coated substrate and 1.2 ml of monomer solution were added into the reaction vessel which was then capped and sealed. The monomer solution was then purged with N_2 for 20 min before heating at 70 °C for 10 min. The reaction vial was then removed from the oil bath and quickly cooled down to room temperature before the sample was taken out. The samples were thoroughly rinsed and sonicated in a good solvent followed by drying using nitrogen.

2.3 Results and Discussion

2.3.1 Synthesis of Polymer Brush Surfaces

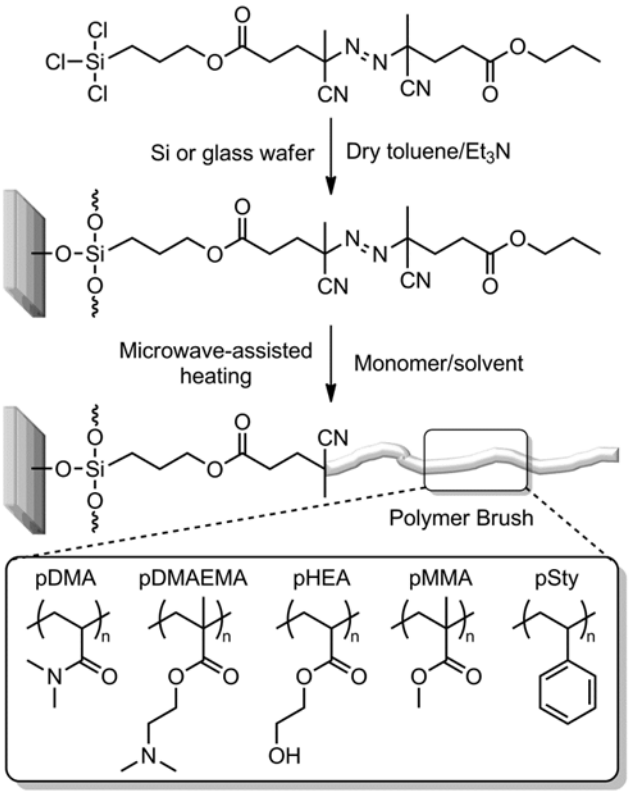

Scheme 2.1 Synthetic scheme for microwave-assisted surface-initiated radical polymerization.

The synthetic strategy for μW-SIP is shown in Scheme 2.1. Conventional free radical polymerization was employed because it is a simple, flexible, and well-studied route to polymer brush surfaces. First, an asymmetric trichlorosilyl-functionalized azo initiator was attached to the hydroxylated surface of a glass or silicon substrate. The average ellipsometric thickness of the initiator layer (4.9 nm) indicated the formation of a multilayer film structure. The initiator functionalized substrates were immersed into a septum-sealed glass vial containing 1.2 mL of monomer solution, and then the solution was purged with nitrogen for 20 min. Surface-initiated polymerizations were conducted

under constant microwave power with simultaneous cooling to maintain the desired reaction temperature (65 °C unless otherwise stated), and for comparative purposes, under conventional heating using a standard oil bath. For μW-SIP reactions, the temperature of the reaction mixture was monitored beneath the reaction vial with an IR sensor within the microwave instrument, as well as inside the reaction vial with a thermocouple inserted through the septum. The actual reaction temperature inside was consistently 5 – 6 °C higher than that measured by the IR sensor; thus, the conventional oil bath was set at 70 °C. Table 2.1 shows the comparison of brush thickness on silicon wafers obtained from μW-SIP and conventional SIP for five monomers (styrene, MMA, DMAEMA, HEA, and DMA) at the same effective solution temperature, monomer concentration, and reaction time. All polymerizations were carried out in benzene with the exception for HEA, which was conducted in water. After polymerization and rinsing the obtained samples with polymer brush on the surface were characterized using gATR-FTIR to confirm the chemical composition. In each case, gATR-FTIR of the polymer brush surfaces showed the expected spectrum indicating no detrimental effects resulted from the microwave irradiation as shown in Figure 2.1.

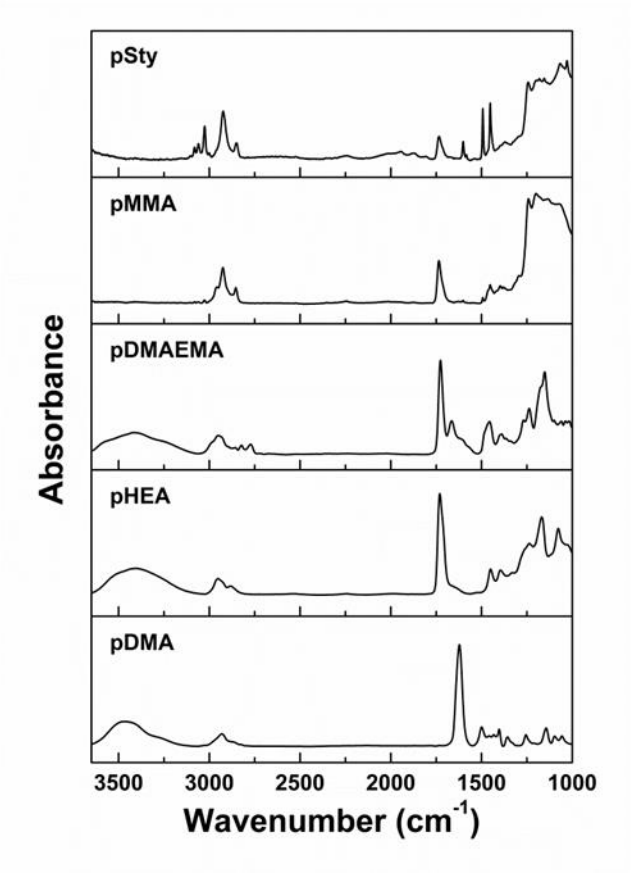

Figure 2.1 gATR-FTIR spectra of polymer brushes synthesized via μW-SIP on SiO_x substrates.

2.3.2 Enhanced Polymer Brush Thickness via Microwave Mediated SIP

The polymer brush thickness values were calculated using a multi-layer model based on Δ and Ψ values which were measured using ellipsometer. The thickness of polymer brush samples synthesized using both microwave radiation (μW-SIP) and SIP under conventional heating conditions are summarized in Table 2.1 and shown in Figure 2.2. μW-SIP yielded a significant enhancement in brush thickness, as compared with conventional SIP, for all monomers investigated in this study. For example, conventional SIP of DMA (4.85 mol/L in benzene, 70 °C) yielded a film thickness of only 2.1 nm after 10 min, whereas μW-SIP of DMA (4.85 mol/L in benzene, 50 W, 65 °C) yielded a film

thickness of 189.5 nm after 10 min; this represents a 90-fold enhancement in film thickness. Similar results were obtained for polar monomers DMAEMA and HEA, which showed a 16-fold and a 3-fold increase in film thickness, respectively, under μW-SIP conditions. More surprisingly, non-polar monomers, which interact to a lesser extent with microwave radiation, also exhibited a significant enhancement in film growth rates under μW-SIP. As shown in Figure 2.2, styrene and MMA showed essentially no film growth after 10 min of conventional SIP (Sty, 1.0 nm; MMA, 0.5 nm), yet showed a 39-fold (38.9 nm) and a 49-fold (24.5 nm) increase, respectively, in film thickness after 10 min of μW-SIP.

Table 2.1

Comparison of Polymer Brush Thickness Obtained From μW-SIP and Conventional SIP

Monomer	Concentration (mol/L)	Power (W)	[a]μW-SIP, 65 °C Thickness (nm)	Conventional SIP, 70 °C Thickness (nm)
Sty	4.36	50	38.9	1.0
MMA	4.69	50	24.5	0.5
HEA	0.066	10	78.4	25.9
DMAEMA	2.98	50	76.9	4.9
DMA	4.85	50	189.5	2.1

[a]Temperature recorded by IR sensor; the actual temperature inside the vial was 5 – 6 °C higher when measured using a thermocouple and digital thermometer.

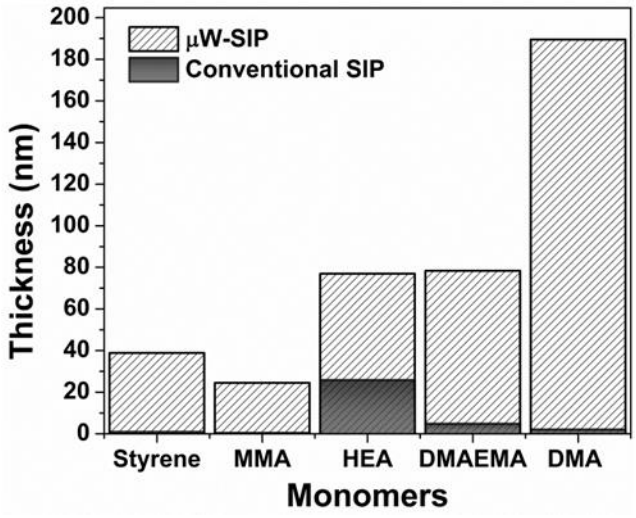

Figure 2.2 Comparison of brush thickness synthesized by μW-SIP and conventional SIP. at the same effective solution temperature, reaction time, and concentration as indicated.

Styrene (4.36 mol/L in benzene, 50 W, 65 °C, 10 min); MMA (4.69 mol/L in benzene, 50 W, 65 °C, 10 min); HEA (0.066 mol/L in water, 10 W, 65 °C, 10 min); DMAEMA (2.98 mol/L in benzene, 50 W, 65 °C, 10 min); DMA (4.85 mol/L in benzene, 65 °C, 10 min). The temperature for conventional SIP was set at 70 °C for each monomer system.

Presently, there is much debate over the origin of reaction enhancements under microwave irradiation, e.g. a specific microwave effect, more efficient heating, or simply differences in the actual and apparent reaction temperatures as recently demonstrated by Kwak and coworkers.[12] Although we have identified the difference between the actual and apparent temperatures of the bulk solutions, we are unable to directly measure the temperature at the silicon surface, thus the latter of the three origins remains a possible cause of the observed SIP reaction enhancements. Doped silicon is known to efficiently absorb microwave energy and heat rapidly.[15, 24] Heat transfer through the doped silicon could result in a temperature gradient at the SIP reaction interface, and if present, would be expected to influence the overall film growth rate by altering the rate of decomposition of surface-bound initiator and/or the rate of propagation. Since neither the interfacial temperature, initiator decomposition rate nor propagation rate can feasibly be measured

for SIP, we performed parallel μW-SIP reactions on doped silicon wafers and microwave transparent glass substrates. Glass slides were cut into small sized pieces (12 mm x 10 mm) followed with a thorough cleaning and were functionalized with azo-initiator. Azo-initiator functionalized glass substrates were then placed back-to-back with initiator-functionalized silicon substrates in the same reaction tube, such that the two substrates experienced identical reaction conditions. Upon the completion of polymerization and cleaning the sample surface were scratched using a blade in such a way that polymers of the scratched surface regions of the surface to be totally removed while the underneath hard substrate remained intact. The scratched samples were characterized using contact mode atomic force microscope (AFM) to measure the height different of the scratched region and neighboring unscratched region. The height difference represents the total film thickness of the sample, i.e. the thickness of initiator and polymer. The thickness of silicon substrates was also measured using ellipsometer and the results are summarized in Table 2.2. μW-SIP of pDMA and pHEA yielded essentially the same film thickness on silicon and glass substrates: pDMA – Si 163 nm, glass 169 nm as shown in Figure 2.3; pHEA – Si 33 nm, glass 36 nm as shown in Figure 2.4, whereas film thickness for pDMAEMA was approximately 15 nm higher on silicon: Si 49 nm, glass 34 nm as shown in Figure 2.5. This comparison should be considered qualitative since it is assumed that the AIBN initiator layer has the same thickness and grafting density on glass as it is on a silicon wafer. Silicon and glass wafers were modified with initiator using the same procedure; however the two types of substrates have different surface hydroxyl content (and thus initiator grafting density), and the accurate thickness measurement of AIBN initiator on glass could not be obtained. Although this is not a direct comparison, these

results warrant additional experiments to further explore the selective heating of the silicon substrate and its possible contribution to the observed reaction enhancements. Regardless of the origin, the enhancements of μW-SIP compared to conventional SIP are readily apparent for each monomer system evaluated in this study.

Table 2.2

AFM Thickness of Scratched Polymer Brush Films

Monomer	Glass AFM Thickness (nm)	Silicon AFM Thickness (nm)	Ellipsometry Thickness (nm)
DMA	169	163	171.0
HEA	36	33	33.8
DMAEMA	34	49	56.2

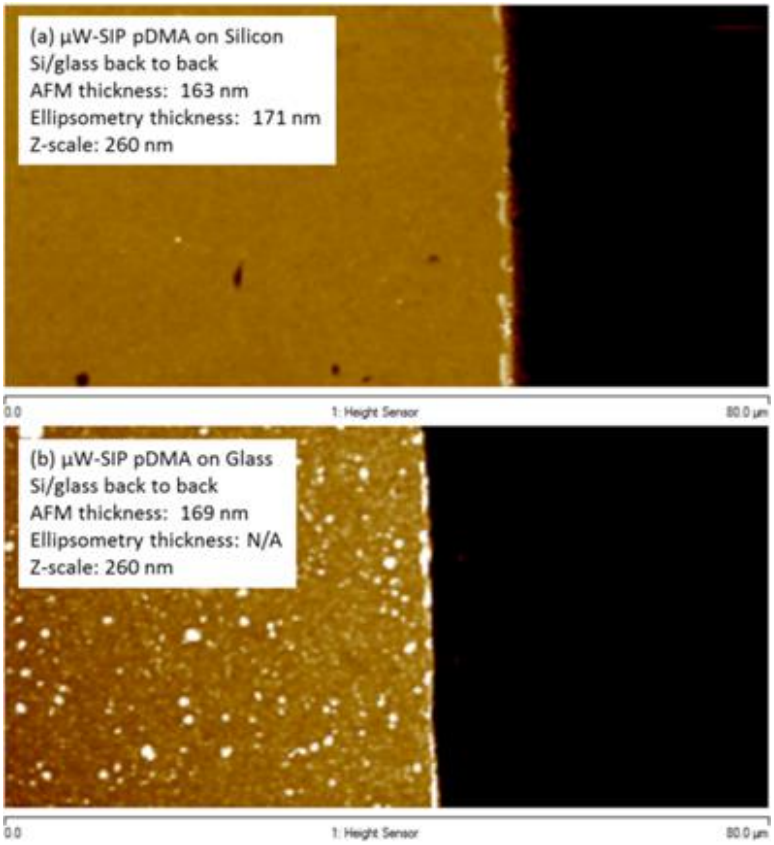

Figure 2.3 Contact mode AFM images of the scratched pDMA brush films prepared via μW-SIP on (a) silicon wafer and (b) glass.

The two substrates were immersed in monomer solution back to back in the same reaction tube (4.85 mol/L in benzene, 65 °C, 10 min).

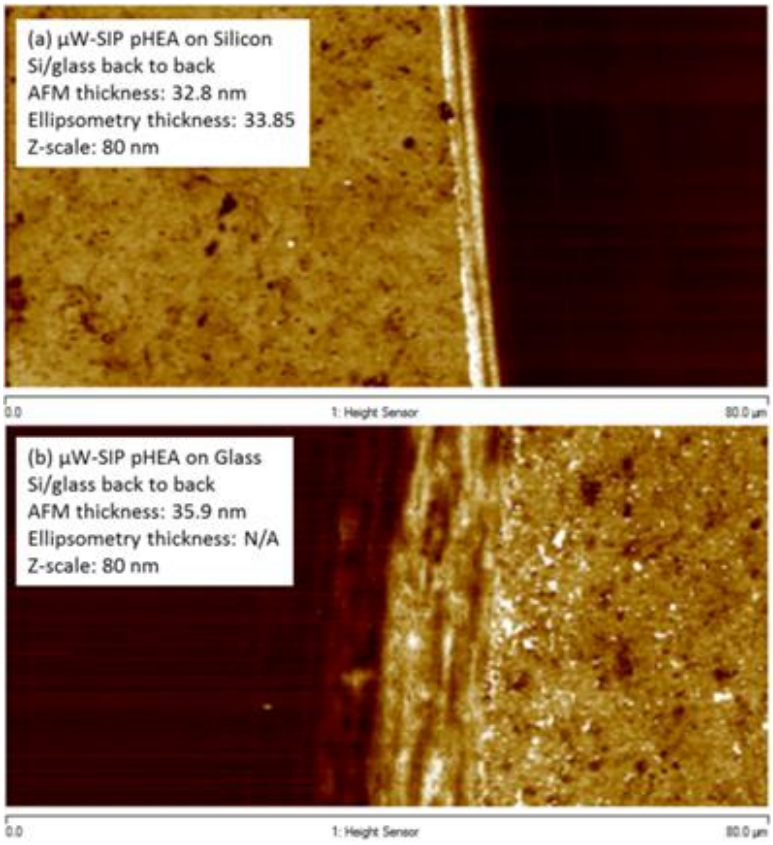

Figure 2.4 Contact mode AFM images of scratched pHEA brush films prepared via µW-SIP on (a) silicon wafer and (b) glass.

The two substrates were immersed in monomer solution back to back in the same reaction tube (0.066 mol/L in water, 10 W, 65 °C, 10 min).

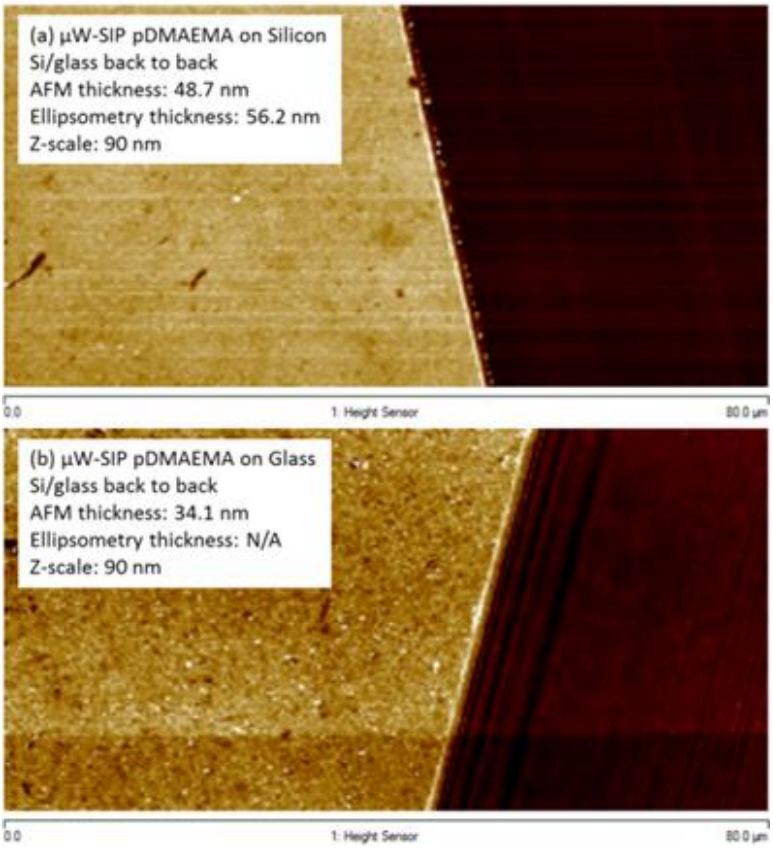

Figure 2.5 Contact mode AFM images of the scratched pDMAEMA brush films prepared via µW-SIP on (a) silicon wafer and (b) glass.

The two substrates were immersed in monomer solution back to back in the same reaction tube (2.98 mol/L in benzene, 65 °C, 10 min).

2.3.3 Reaction Time and Concentration

To further investigate the µW-SIP process, polymer brush thickness was evaluated as a function of reaction time and concentration. Figure 2.6a shows the evolution of film thickness with time for µW-SIP of DMA, DMAEMA, and HEA. DMA showed an immediate increase in thickness at very short reaction times (2 min, 182 nm) and then gradually increased, almost plateauing with additional reaction time. While the enhanced polymerization behavior of DMA is consistent with microwave-assisted solution polymerizations previously reported by Roy et al.,[9] the rapid plateau of film

thickness for DMA suggests that a relatively high concentration of radicals early in the reaction leads to both a high polymerization rate and increased termination. The relatively less reactive DMAEMA and HEA monomers show similar trends as a function of reaction time, but exhibit a more gradual increase in film thickness.

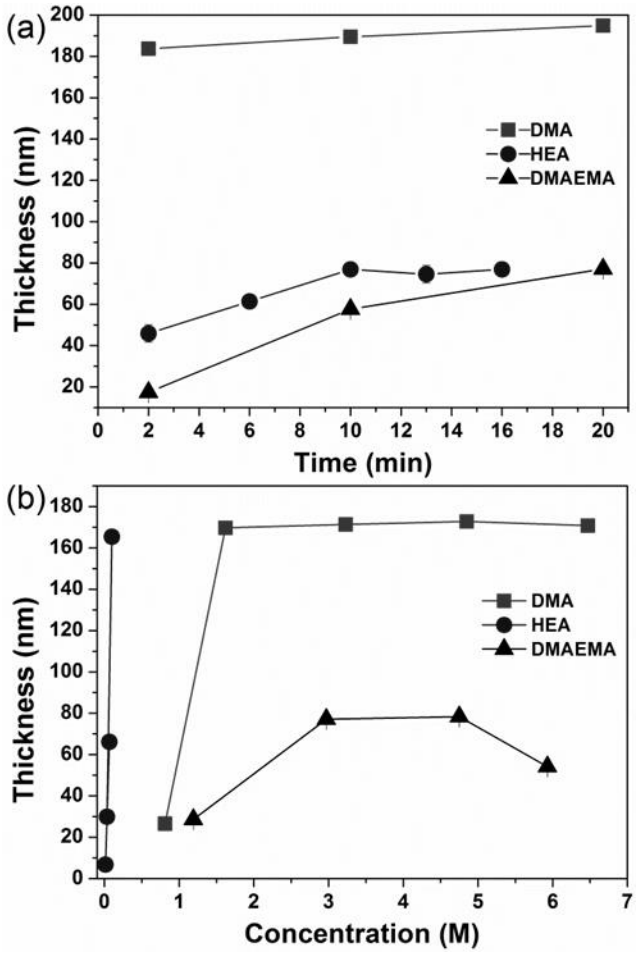

Figure 2.6 Plots of (a) thickness versus time and (b) thickness versus monomer concentration.

(a) Thickness versus time plots for DMA (4.85 mol/L in benzene, 50 W, 65 °C), HEA (0.066 mol/L in water, 10 W, 65 °C), and DMAEMA (2.98 mol/L in benzene, 50 W, 65 °C). (b) Thickness versus monomer concentration plots for DMA (benzene, 50 W, 65 °C, 10 min), HEA (water, 25 W, 65 °C, 10 min), and DMAEMA (benzene, 50 W, 65 °C, 10 min). Some error bars are contained within the data point.

Figure 2.6b shows the evolution of film thickness with increasing monomer concentration for DMA, DMAEMA, and HEA. For conventional SIP, there typically exists a linear relationship between film thickness and monomer concentration observed at constant reaction time.[25] However, for μW-SIP of polar monomers in non-polar solvents (or vice versa), as in the case of DMA and DMAEMA in benzene, the interplay between monomer concentration and the change in polarity of the reaction mixture as concentration increases has an evident effect on brush thickness. At low monomer concentrations (0.81 mol/L for DMA and 1.19 mol/L for DMAEAM), the film thickness is dictated both by low concentration and the mostly non-polar nature of the reaction mixture, which absorbs microwave radiation less efficiently. As shown in Figure 2.6b, there appears to be an optimal concentration and polarity range that provides a maximum film thickness for a given reaction time. At higher monomer concentrations, the high polarity of the reaction mixture, and consequently strong absorption of microwave radiation leads to a decrease in film thickness. In fact, μW-SIP of DMA in bulk monomer led to gelation of the reaction mixture and minimal brush growth. Similar results of increased side reactions and loss of polymerization control have been reported for microwave-assisted solution polymerization of DMA in dimethylformamide – a high microwave absorbing solvent[9]. When both monomer and solvent are polar, such as the case of HEA in water, the change in polarity of the reaction mixture with increasing monomer concentration is minimal, and μW-SIP exhibited a more traditional relationship between film thickness and concentration as shown for HEA in Figure 2.6b. Employing higher HEA concentrations (i.e. > 0.1 mol/L) led to extremely thick, heterogeneous films and partial gelation of the reaction mixture. Strikingly, thick pHEA brushes were

obtained by μW-SIP at extremely low monomer concentrations. For instance, a 165 nm pHEA brush was achieved in 10 min at 0.1mol/L HEA.

2.3.4 Radiation Power

As previously mentioned, all μW-SIP reactions were performed under constant microwave irradiation power (50 W). The success of initial experiments at low power values prompted us to explore the effect of power on brush thickness. Figure 2.7 shows the evolution of brush thickness on silicon wafers as a function of microwave power for DMA, DMAEMA, and HEA, with the upper power values for each monomer system limited by our ability to accurately maintain a constant temperature with simultaneous cooling. An increase in microwave power while maintaining a constant solution temperature had a detrimental effect on brush thickness in each monomer system. We speculate that an increase in power may result in a greater absorption of microwave radiation by the doped silicon wafer leading to more selective heating of the substrate. A higher temperature at the silicon interface could alter the rate of initiator decomposition and increase the occurrence of bimolecular termination, both of which would be detrimental to the brush grafting density, molecular weight, and ultimately thickness. However, a more detailed investigation of the effect of microwave power on brush properties is required – particularly on microwave transparent substrates such as undoped silicon wafer or glass.

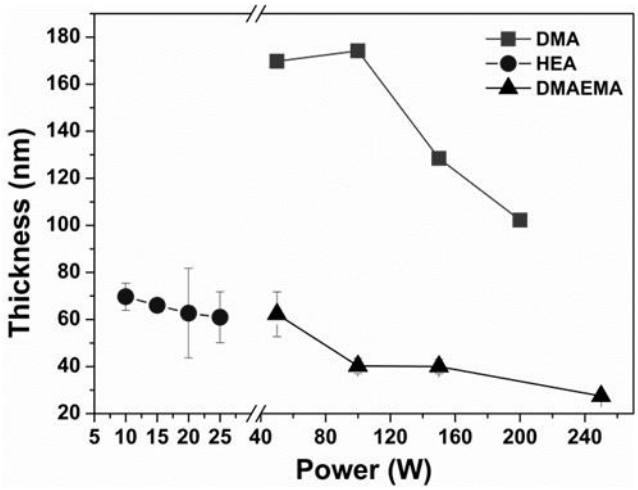

Figure 2.7 Thickness versus microwave irradiation power for DMA, HEA, and DMAEMA.

DMA (4.85 mol/L in benzene, 65 °C, 10 min), HEA (0.066 mol/L in water, 65 °C, 10 min), and DMAEMA (2.98 mol/L in benzene, 65 °C, 10 min), Error bars represent one standard deviation of the data. Some error bars are contained within the data point.

2.4 Conclusion

In summary, the use of μW-SIP enables rapid synthesis of polymer brush surfaces from a variety of monomers. The effects of reaction time, monomer concentration, and microwave power on brush thickness were reported. Not only does μW-SIP reduce the time necessary to achieve a desired thickness, but in many cases, it may reduce the concentration of monomer needed for the polymerization. The μW-SIP strategy was demonstrated with conventional radical polymerization on flat silicon and glass substrates, but should also find applicability toward controlled radical SIP techniques and a broader range of substrates including membranes and nanoparticles.

2.5 Acknowledgements

This work was financially supported by the National Science Foundation CAREER Award (DMR-1056817). The acquisition of the AFM instrumentation used in

this work was enabled via partial funding from the Office of Naval Research (Award N00014-07-1-1057).

2.6 References

1. Kappe, C. O., *Angew. Chem. Int. Ed.* **2004,** *43* (46), 6250-6284.
2. Ebner, C.; Bodner, T.; Stelzer, F.; Wiesbrock, F., *Macromolecular Rapid Comm.* **2011,** *32* (3), 254-288.
3. Hoogenboom, R.; Schubert, U. S., *Macromol. Rapid Commun.* **2007,** *28* (4), 368-386.
4. Kempe, K.; Becer, C.; Schubert, U., *Macromolecules* **2011,** *44* (15), 5825-5842.
5. Zhu, J.; Zhu, X.; Zhang, Z.; Cheng, Z., *J. Polym. Sci., Part A: Polym. Chem.* **2006,** *44* (23), 6810-6816.
6. Brown, S. L.; Rayner, C. M.; Perrier, S., *Macromol. Rapid Commun.* **2007,** *28* (4), 478-483.
7. Brown, S. L.; Rayner, C. M.; Graham, S.; Cooper, A.; Rannard, S.; Perrier, S., *Chem. Commun.* **2007,** (21), 2145-2147.
8. Roy, D.; Sumerlin, B. S., *Polymer* **2011,** *52* (14), 3038-3045.
9. Roy, D.; Ullah, A.; Sumerlin, B. S., *Macromolecules* **2009,** *42* (20), 7701-7708.
10. Chen, G.; Zhu, X.; Cheng, Z.; Lu, J.; Chen, J., *Polym. Int.* **2004,** *53* (4), 357-363.
11. Zhang, H.; Schubert, U. S., *Macromol. Rapid Commun.* **2004,** *25* (13), 1225-1230.
12. Kwak, Y.; Mathers, R. T.; Matyjaszewski, K., *Macromol Rapid Comm* **2012,** *33* (1), 80-86.
13. Boukherroub, R.; Petit, A.; Loupy, A.; Chazalviel, J.-N.; Ozanam, F., *J. Phys. Chem. B* **2003,** *107* (48), 13459-13462.
14. Liu, X.; Han, H.-M.; Liu, H.-B.; Xiao, S. J., *Surface Sci.* **2010,** *604* (15-16), 1315-1319.
15. Petit, A.; Delmotte, M.; Loupy, A.; Chazalviel, J.; Ozanam, F.; Boukherroub, R., *J. Phys. Chem. C* **2008,** *112* (42), 16622-16628.
16. Haensch, C.; Erdmenger, T.; Fijten, M.; Hoeppener, S.; Schubert, U. S., *Langmuir* **2009,** *25* (14), 8019-8024.
17. Liu, X.; Zheng, H. N.; Ma, Y. Z.; Yan, Q.; Xiao, S. J., *J. Colloid Interf. Sci.* **2011,** *358* (1), 116-122.
18. Jhaveri, S. B.; Carter, K., *Langmuir* **2007,** *23* (16), 8288-8290.
19. Jhaveri, S.; Peterson, J.; Carter, K., *Langmuir* **2009,** *25* (16), 9552-9556.
20. Ofir, Y.; Moran, I. W.; Subramani, C.; Carter, K. R.; Rotello, V. M., *Adv. Mater.* **2010,** *22* (32), 3608-3614.
21. Barbey, R.; Lavanant, L.; Paripovic, D.; Schüwer, N.; Sugnaux, C.; Tugulu, S.; Klok, H.-A., *Chem. Rev.* **2009,** *109* (11), 5437-5527.
22. Ayres, N., *Polym. Chem.* **2010,** *1* (6), 769-777.
23. Patton, D. L.; Page, K. A.; Xu, C.; Genson, K. L.; Fasolka, M. J.; Beers, K. L., *Macromolecules* **2007,** *40* (17), 6017-6020.
24. Thompson, K.; Booske, J.; Gianchandani, Y.; Cooper, R., *IEEE Elec. Dev. Lett.* **2002,** *23* (3), 127-129.

25. Murata, H.; Prucker, O.; Rühe, J., *Macromolecules* **2007,** *40* (15), 5497-5503.

CHAPTER III - CONTROLLED HETEROGEITY OF TAPERED BLOCK COPOLYMER BRUSH VIA POST POLYMERIZATION MODIFICATION

3.1 Introduction

In the field of polymer surface engineering, the ability to intentionally control the composition, distribution and spatial arrangement of functional moieties within polymer thin films using straightforward and efficient chemistries is of great interest. Advances in controlled surface-initiated polymerization (SIP) techniques have undoubtedly provided polymer chemists with a powerful toolset to tailor these parameters for polymer brush surfaces given knowledge of reaction conditions, reactivity ratios, and order of monomer addition; however, challenges remain particularly regarding direct polymerization of monomers with complex and reactive pendent functionality.[1-2] In this regard, the combination of surface-initiated polymerization and post-polymerization modification (PPM) addresses the limit of direct polymerization via installation of functional moieties following polymerization using chemoselective reactions and has been demonstrated as a versatile method for preparing multifunctional polymer brush surfaces.[3-7] Recently, a number of functional polymer brush surfaces with chemical and biological properties such as patterning,[8-11] catalysis,[12-13] controlled release,[14] separations,[15] barrier properties,[16] and biological activity[17-19] have been fabricated via the post-modification approach.

For polymer brushes in the high grafting density regime, segmental repulsion and overlap of polymer chains stretch the chains perpendicular to the surface and reduces the conformational entropy.[20-21] Upon post-modification of polymer brush, the addition of reactive moieties onto the already stretched polymer chains further increases the

segmental repulsion rendering the diffusion of reactive moieties from solution to the polymer brush more difficult. The effectiveness of the PPM process of polymer brush in terms of depth of penetration and homogeneity of the modified brush is thus governed by the reaction conditions (i.e. intrinsic post-modification reaction rate and efficiency) and the parameters that influence mass transport into the brush, including grafting density, film thickness, polymer chain stiffness, size or molecular weight (MW) of the free-moving modifier, and solvent quality. Therefore, it can be deduced that increases in thickness and grafting density of polymer brush and larger MW of the modifier will decrease the efficacy and depth of penetration of the PPM resulting in a brush surface with greater compositional heterogeneity. Heterogeneous brush modification may be undesirable in some applications; however, exploiting the limited ability of modifiers to penetrate reactive brush surfaces will undoubtedly provide opportunities to design complex brush structures unattainable by direct polymerization.

Despite the extensive applications of PPM in the literature, relatively few reports have investigated the influence of the aforementioned parameters on the spatial distribution of functional moieties within post-modified polymer brush films. Recently, Schuh and Rühe reported the reaction and penetration of active ester brush surfaces with amine-functionalized poly(ethylene glycol) (PEG-NH_2).[22] The results showed that the MW of PEG-NH_2 played the most important role on the PPM while other parameters such as the grafting density, film thickness and the percentage of active ester moiety of the brush only have minor effects. Using neutron reflectivity (NR) Schüwer and coworkers studied the PPM process and the distribution of small molecule modifiers on p-nitrophenyl chloroformate (NPC) pre-activated poly(hydroxyethyl methacrylate)

(pHEMA) brushes and the effectiveness of the PPM was found to be dependent on grafting density, brush thickness and polarity of the amino acid modifier.[23] These results provided one of the first high-resolution snapshots of the compositional gradients and heterogeneity within the ultrathin brush films. However, a significant drawback of Schuwer's system was the need for "pre-activation" of the pHEMA brush hydroxyl moieties with NPC – a PPM process itself determined by the authors to be less than quantitative – prior to the PPM aminolysis reaction with amino acids. Thus, the extent of penetration and the spatial distribution of amino acids observed by neutron reflectivity were directly dependent on and limited by the extent of NPC activation – leaving an incomplete picture of the PPM process on a fully reactive brush system.

Previously, our group utilized base-catalyzed thiol-isocyanate chemistries as a modular PPM toolset to fabricate multicomponent surfaces.[24-25] The thiol-isocyanate reaction has a high reaction rate and efficiency thus rendering it an ideal platform to the probe the spatial distribution of modifiers within the brush. In this study, we use neutron reflectometry to investigate the thiol-isocyanate postmodification of poly(2-isocyanatoethyl methacrylate) (pNCOMA) brush surfaces with two deuterated thiols to determine the extent of penetration and spatial distribution of two chemically comparable *d*-thiols (d_7-propanethiol or d_7-PPT and d_{25}-dodecanethiol or d_{25}-DDT) differing only in molecular weight. With knowledge of vertical composition profiles as a function of thiol MW at hand, we exploit the limited mass transport aspects of PPM to intentionally generate tapered brush surfaces using a two-step PPM process – wherein a pNCOMA brush is first reacted with the larger MW d_{25}-DDT and then backfilled with the lower

MW d_7-PPT. To our knowledge, this represents the first tapered brush synthesized via a PPM process, and remarkably, without the use of controlled SIP techniques.

3.2 Experimental Section

3.2.1 Materials

All reagents and solvents were obtained at the highest purity available from Aldrich Chemical Company or Fisher Scientific and used without further purification unless otherwise specified. Photo-initiator precursor of 2-Hydroxy-4'-(2-hydroxyethoxy)-2-methylpropiophenone (HPP, Irgacure 2959) was purchased from Ciba Specialty Chemicals. The monomer of 2-isocyanatoethyl methacrylate was purchased from TCI America and passed through columns of neutral alumina to remove the BHT inhibitor before use. Deuterated thiols of 1-propane-d_7-thiol (d_7-PPT) and 1-dodecane-d_{25}-thiol (d_{25}-DDT) were purchased from CDN Isotopes in sealed ampules and used as received. Single sided polished silicon wafers were purchased from University Wafers.

3.2.2 Characterization

A Varian Mercury Plus 300MHz NMR spectrometer operating at a frequency of 300 MHz with VNMR 6.1C software was used for proton and carbon analysis. Ellipsometry measurements were carried out using a Gaertner Scientific Corporation LSE ellipsometer with a 632.8 nm laser at 70° from the normal. The refractive indices of 3.86, 1.45, 1.43 and 1.50 for silicon, oxide layer, photoinitiator monolayer, and all polymer layers, respectively, were used to calculate polymer brush thickness using multilayer layer model.[26-27] The chemical composition of polymer brush surfaces was characterized using grazing angle attenuated total reflectance Fourier transform infrared spectroscopy (gATR-FTIR) using a ThermoScientific FTIR instrument (Nicolet 8700) equipped with a

VariGATR™ accessory (grazing angle 65°, germanium crystal; Harrick Scientific). The VariGATR™ attachment and FTIR instrument were under constant purging of N_2 gas along the infrared beam pathway to reduce the influence of CO_2 and H_2O in air. All spectra were collected with a resolution of 4 cm^{-1} by accumulating a minimum of 128 scans per sample and the spectra were analyzed and processed using Omnic software. Atomic force microscopy (AFM) was performed using a Bruker Icon Dimension instrument in tapping mode in order to measure the surface roughness and the film thickness of scratched brush surfaces. The polymer brush surfaces were scanned with T300R-25 probes (Bruker AFM Probes) with a spring constant of 40 N/m. Neutron reflectometry (NR) characterization of polymer brush samples was performed at the Spallation Neutron Source (SNS) at Oak Ridge National Laboratory (ORNL) using the Liquids Reflectometer (LR) under standard collection parameters. The LR collects specular reflectivity data in a continuous wavelength band (set to 2.5 Å < λ < 6.0 Å) at several different incident angles; for our work θ = 0.19°, 0.27°, 0.34°, 0.62°, 1.12°, and 2.01° were used. As a result of these instrument settings, data was acquired over a wave vector transfer ($Q = 4\pi \sin\theta/\lambda$) range of 0.006 $Å^{-1} < Q < 0.176$ $Å^{-1}$. Data was collected at each angle with incident beam slits set to maintain a constant relative wavevector resolution of $\delta Q/Q = 0.078$, allowing the data obtained at different θ to be stitched together into a single reflectivity curve. The neutron refractive index depends on the scattering length density (SLD), Σ, which is determined using the equation $\Sigma = b/V$, where b is the monomer scattering length (sum of scattering lengths of constituent atomic nuclei) and V is the monomer volume. Initial analysis of the NR data was done with the Motofit package and Igor Pro 6.3 software (Wavemetrics) by fitting the reflectivity

profiles (R-q plots) to model scattering length density (SLD) profiles.[28] The model SLD profiles of polymer brush samples were constructed from five to six layers (Si, SiO2, unmodified pNCOMA, postmodified pNCOMA, hydrated pNCOMA, and air). The SLD profiles were then optimized using a genetic algorithm to minimize the χ^2 between the measured and calculated reflectivities by varying layer thicknesses, interfacial roughnesses, and SLD values.

3.2.3 Cleaning of Silicon Substrates

Silicon wafers were cut into appropriate sized pieces and cleaned by sonication in a DP2300 ultra-high performance general purpose cleaner and degreaser (Branson Ultrasonics Corp) for 5 minutes. The substrates were then wiped gently with a cotton-tipped applicator to remove residue silicon dust from the surface. The substrates were then placed in deionized water and sonicated for 10 min. The wafers were then placed into an RCA-1 solution (deionized water: 27% ammonium hydroxide: 30% hydrogen peroxide 5:1:1) for 15 min at 70 °C followed with extensively rinsing with deionized water to remove any organic residues. The clean substrates were dried under a stream of N_2, and treated with UV ozone for 1 h before storing in an oven at 140 °C. Silicon wafers (2" diameter) used for neutron reflectivity studies were treated in a similar manner without cutting.

3.2.4 Immobilization of HPP-Trichlorosilane (Irgacure 2959) Photoinitiator

HPP-trichlorosilane photoinitiator was synthesized following previous literature procedures as shown in Scheme 3.1.[8, 24, 27] The previously cleaned silicon wafers were transferred into a glove box where the silicon substrates were placed into a toluene solution of HPP-trichlorosilane (4 mmol) and excess triethylamine at room temperature

for 3 h without stirring. Upon removal from the solution, the samples were thoroughly rinsed using toluene before drying under a stream of N_2. The initiator-functionalized silicon wafers were stored in toluene at -20 °C under darkness until use. The acetate protection group was removed by placing the initiator-functionalized wafers in a suspension of 120 mg K_2CO_3 in 6 mL methanol containing 75 µL H_2O for 1 h followed by subsequent washing with water, methanol, and toluene. The wafers with deprotected initiator on the surface were dried with a stream on N_2.

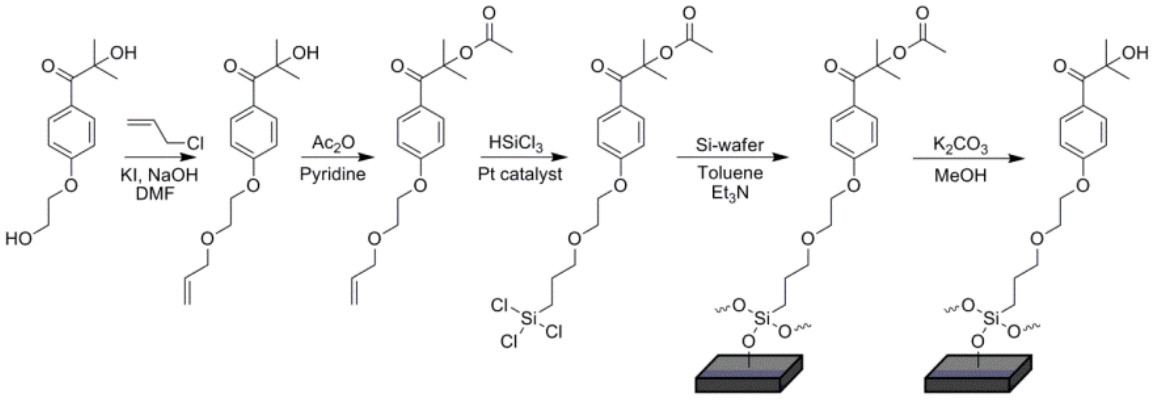

Scheme 3.1 Synthesis of surface-reactive photoinitiator and immobilization onto silicon surfaces.

3.2.5 Surface-initiated Polymerization (SIP) of pNCOMA Polymer Brush

The photoinitiator functionalized substrates were inserted into a microchannel reactor containing 2-isocyanatoethyl methacrylate (NCOMA) (3.5 mol/L in dry THF) and irradiated with $UV_{\lambda max,\ 365nm}$ light (~140 mW/cm^2) under an inert atmosphere for various times to achieve the desired brush thicknesses. After extensive washing in dry THF and toluene, the brush surfaces were dried using a stream of N_2.

3.2.6 PPM of pNCOMA Brush via Thiol-Isocyanate (Thiol-NCO) "Click" Reactions

All thiol-isocyanate reactions were catalyzed using 1,8-diazabicyclo[5.4.0]undec-7-ene (DBU) under ambient laboratory conditions (i.e. room temperature and normal

atmosphere). Reaction mixtures were not degassed prior to use. Solutions of either d_7-PPT or d_{25}-DDT and DBU catalyst (thiol: DBU; 0.01 mol/L:2×10^{-3} mol/L) in THF were prepared and placed into the reaction vessel containing the isocyanate-functionalized polymer brush and subsequently allowed to react for 1 h (unless otherwise specified) to facilitate functionalization via thiol-isocyanate click reactions. For the creation of tapered copolymer brushes, a solution of d_{25}-DDT and DBU catalyst (thiol:DBU; 0.01 mol/L:2×10^{-3} mol/L) in THF was prepared and placed into the reaction vessel containing the isocyanate-functionalized polymer brush and allowed to react for 15 min before removing the substrate, washing with THF and toluene, and drying under a stream of N_2. Subsequently, a solution of d_7-PPT and DBU catalyst (thiol: DBU; 0.01 mol/L:2×10^{-3} mol/L) in THF was prepared. The substrate previously reacted with d_{25}-DDT was immersed in the d_7-PPT solution and allowed to react for 4 h to backfill any remaining pendent isocyanate functionalities. After the reaction, the substrate was washed with THF and toluene followed by drying under a stream of N_2.

3.3 Results and Discussion

3.3.1 Polymer Brush Synthesis and PPM

Polymer brushes of 2-isocyanatoethyl methacrylate (NCOMA) were synthesized by surface-initiated photopolymerization on photoinitiator-modified silicon substrates (50 mm diameter$\times$0.5 mm thickness). After thoroughly removing physically absorbed polymer by extensive rinsing with dry THF, the average thickness of the unmodified pNCOMA brush samples was determined by ellipsometry. The polymer brushes were then post-modified using a single step DBU catalyzed thiol-isocyanate click reaction in THF, according to Scheme 3.2. Two deuterated thiols, d_7-PPT (MW 77.16 g/mol) and

d_{25}-DDT (MW 227.25 g/mol) were used as modifiers to investigate the effect of modifier MW on the depth of penetration and overall distribution of modifiers within post-modified brushes. Upon exposure to the thiol solution, the pendant NCO moieties on the polymer chains react quickly with the thiol modifier forming thiourethane linkages. The highly efficient single step PPM avoids the complications associated with any pre-activation steps and allows better analysis of the PPM process using neutron reflectometry.

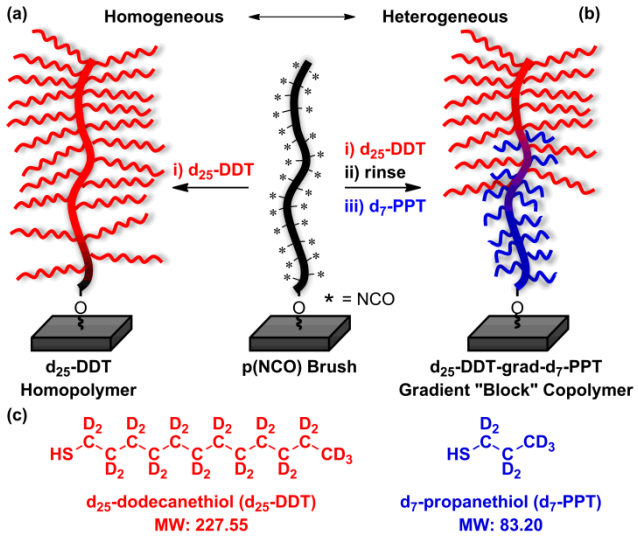

Scheme 3.2 Postmodification of pNCOMA polymer brush with (a) d_{25}-DDT and (b) heterogeneous, complex architecture polymer brush surfaces via postpolymerization modification using thiol-isocyanate click chemistry.

3.3.2 Neutron Reflectometry

Neutron reflectometry (NR) was conducted at the Spallation Neutron Source (SPS) at Oak Ridge National Lab (ORNL). NR is a powerful diffraction-based technique for probing the structure of ultrathin films such as post-modified polymer brush surfaces.[23, 29-30] NR experiments utilize isotopic nuclei with different neutron scattering lengths that provide significant scattering contrast to elucidate sub-layer structural information. In

our investigation, deuterated thiols of different sizes and degree of deuteration (d_7-PPT and d_{25}-DDT) were used for post-polymerization modification of pNCOMA polymer brushes to label the post-modified regions. The data directly collected from NR experiments are reflectivity profiles (R-q plots) which can be fitted with a multilayer model that consisted of substrate, intermediate (initiator) layer, and polymer brush layers to minimize the χ^2 between the experimental and calculated reflectivity profiles. The SLD profiles of the optimized multilayer models contain the information of post-modifier distribution – labeled by isotopic nuclei – along the normal direction of the film.

3.3.3 Estimation of Mass Density for SLD Analysis

The SLD values for prototypical polymers can be calculated using the NIST SLD calculator provided the specific chemical composition and mass density, ρ, are known. The mass density of NCOMA monomer is 1.098 g/cm^3. The mass density of unmodified and thiol-modified pNCOMA polymer brushes, however, are not readily available in the literature. Therefore, good estimations of the mass density (ρ) values for the polymer brushes are needed before addressing the NR data. To begin, pNCOMA polymer brushes with dry thickness values of 117 nm and 25 nm were synthesized and characterized via neutron reflectometry. Figure 3.1a and 3.1b show the SLD profiles and reflectivity data (insert, multiplied by Q^4) obtained by fitting the experimental data for the 117 nm and 25 nm samples, respectively. The SLD profiles for the pNCOMA brushes show similar features with two abrupt transitions at the Si/SiO_2 and SiO_2/pNCOMA brush interfaces, followed by a convergence to a constant SLD value (1.94×10^{-6} Å^{-2}) before a smooth polymer to air transition is observed. In both profiles, the plateau regions with the constant SLD value of 1.94×10^{-6} Å^{-2} correspond to homogeneous regions of unmodified

pNCOMA within each sample. As expected, the plateau in the SLD profile of the thicker pNCOMA brush (117 nm) sample covers a much wider range than that of the thinner sample (25 nm).

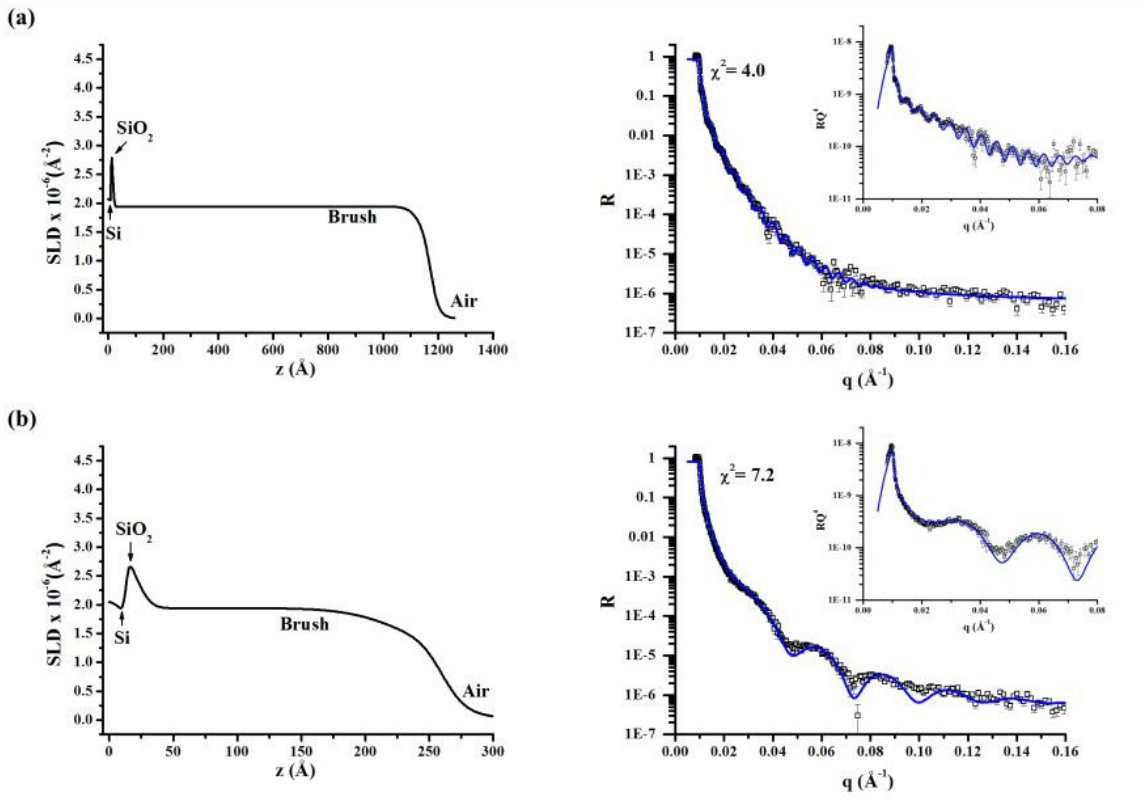

Figure 3.1 Neutron SLD profiles and reflectivity data of R-q profiles for the unmodified pNCOMA brush of (a) 117 and (b) 25 nm, respectively.

The experimental reflectivity data were shown in open symbols and fittings in blue lines. The inset shows the reflectivity data profiles (multiplied by Q^4).

It is worth mentioning that by assuming the mass density of the pNCOMA brush to be 1.00 g/cm^3, the SLD of unmodified polymer brush was calculated to be 1.54×10^{-6} Å^{-2}. The higher SLD value (1.94×10^{-6} Å^{-2}) obtained from the fitted NR data indicates that the mass density of pNCOMA brush is larger than 1.00 g/cm^3. The mass density, ρ, of polymer brush samples can be estimated based on Equation 1.

$$\rho = \frac{\Sigma_{FIT}}{\Sigma_{\mathbf{CAL}}} \quad \text{Equation 1}$$

In Equation 1, Σ_{FIT} is the SLD value of a polymer brush sample obtained by fitting the multilayer model to measured reflectivity data, Σ_{CAL} is the SLD value of the same polymer brush sample calculated using the NIST SLD calculator by assuming mass density equals to 1.00 g/cm^3, respectively. Based Equation 1, the mass density of pNCOMA brush was calculated as 1.26 g/cm^3. The estimated mass density of the unmodified NCOMA polymer brush was considered reasonable in comparison to the mass densities for similar linear poly(methacrylates). Next, the mass density of the polymer brushes postmodified with deuterated thiol was calculated using the weighted harmonic mean of the mass densities of unmodified pNCOMA brush and deuterated thiols, as shown in Equation 2.

$$\rho_{modified} = \frac{M_{pNCOMA}+M_{d-thiol}}{M_{pNCO}/\rho_{pNCOMA}+M_{d-thiol}/\rho_{d-thiol}} \quad \text{Equation 2}$$

In Equation 2, ρ_{pNCOMA} and $\rho_{\text{d-thiol}}$ are the mass density of the unmodified pNCOMA polymer brush and deuterated thiol; M_{pNCOMA} and $M_{\text{d-thiol}}$ are the molecular weight of respective repeating units. In Equation 2, the mass density of deuterated thiols ($\rho_{\text{d-thiol}}$) can be calculated based on Equation 3 by assuming that the sizes of deuterium and hydrogen atoms are equivalent.

$$\rho_{d-thiol} = \frac{M_{d-thiol}}{M_{thiol}}\rho_{thiol} \quad \text{Equation 3}$$

In Equation 3 ρ_{thiol}, and $\rho_{\text{d-thiol}}$ are the mass density of corresponding non-deuterated thiols, respectively. $M_{\text{d-thiol}}$ and M_{thiol} are the molecular weight of the deuterated and non-deuterated thiols, respectively. The mass densities of d_7-PPT and d_{25}-

DDT were estimated to be 0.896 g/cm^3 and 0.950 g/cm^3, respectively. The mass densities of deuterated PPT and DDT modified pNCOMA polymer brushes with full isocyanate conversion were then calculated to be 1.10 g/cm^3 and 1.05 g/cm^3, respectively. The SLD values and corresponding mass densities of unmodified pNCOMA, d_7-PPT modified pNCOMA, and d_{25}-DDT modified pNCOMA brush samples are shown in Table 3.1.

Table 3.1

SLD and Corresponding Mass Density

	Experimental		Theoretical	
	SLD ($\times 10^{-6}$ Å^{-2})	Density (g/cm^3)	SLD ($\times 10^{-6}$ Å^{-2})	Density (g/cm^3)
Bulk Si	2.07	2.33	2.07	2.33
SiOx	3.14	2.65	3.14	2.65
pNCOMA	1.94	1.26[a]	1.54	1.00
pNCOMA-d_7-PPT	3.09	1.16[a]	2.94	1.10
			2.66	1.00
pNCOMA-d_{25}-DDT	4.60	1.02[a]	4.74	1.06
			4.49	1.00

a Calculated based on MOTOFIT of NR data

3.3.4 Effect of Molecular Weight of Thiols on PPM

To study the size effect of the post-modifier on the PPM penetration depth, two deuterated thiols of different sizes and molecular weight, d_7-PPT and d_{25}-DDT were chosen to postmodify the NCOMA polymer brush. Explicit grafting density was not determined since the reactive nature of the pNCOMA free polymer formed in solution complicated GPC analysis in the unmodified form; however, the grafting density and original thickness of the NCOMA brushes (127±3 nm) were held constant using fixed polymerization time and monomer concentration, respectively, for both samples before

modification.[22] Following d_7-PPT modification of the pNCOMA brush with an initial thickness of 130 nm, as shown in Figure 3.2a, the SLD profile displayed a gradual increase in the SLD value that covered a range of 63 nm along the normal direction from the SiO_2/brush interface before reaching a maximum constant SLD value (3.09×10^{-6} Å^{-2}). The high SLD value is due to the presence of a large amount of deuterium nuclei in the d7-PPT modified sub-layer. The SLD can be calculated by the scattering length contribution of every atom within a unit cell. The coherent scattering length of deuterium nuclei (6.671×10^{-15} m) is higher than that of hydrogen (-3.7406×10^{-15} m). In contrast, the mass density change of polymer brush after the modification was less significant. As a result, the presence of deuterium atoms within the deuterated thiol modified pNCOMA brush resulted in higher SLD values.

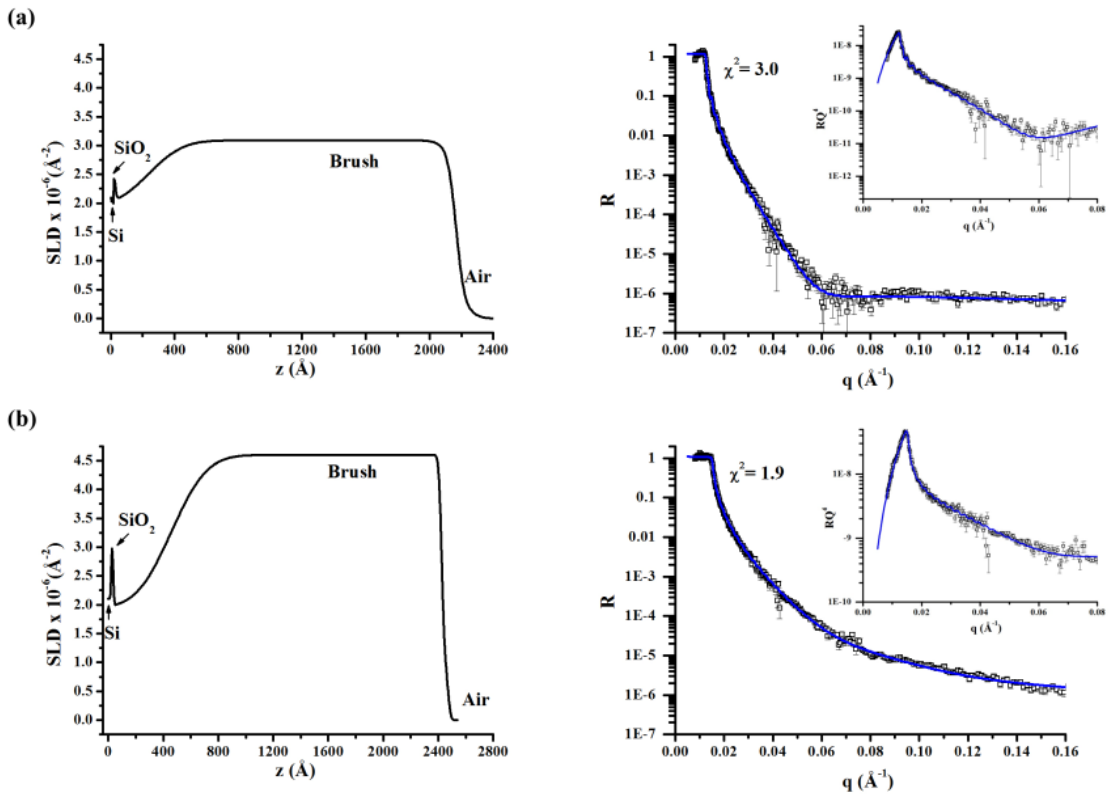

Figure 3.2 Neutron SLD profiles and reflectivity data of R-q profiles of pNCOMA modified with (a) d_7-PPT and (b) d_{25}-DDT, respectively.

The experimental reflectivity data were shown in open symbols and fittings in blue lines. The inset shows the reflectivity data profiles (multiplied by Q^4).

In Figure 3.2a, the region with constant SLD value (3.09×10^{-6} Å^{-2}) that extends from ~50 nm from the substrate to the polymer/air interface at 218 nm represents the fully post-modified layer. For d_7-PPT modified NCOMA polymer, the fitted SLD value of 3.09×10^{-6} Å^{-2} corresponds to a mass density of 1.16 g/cm^3. The result of fitted SLD is consistent with the calculated SLD estimated in Table 3.1 (SLD 2.94×10^{-6} Å^{-2}, ρ 1.10 g/cm^3). The SLD values of the two methods show less than 5% difference. The SLD gradually decreases from the plateau region to the substrate suggesting the presence of a d_7-PPT concentration gradient. Fully modified polymer brush at the outskirt region of the

film gradually transits to partially modified brush near the substrate/polymer interface. The experimental fit of the reflectivity data indicates that at least 70% (148 nm) of the total film thickness is fully modified with d_7-PPT and about 29% (63 nm) of the thickness exhibits a concentration gradient. After PPM with d_{25}-DDT, as shown in Figure 3.2b, greater heterogeneities in the SLD profile of polymer brush (original thickness 123 nm) were observed with the plateau region at the outskirt region of the profile with a higher SLD value (4.60×10^{-6} Å^{-2}). The plateau with constant SLD value at the outskirt of the film represents the fully post-modified region. For d_{25}-DDT modified polymer brush, the fitted SLD (4.60×10^{-6} Å^{-2}) corresponds to a mass density of 1.02 g/cm^3. The result of fitted SLD is consistent with the calculated SLD estimated in Table 3.1 (SLD 4.74×10^{-6} Å^{-2}, ρ 1.06 g/cm^3). The SLD values of the two methods show less than 3% difference. The SLD gradient of the d_{25}-DDT modified polymer brush was larger than that of d_7-PPT modified brush. As shown in Figure 3.2b, the gradient region spanned to 42% (102 nm) of the total thickness from the polymer/substrate interface. The SLD gradient of both d_7-PPT and d_{25}-DDT modified polymer brushes at the near substrate region of the film suggests that there were NCO moieties at the innermost region of the brush remained unreacted after PPM. Upon exposure to deuterated thiols, the NCO groups at the outskirt of the polymer brush quickly react and form thiourethane alkyl moieties. The addition of NCO groups onto polymer chain greatly increases the segmental repulsion and hampers the penetration of thiol modifiers into the innermost layer of the film from solution. Unable to be reached by deuterated thiols, NCO groups near the substrate/polymer interface have low conversions after PPM, and consequently, less deuteration resulting in the low SLD value. The fact that the gradient of the d_{25}-DDT modified sample is

significantly greater than the component gradient of d_7-PPT modified film in both range and slope suggests that the size of the modifier impacts mass transport into the brush. Although the results were based on NR snapshots of one postmodification time (1 hour), these results are in good agreement with trends reported by Schuh and Schüwer and elucidate the effect of thiol molecular weight (or molecular size) on the PPM process for polymer brushes.[22-23]

3.3.5 Effect of Polymer Brush Thickness on PPM

The change in polymer brush thickness before and after PPM was also examined. The thickness of post modified polymer brush samples was measured using the AFM scratch method. The results of thickness ratio of post modified polymer brush over unmodified brush are shown in Table 3.2.

Table 3.2

Polymer Brush Thickness Before and After PPM

	Thickness (nm) Before PPM[a]	After PPM[b]	Thickness Ratio
pNCOMA-d_7-PPT	130	218	1.67
pNCOMA-d_{25}-DDT	123	245	1.99
	29.0	84.7	2.92
Tapered polymer brush			
DDT-PPT	125	270	2.16
PPT-DDT	92.5	174	1.88

a Based on ellipsometry measurement; b based on NR fitting and AFM measurement

Based on the principle of mass conservation, the thickness ratio of pNCOMA polymer brush post-modified at full conversion over its original thickness can be calculated using Equation 4,

$$\frac{T_2}{T_1} = \frac{V_2}{V_1} = \frac{M_2/\rho_2}{M_1/\rho_1} = \frac{M_2}{M_1}\frac{\rho_1}{\rho_2} \quad \text{Equation 4}$$

in which T_i denotes the film thickness, V_i represents the volume occupied by the film, M_i and ρ_i are the repeating unit molecular weight and mass density. The subscriptions 1 and 2 represent polymer brushes before and after modification, respectively.[5] For the d_7-PPT modified pNCOMA brush with an original thickness (T_1) of 130 nm, the $M_2\rho_1/M_1\rho_2$, was calculated to be 1.67 and was equivalent to the experimental T_2/T_1 ratio. The results show that, for the small modifier (d_7-PPT), quantitative conversion can be achieved for thick pNCOMA brush (130 nm).

The T_2/T_1 ratio of d_{25}-DDT modified pNCOMA brush at full conversion can be calculated to be 3.04 based on Equation 4. For the sample with an original brush thickness (T_1) of 123 nm, the experimental thickness ratio (T_2/T_1) was only 1.99. The fact that the experimental thickness ratio was significantly smaller than the 100% conversion value indicated that a large amount of NCO groups remained unreacted after PPM. Given the high efficiency of the thiol-isocyanate reaction, the low conversion of PPM can only be explained by the lack of full penetration of the d_{25}-DDT into the brush. By reducing the thickness of unmodified pNCOMA brush one would expect to reduce the penetration barrier for DDT and to improve the overall PPM conversion. To test the hypothesis, a pNCOMA brush sample with an original thickness of 29 nm was synthesized and reacted with d_{25}-DDT under identical conditions (1 hour). The thickness increased to 84.7 nm and the T_2/T_1 ratio was 2.92. Although still smaller than the 100% value (3.04), it was significantly higher than that of the thicker brush film. As shown in Figure 3.3 the compositional gradient at the near substrate region of the SLD profile of the thin polymer brush sample is much smaller than the gradient of thick polymer brush shown in Figure 3.2. The results show that, for thick pNCOMA brush (130 nm),

quantitative conversion can be achieved using the small modifier (d_7-PPT). The results show that, for the large modifier (d_{25}-DDT), the thickness of pNCOMA brush affects the PPM conversion and compositional gradient at the inner part of the brush. Reducing unmodified brush thickness increases the overall conversion and reduces the compositional gradient.

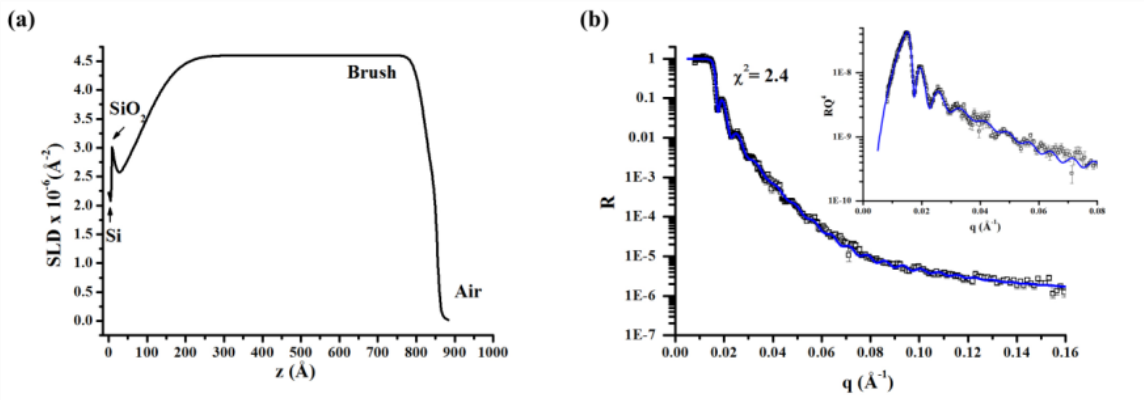

Figure 3.3 Neutron SLD profiles (a) and reflectivity data (b) of R-q for pNCOMA brush with an original thickness of 29 nm modified with d_{25}-DDT.

The experimental reflectivity data were shown in open symbols and fittings in blue lines. The inset shows the reflectivity data profiles (multiplied by Q^4).

3.3.6 Tapered Copolymer via Sequential PPM

While the synthesis of a polymer brush with homogeneous structure is indeed important, our findings that reactive functional groups in the near-substrate region of the polymer brush can be preserved after PPM due to diffusion limitations of incoming modifiers open the door to greater opportunities for designing and synthesizing complex polymer brush architectures with multiple components and heterogeneity. Given that the PPM reaction rate is exceedingly fast, the progression of the thiol-isocyanate reaction within the film is predominately dependent on the mass transport of the thiol molecules from solution into the brush. The diffusion process becomes more difficult with

increasing reaction time due to increasing steric hindrance and segmental repulsion.[22] A short PPM reaction time yields a polymer brush with a fully converted layer near the air interface and a partially converted inner layer approaching the near-substrate region. The unreacted NCO moieties in the inner region of the brush remain available for further postmodification using a second modifier, with proper tuning of the PPM conditions, resulting in a tapered copolymer architecture without using controlled polymerization technique.

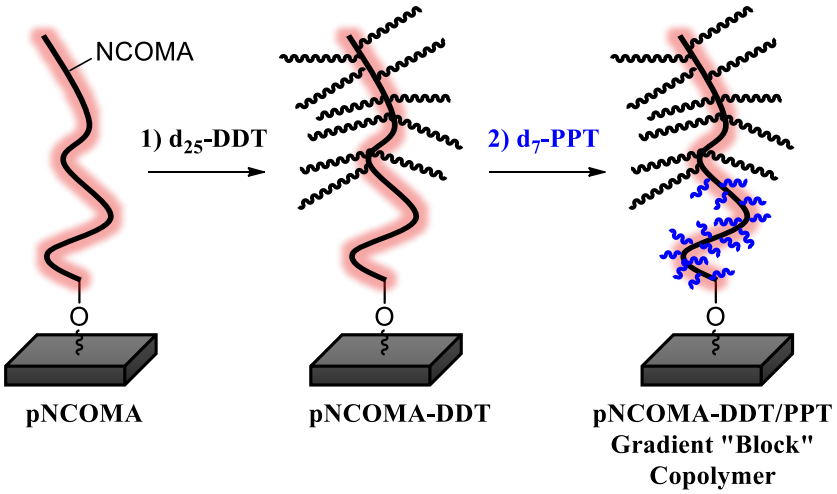

Scheme 3.3 Synthesis of tapered copolymer brush via sequential thiol PPM of pNCOMA brush.

As a proof of concept, tapered copolymer brushes with compositional heterogeneity along the vertical direction were synthesized using a sequential PPM process with d_7-PPT and d_{25}-DDT as shown in Scheme 3.3. The chemical compositions of pNCOMA polymer brushes modified with equivalent non-deuterated thiols were first characterized using grazing angle attenuated total reflection FTIR as shown in Figure 3.4. The strong absorption at 2250 cm^{-1} corresponding to the isocyanate functional group decreased in intensity after the first DDT modification and nearly disappeared after the

second modification with PPT. The peak at ~3300 cm^{-1} represents the N-H stretch of the thiourethane groups. The longer reaction time in the second thiol modification step allows sufficient time for the smaller PPT molecules to penetrate through the DDT-modified outer layer and into the inner unmodified region of the brush.

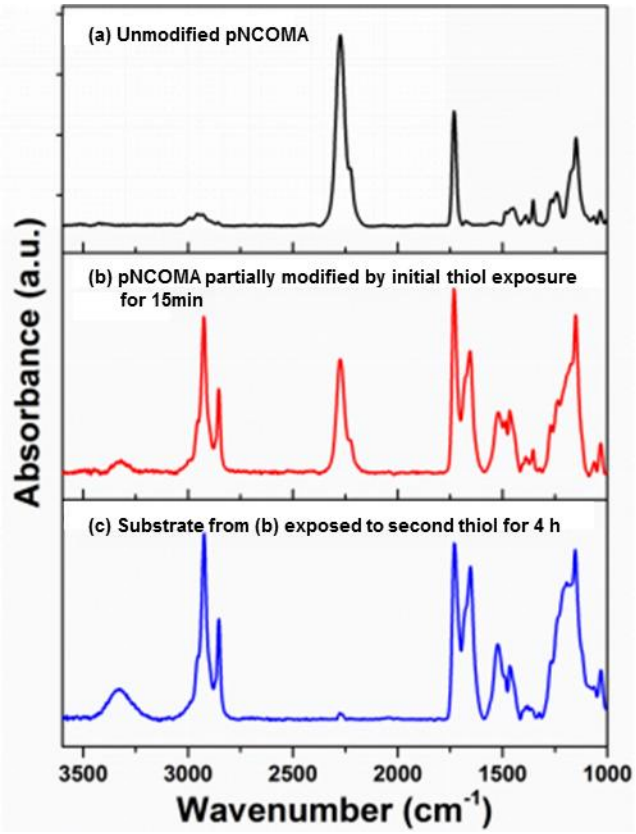

Figure 3.4 Grazing angle FTIR of (a) unmodified pNCOMA brush, (b) a partially modified pNCOMA brush with DDT and (c) a sequentially modified pNCOMA brush first with DDT followed with PPT.

These results provided the impetus for the following neutron reflectometry studies. For NR, pNCOMA brush surfaces were first placed in a THF solution of d_{25}-DDT (0.01 mol/L d_{25}-DDT and 0.002 mol/L DBU) for 15 min. Following a rinse with anhydrous THF, the same samples were exposed to a THF solution of d_7-PPT (0.01 mol/L d_7-PPT and 0.002 mol/L DBU) for 4 hours to allow consumption of the isocyanate

groups remaining at greater penetration depths. Importantly, the difference in isotopic labeling between d_7-PPT and d_{25}-DDT provides significant scattering contrast to allow elucidation of the respectively modified regions of the brush.

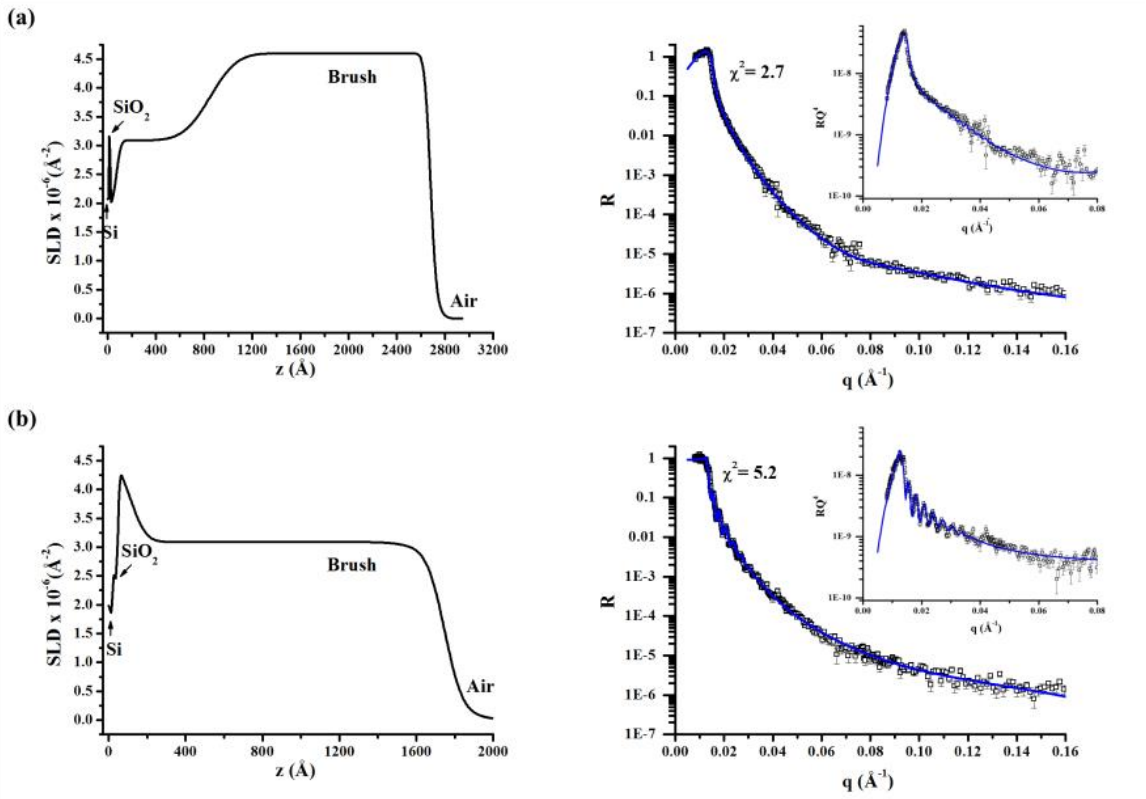

Figure 3.5 Neutron SLD profiles and neutron reflectivity profiles of pNCOMA brush sequentially modified with (a) d_{25}-DDT first then reacted with d_7-PPT and (b) d_7-PPT first then reacted with d_{25}-DDT, respectively.

The experimental reflectivity data were shown in open symbols and fittings in blue lines. The insets show the reflectivity data profiles (multiplied by Q^4).

Figure 3.5a shows the reflectivity data and corresponding SLD profile for the DDT-PPT sequentially modified brush sample. The SLD profile consists of two homogeneous plateaus. The outer plateau (SLD 4.60×10^{-6} Å^{-2}) ranging from the air/polymer interface to ~50 % (136 nm) of the film corresponds to the d_{25}-DDT fully modified region. From 136 nm, the SLD plateau gradually transitions to another ~8%

(22 nm) homogeneous layer (SLD 3.09×10^{-6} Å^{-2}) consistent with the d_7-PPT modified layer. The gradient between two homogenous regions ranges over a range of ~36% of the film thickness (96 nm). The SLD profile converged to values close to the unmodified NCOMA polymer brush as the innermost end of the film. The SLD profile in Figure 3.5a demonstrated that, despite a crowded d_{25}-DDT modified outskirt, small alkyl thiols such as d_7-PPT can still diffuse to the inner part of the polymer brush and react with NCO moieties. The SLD results are consistent with thickness measurements. The original thickness (125 nm), the sequentially modified thickness (270 nm), and the thickness ratio (2.16) of the DDT-PPT sequentially modified pNCOMA brush sample are shown in Table 3.2. The thickness ratio of the DDT-PPT sequentially modified sample (2.16) is higher than the thickness ratio of DDT modified pNCOMA brush sample (1.99) of similar thickness. In the second step modification, d_7-PPT reacted with the NCO groups that remained unreacted after the first modification at the innermost part of the polymer brush and resulted in a higher thickness and thickness ratio. The SLD profile described in Figure 3.5a is consistent with a tapered copolymer brush structure. Previous examples of block copolymer[31-32] and copolymer brush surfaces[33] have all required sequential or gradual monomer additions with controlled polymerizations. Here, we have shown that polymer brushes with layered vertical architecture and compositional heterogeneity can be successfully synthesized without the use of controlled polymerization techniques.

For comparison, pNCOMA brush with reversed sequential modification (d_7-PPT first, d_{25}-DDT later) was carried out in a similar manner. Similarly, pNCOMA brush surfaces were first placed in a THF solution of d_7-PPT (0.01 mol/L d_7-PPT and 0.002 mol/L DBU) for 15 min. Following a rinse with anhydrous THF, the same samples were

exposed to a THF solution of d_{25}-DDT (0.01 mol/L d_{25}-DDT and 0.002 mol/L DBU) for 4 hours to allow consumption of the isocyanate groups remaining at greater penetration depths. The SLD profile for the reversed sequentially modified brush (PPT-DDT) is shown in Figure 3.5b. The majority of the polymer brush (~83% or 144 nm) consists of the d_7-PPT modified pNCOMA brush with SLD of 3.09×10^{-6} Å^{-2}. At a penetration depth of 144 nm from polymer/air interface, the SLD profile gradually increases to 4.25×10^{-6} Å^{-2}. Notably, this value is smaller than the SLD value of d_{25}-DDT fully modified brush (4.60×10^{-6} Å^{-2}). Despite the prolonged reaction time of the second step, the segmental repulsion of d_7-PPM modified polymer brush posed greater hindrance on the transport of d_{25}-DDT into the inner region of the film and prevents the formation of a homogeneous layer fully modified by d_{25}-DDT at the inner layer of the film. The SLD results are consistent with thickness measurements. The original thickness (92.5 nm), the sequentially modified thickness (174 nm), and the thickness ratio (1.88) of the DDT-PPT sequentially modified pNCOMA brush sample are shown in Table 3.2. The thickness ratio of the PPT-DDT sequentially modified sample (1.88) is higher than the thickness ratio of DDT modified pNCOMA brush sample (1.67). In the second step modification, d_{25}-DDT reacted with the NCO groups that remained unreacted after the first step modification at the innermost part of the polymer brush and resulted in a higher thickness.

3.4 Conclusion

In conclusion, the distribution of deuterated thiourethane alkyl pendent moieties along the vertical direction following post-polymerization modification (PPM) of NCO-functionalized polymer brush surfaces has been drawn using neutron reflectometry analysis and highly efficient NCO-thiol reactions. We have shown that, given equivalent

conditions, the size or the molecular weight of reactive modifiers and unmodified polymer brush thickness play important roles on the penetration depth of modifier and affect the concentration gradient near the substrate/polymer interface within the polymer brush. By applying a sequential PPM strategy, we provided a straightforward, yet unconventional approach to design and synthesis tapered copolymer brushes with complex architectures. Tapered copolymers are particularly interesting as they have shown unique mechanical and interfacial properties in other bulk systems,[34-35] but are relatively unexplored as brush systems.[33] Using the information of limited mass transport of reactive moieties from solution into polymer brush surfaces, the first tapered copolymer brush surface was fabricated without the use of controlled polymerization techniques. These findings shed light on encouraging opportunities to design functionally and architecturally complex polymer surfaces with controlled heterogeneity by tuning the mass transport of reactive modifiers into brush surfaces – surfaces with structure and functionality unattainable by conventional routes that may exhibit new and unique properties.

3.5 Acknowledgement

The author gratefully acknowledges financial support from the National Science Foundation (NSF CAREER DMR-1056817). Funding for neutron beam time and travel to SNS were provided by the Department of Energy, Office of Basic Energy Sciences, through the EPSCoR Grant, DE-FG02-08ER46528 and by the UT-ORNL Joint Institute for Neutron Sciences (JINS). We thank Dr. Bradley Lokitz and Dr. John Ankner from ORNL for helpful discussions regarding NR.

3.6 References

1. Barbey, R.; Lavanant, L.; Paripovic, D.; Schüwer, N.; Sugnaux, C.; Tugulu, S.; Klok, H.-A., Polymer Brushes via Surface-Initiated Controlled Radical Polymerization: Synthesis, Characterization, Properties, and Applications. *Chemical Reviews* **2009,** *109* (11), 5437-5527.
2. Ayres, N., Polymer brushes: Applications in biomaterials and nanotechnology. *Polym. Chem.* **2010,** *1* (6), 769-777.
3. Arnold, R. M.; Huddlestona, N. E.; Locklin, J., Utilizing click chemistry to design functional interfaces through post-polymerization modification. *J. Mater. Chem.* **2012,** *22*, 19357-19365.
4. Galvin, C. J.; Genzer, J., Applications of surface-grafted macromolecules derived from post-polymerization modification reactions. *Progress in Polymer Science* **2012,** *37* (7), 871-906.
5. Murata, H.; Prucker, O.; Rühe, J., Synthesis of Functionalized Polymer Monolayers from Active Ester Brushes. *Macromolecules* **2007,** *40* (15), 5497-5503.
6. Günay, K. A.; Schüwer, N.; Klok, H.-A., Synthesis and post-polymerization modification of poly(pentafluorophenyl methacrylate) brushes. *Polymer Chemistry* **2012,** *3* (8), 2186.
7. Gauthier, M. A.; Gibson, M. I.; Klok, H. A., Synthesis of functional polymers by post-polymerization modification. *Angew Chem Int Ed Engl* **2009,** *48* (1), 48-58.
8. Hensarling, R. M.; Doughty, V. A.; Chan, J. W.; Patton, D. L., "Clicking" Polymer Brushes with Thiol-yne Chemistry: Indoors and Out. *J. Am. Chem. Soc.* **2009,** *131* (41), 14673-14675.
9. Arumugam, S.; Popik, V. V., Attach, Remove, or Replace: Reversible Surface Functionalization Using Thiol-Quinone Methide Photoclick Chemistry. *J Am Chem Soc* **2012,** *134* (20), 8408-8411.
10. Orski, S. V.; Poloukhtine, A. A.; Arumugam, S.; Mao, L.; Popik, V. V.; Locklin, J., High Density Orthogonal Surface Immobilization via Photoactivated Copper-Free Click Chemistry. *J Am Chem Soc* **2010,** *132* (32), 11024-11026.
11. Choi, J.; Schattling, P.; Jochum, F. D.; Pyun, J.; Char, K.; Theato, P., Functionalization and patterning of reactive polymer brushes based on surface reversible addition and fragmentation chain transfer polymerization. *Journal of Polymer Science Part A: Polymer Chemistry* **2012,** *50* (19), 4010-4018.
12. Proch, S.; Mei, Y.; Villanueva, J. M.; Lu, Y.; Karpov, A.; Ballauff, M.; Kempe, R., Suzuki- and Heck-Type Cross-Coupling with Palladium Nanoparticles Immobilized on Spherical Polyelectrolyte Brushes. *Adv. Synth. Catal* **2008,** *350*, 493-500.
13. Tam, T. K.; Zhou, J.; Pita, M.; Ornatska, M.; Minko, S.; Katz, E., Biochemically Controlled Bioelectrocatalytic Interface. *J. Am. Chem. Soc.* **2008,** *130* (33), 10888-10889.
14. Kumar, S.; Dory, Y. L.; Lepage, M.; Zhao, Y., Surface-Grafted Stimuli-Responsive Block Copolymer Brushes for the Thermo-, Photo- and pH-Sensitive Release of Dye Molecules. *Macromolecules* **2011,** *44* (18), 7385-7393.
15. Sun, X. L.; Stabler, C. L.; Cazalis, C. S.; Chaikof, E. L., Carbohydrate and protein immobilization onto solid surfaces by sequential Diels-Alder and azide-alkyne cycloadditions. *Bioconjugate Chem* **2006,** *17* (1), 52-57.

16. Brantley, E. L.; Holmes, T. C.; Jennings, G. K., Blocklike Fluorocarbon and Hydrocarbon Copolymer Films via Surface-Initiated ATRP and Postpolymerization Reactions. *Macromolecules* **2005,** *38* (23), 9730-9734.
17. Cullen, S. P.; Liu, X.; Mandel, I. C.; Himpsel, F. J. H.; Gopalan, P., Polymeric Brushes as Functional Templates for Immobilizing Ribonuclease A: Study of Binding Kinetics and Activity. *Langmuir* **2008,** *24* (3), 913-920.
18. Paripovic, D.; Hall-Bozicb, H.; Klok, H.-A., Osteoconductive surfaces generated from peptide functionalized poly(2-hydroxyethyl methacrylate-co-2-(methacryloyloxy)ethyl phosphate) brushes. *J. Mater. Chem.* **2012,** *22*, 19570-19578.
19. Glinel, K.; Jonas, A. M. J.; Jouenne, T.; Leprince, J.; Galas, L.; Huck, W. T. S., Antibacterial and Antifouling Polymer Brushes Incorporating Antimicrobial Peptide. *Bioconjugate Chem.* **2009,** *20* (1), 71-77.
20. Milner, S. T., Polymer Brushes. *Science* **1991,** *251* (4996), 905-914.
21. Chen, W. Y.; Zheng, J. X.; Cheng, S. Z.; Li, C. Y.; Huang, P.; Zhu, L.; Xiong, H.; Ge, Q.; Guo, Y.; Quirk, R. P.; Lotz, B.; Deng, L.; Wu, C.; Thomas, E. L., Onset of tethered chain overcrowding. *Phys Rev Lett* **2004,** *93* (2), 028301.
22. Schuh, C.; Rühe, J., Penetration of Polymer Brushes by Chemical Nonidentical Free Polymers. *Macromolecules* **2011,** *44* (9), 3502-3510.
23. Schüwer, N.; Geue, T.; Hinestrosa, J. P.; Klok, H.-A., Neutron Reflectivity Study on the Postpolymerization Modification of Poly(2-hydroxyethyl methacrylate) Brushes. *Macromolecules* **2011,** *44*, 6868-6874.
24. Hensarling, R. M.; Rahane, S. B.; Leblanc, A. P.; Sparks, B. J.; White, E. M.; Locklin, J.; Patton, D. L., Thiol-isocyanate "click" reactions: Rapid development of functional polymeric surfaces. *Polym. Chem.* **2011,** *2* (1), 88-90.
25. Rahane, S. B.; Hensarling, R. M.; Sparks, B. J.; Stafford, C. M.; Patton, D. L., Synthesis of multifunctional polymer brush surfaces via sequential and orthogonal thiol-click reactions. *J. Mater. Chem.* **2012,** *22* (3), 932-943.
26. Beinhoff, M.; Frommer, J.; Carter, K. R., Photochemical Attachment of Reactive Cross-Linked Polymer Films to Si/SiO2 Surfaces and Subsequent Polymer Brush Growth. *Chem. Mater.* **2006,** *18* (15), 3425-3431.
27. Schuh, C.; Santer, S.; Prucker, O.; Rühe, J., Polymer Brushes with Nanometer-Scale Gradients. *Advanced Materials* **2009,** *21* (46), 4706-4710.
28. Nelson, A., Co-refinement of multiple-contrast neutron/X-ray reflectivity data using MOTOFIT. *Journal of Applied Crystallography* **2006,** *39*, 273-276.
29. Lokitz, B. S.; Wei, J.; Hinestrosa, J. P.; Ivanov, I.; Browning, J. F.; Ankner, J. F.; Kilbey, S. M.; Messman, J. M., Manipulating Interfaces through Surface Confinement of Poly(glycidyl methacrylate)-block-poly(vinyldimethylazlactone), a Dually Reactive Block Copolymer. *Macromolecules* **2012,** *45* (16), 6438-6449.
30. Soto-Cantu, E.; Lokitz, B. S.; Hinestrosa, J. P.; Deodhar, C.; Messman, J. M.; Ankner, J. F.; Kilbey Ii, S. M., Versatility of Alkyne-Modified Poly(Glycidyl Methacrylate) Layers for Click Reactions. *Langmuir* **2011,** *27* (10), 5986-5996.
31. Zhao, B.; Brittain, W. J., Polymer brushes: surface-immobilized macromolecules. *Prog. Polym. Sci.* **2000,** *25* (5), 677-710.
32. Edmondson, S.; Osborne, V. L.; Huck, W. T. S., Polymer brushes via surface-initiated polymerizations. *Chem. Soc. Rev.* **2004,** *33* (1), 14-22.

33. Xu, C.; Wu, T.; Mei, Y.; Drain, C. M.; Batteas, J. D.; Beers, K. L., Synthesis, and Characterization of Tapered Copolymer Brushes via Surface-Initiated Atom Transfer Radical Copolymerization. *Langmuir* **2005,** *21* (24), 11136-11140.
34. Kuan, W.-F.; Roy, R.; Rong, L.; Hsiao, B. S.; Epps, T. H., Design, and Synthesis of Network-Forming Triblock Copolymers Using Tapered Block Interfaces. *ACS Macro Lett.* **2012,** *1* (4), 519-523.
35. Roy, R.; Park, J. K.; Young, W.-S.; Mastroianni, S. E.; Tureau, M. v. S.; Epps, T. H., Double-Gyroid Network Morphology in Tapered Diblock Copolymers. *Macromolecules* **2011,** *44* (10), 3910-3915.

3.7 Appendix Controlled Heterogeity of Tapered Block Copolymer Brush Via Post-Polymerization Modification

Table A.1

Mass Density of Monomers and Polymers

Name	**Mass Density (ρ, g/cm^3)**
NCOMA	1.098
pNCOMA	1.260a
PPT	0.820
d7-PPT	0.919a
DDT	0.845
D25-DDT	0.950a
pNCOMA-d7-PPT	1.162a
pNCOMA-d25-DDT	1.024a
MMA	0.940
pMMA	1.180
ethyl methacrylate (EMA)	0.917
pEMA	1.110
propyl methacrylate (PMA)	0.902
pPMA	1.080
butyl methacrylate (BMA)	0.894
pBMA	1.070

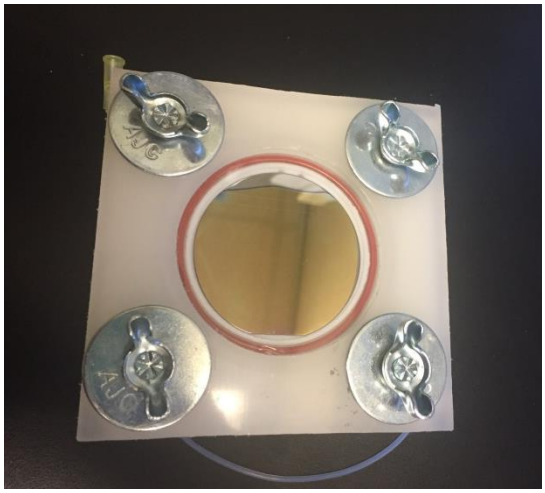

Figure A.1 Microchannel reactor for the polymerization of 2-inch wafers.

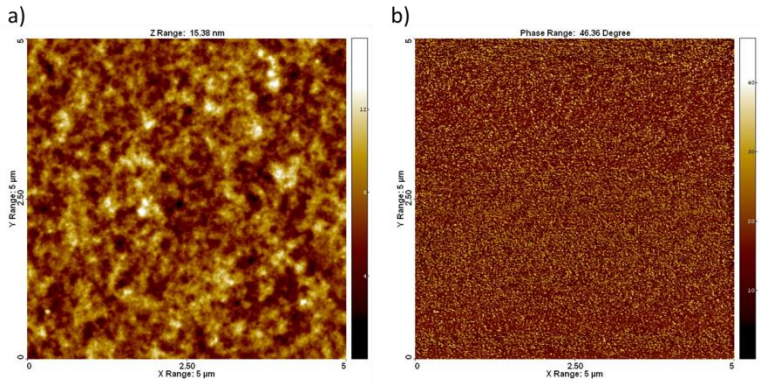

Figure A.2 AFM images (5×5 µm) of unmodified pNCOMA brush; a) height and b) phase.

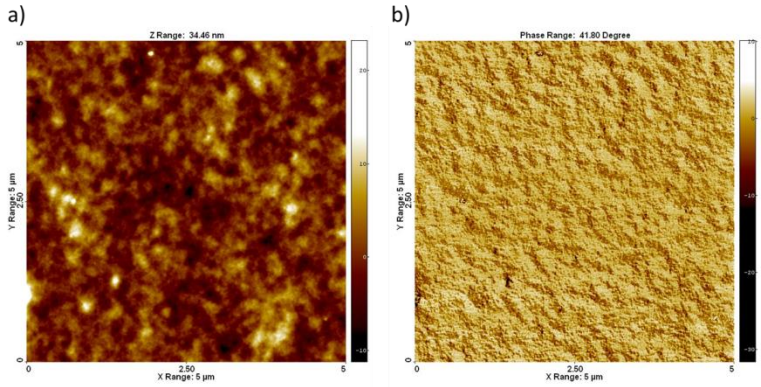

Figure A.3 AFM images (5×5 µm) of d_7-PPT modified pNCOMA brush; a) height and b) phase.

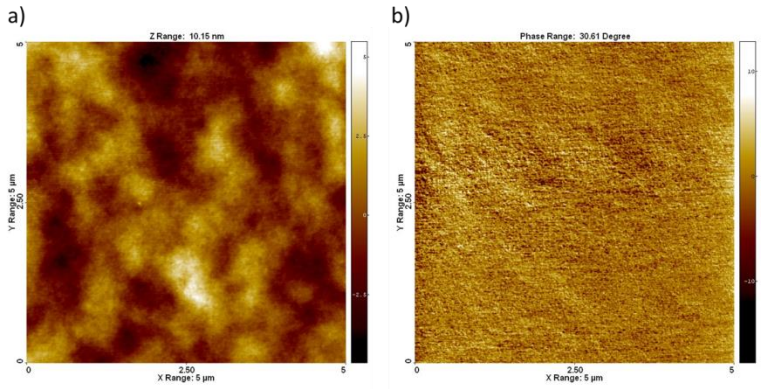

Figure A.4 AFM images (5×5 μm) of d_{25}-DDT modified pNCOMA brush; a) height and b) phase.

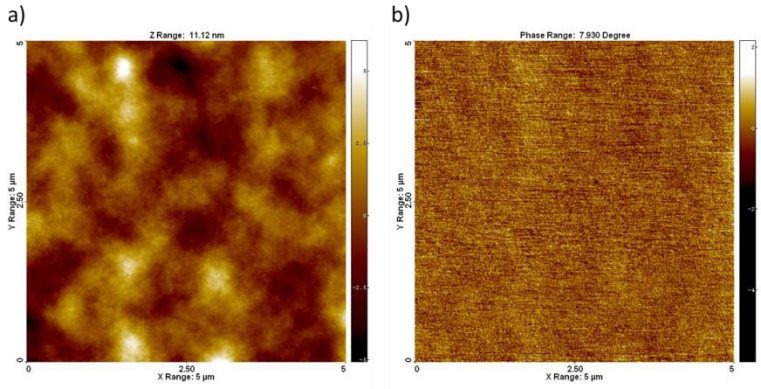

Figure A.5 AFM images (5×5 μm) of sequentially modified pNCOMA brush with d_{25}-DDT and d_7-PPT; a) height and b) phase.

Table A.2

RMS Roughness Measurements

Roughness Measurements from AFM	
Layer	**RMS Roughness (nm)**
unmodified pNCOMA	1.61 ± 0.2
modified pNCOMA-d_7-PPT	2.75 ± 0.4
modified pNCOMA-d_{25}-DDT	1.05 ± 0.2
Tapered block copolymer – d_{25}-DDT/d_7-PPT	1.01 ± 0.2

CHAPTER IV – AN EFFICIENT ROUTE TOWARD PENDENT THIOL POLYMER BRUSH SURFACE AND POST-POLYMERIZATION MODIFICATION PLATFORM

4.1 Introduction

Engineering polymer brush surfaces with desired chemical functionality is of great interests in various applications.[1-4] Two strategies have been developed to fabricate functionalized polymer brush surfaces, including i) direct polymerization of monomers containing the desired functional moieties as pendent groups, and ii) postpolymerization modification (PPM) of the polymer brush. The direct polymerization method, while seemingly straightforward, is limited by the intrinsic intolerance of monomers carrying reactive functional groups with various polymerization mechanisms and conditions (e.g. thiol and radical polymerization). To address the disadvantages of the direct polymerization method, the PPM approach is often preferred.[5] In the PPM approach, monomers carrying chemoselective moieties that are unreactive or inert under polymerization conditions are first subjected to surface-initiated polymerization to incorporate these moieties into the polymer brush structure. Using the initially inert chemical moieties as reactive handles for further modifications, the PPM method enables the versatile and modular transformation of physical and chemical properties of surfaces via efficient modification chemistries. PPM of polymer brushes are based on reactions with high efficacy such as amidation of active esters,[6-8] copper catalyzed azide-alkyne cycloaddition (CuAAC),[9-11] epoxy ring opening reactions,[12-14] Diels-Alder cycloadditions,[15-22] nitroxide photoclick reactions,[23] and thiol-based reactions.[24]

Thiols are versatile functional groups that react with a wide range of functional groups such as alkenes,[21-22, 25-28] alkynes,[26, 29-30] isocyanates,[31] epoxides,[32] and

halogens.[33-35] These thiol-based reactions provide an efficient and modular strategy towards engineering multifunctional surfaces.[36-38] Specifically, thiol-ene reactions exhibit high efficiency and rapid reaction rates in the presence of O_2 and moisture at room temperature.[39-41] Immobilizing thiols onto the polymer brush as pendent reactive handles opens the door to the wide range of acrylates, methacrylates, and maleimides as modifiers – all of which are capable of carrying libraries of additional functionality that can be exploited for potential applications.

The integration of thiols as functional groups on polymer brush platforms has been a challenging task due to the intrinsic reactivity of thiols (e.g. large chain transfer constants) under radical polymerization conditions. The synthesis of polymers with polyfunctional thiols often requires protection/deprotection reactions under harsh conditions that can damage the polymer brush surface (conversion of bromo groups to thioesters followed with reflux under basic conditions).[42-43] Recently, our group reported a method of fabricating polymer brush surfaces containing pendent polyfunctional thiols as a PPM platform using a pre-synthesized modifier that contains a photo-caged thiol moiety. The method required pre-synthesis of the protected thiol modifier and the deprotection step involved a number of side reactions and byproducts which limited its potential application.[44]

In this chapter, we report a straightforward approach that utilizes cystamine-modified poly(styrene-alt-maleic anhydride) (pSMA) brush to prepare polymer brush surfaces containing pendent polyfunctional thiols along the polymer chain as a PPM platform for further thiol-ene modifications. Furthermore, the pSMA brush itself was

found to be a modular and versatile platform for PPM via efficient amine-anhydride reactions that endow the brush surface with a broad range of functionalities.

4.2 Experimental Section

4.2.1 Materials

Maleic anhydride, acetonitrile, cystamine dihydrochloride, triethylamine, tris(2-carboxylethyl) phosphine hydrochloride (TCEP), phosphate-buffered saline (PBS) buffer solution, propylamine, allylamine, propargylamine, dopamine hydrochloride, N-methylmaleimide, N-phenylmaleimide, poly(ethylene glycol) methacrylate (PEGMA, MW 360) and 1,8-diazabicyclo(5.4.0)undec-7-ene (DBU) were purchased from Sigma-Aldrich and used as received. Aminopropylisobutyl POSS was purchased from Hybrid Plastics and used as received. Styrene was purchased from Sigma-Aldrich and was purified by passing through an alumina column to remove inhibitor before use. Silicon wafers (orientation <100>, native oxide) were purchased from University Wafer. Plasma cleaning of the silicon substrates was done using a plasma cleaner from Harrick Plasma with air as the feed gas. An azo-based trichlorosilane initiator for surface-initiated polymerization was synthesized according to literature procedures.[45-46]

4.2.2 Instrumentation and Characterization

Ellipsometry measurements were carried out using a Gartner Scientific Corporation LSE ellipsometer with a 632.8 nm laser at 70° from the normal. Multiple thickness measurements were taken for each sample to better estimate the estimate the uncertainty in the measurements. Grazing angle attenuated total reflection FTIR (gATR-FTIR) analysis was carried out using a Thermo Scientific FTIR (Nicolet 8700) equipped with a VariGATR™ accessory (grazing angle 65°, germanium crystal; Harrick

Scientific). Spectra were collected with a resolution of 4 cm^{-1} by accumulating a minimum of 128 scans per sample. All spectra were collected while purging the VariGATR™ attachment and FTIR instrument with nitrogen along the infrared beam path to minimize the peaks corresponding to atmospheric moisture and CO_2. Spectra were analyzed and processed using Omnic software. Static water contact angles of polymer brush surfaces were measured using 6 μL water droplets on a Rame-hart goniometer. See Table B1 in the Appendix for water contact angle measurements.

4.2.3 Cleaning of Silicon Substrates

Silicon wafers were cut into 1.2 cm × 1.2 cm pieces. Diced wafers were cleaned sequentially in DI water, ethanol, THF, and toluene under ultrasonication and dried using nitrogen. Cleaned wafers were transferred to plasma cleaner and were exposed to plasma radiation for 15 min. The cleaned substrates were stored in an oven at 120 °C before functionalization.

4.2.4 Immobilization of Initiator onto Silicon Substrates

Cleaned silica substrates were transferred into dry, septum-sealed test tubes containing a toluene solution of initiator (4 mmol, 13 mL) and triethylamine (0.2 mL) and were allowed to react for 45 min. Substrates were then rinsed and sonicated in toluene and dried under a stream of nitrogen. If not used immediately, initiator functionalized substrates were stored in the dark at -20 °C in toluene.

4.2.5 Surface-Initiated Polymerization of pSMA Brush

A substrate with the azo-based initiator was placed in a sealed test tube and purged with nitrogen. In a separate Schlenk tube, styrene (1.0 mL, 0.91 g, 8.7 mmol) and maleic anhydride (1.0 g, 10.2 mmol) were dissolved in anhydrous acetonitrile (10.0

mL) and the solution was subjected to three freeze-pump-thaw cycles to remove oxygen. For each polymerization, 1.5 mL of the degassed monomer solution was then transferred via cannula into the test tube containing the substrate. The SMA solution containing the initiator-functionalized substrate was heated at 95 °C for various times to obtain polymer brushes of different thickness. After polymerization, pSMA brush modified substrates were removed from the reaction solution and cleaned by repeated rinsing and ultrasonication in acetonitrile to remove any physically adsorbed polymers from the surface. Brush samples were finally dried with nitrogen.

4.2.6 PPM of pSMA Brush with Cystamine Dihydrochloride

Cystamine dihydrochloride (40 mg, 0.178 mmol) and triethylamine (50 μL, 36.3 mg, 0.359 mmol) were dissolved in 4.0 mL of solvent mixture that contained 50% DI water and 50% acetonitrile. A pSMA brush substrate was placed in the cystamine solution for 20 min at room temperature to ensure high anhydride conversion. The postmodified substrates were thoroughly rinsed using DI water and dried with nitrogen.

4.2.7 Reduction of Cystamine Modified pSMA Brush

A substrate with cystamine postmodified pSMA brush was placed in a solution of TCEP (60 mg, 0.21mmol) in 6 mL of acetonitrile: PBS solvent mixture (50:50 by volume) in a sealed test tube. The TCEP solution containing the cystamine postmodified pSMA brush substrate was under constant nitrogen purging for 16 h. The substrate was then removed, rinsed thoroughly using DI water, and dried with nitrogen.

4.2.8 PPM of Thiol Pendent Polymer Brush with N-Methylmaleimide

A silicon substrate with reduced cystamine-modified pSMA brush was placed in an acetonitrile solution of N-methylmaleimide (0.15 mol/L) and DBU (0.022 mol/L) for

72 hours at room temperature. The substrate was then removed, rinsed thoroughly using acetonitrile, and dried with nitrogen.

4.2.9 PPM of Thiol Pendent Polymer Brush with N-Phenylmaleimide

Silicon substrate with reduced cystamine-modified pSMA brush was placed under an acetonitrile solution of *N*-phenylmaleimide (0.096 mol/L) and DBU (0.022 mol/L) for 72 hours at room temperature. The substrate was then removed, rinsed thoroughly using acetonitrile, and dried with nitrogen.

4.2.10 PPM of Thiol Pendent Polymer Brush with Poly(ethylene glycol) methacrylate

Silicon substrate with reduced cystamine-modified pSMA brush was placed under an acetonitrile solution of poly(ethylene glycol) methacrylate (PEGMA, MW 360, 0.50 mol/L) and DBU (0.067 mol/L) for 72 hours at room temperature. The substrate was then removed, rinsed thoroughly using DI water, and dried with nitrogen.

4.2.11 PPM of pSMA Surfaces Using Propylamine

Silicon substrate with pSMA brush was placed under acetonitrile solution of propylamine (0.12 mol/L) for 20 min at room temperature to allow near quantitative conversion. The substrate was then removed, rinsed thoroughly using acetonitrile, and dried with nitrogen.

4.2.12 PPM of pSMA Surfaces Using Allylamine

Silicon substrate with pSMA brush was placed under acetonitrile solution of allylamine (0.13 mol/L) for 20 min at room temperature to allow near quantitative conversion. The substrate was then removed, rinsed thoroughly using acetonitrile, and dried with nitrogen.

4.2.13 PPM of pSMA Surfaces Using Propargylamine

Silicon substrate with pSMA brush was placed under acetonitrile solution of propargylamine (0.16 mol/L) for 20 min at room temperature to allow near quantitative conversion. The substrate was then removed, rinsed thoroughly using acetonitrile, and dried with nitrogen.

4.2.14 PPM of pSMA Surfaces Using Aminopropyilsobutyl POSS

Silicon substrate with pSMA brush was placed under acetonitrile solution of aminopropylisobutyl POSS (0.057 mol/L) for 120 min at 50 °C. The substrate was then removed, rinsed thoroughly using acetonitrile, and dried with nitrogen.

4.2.15 PPM of pSMA Surfaces Using Dopamine Hydrochloride

Silicon substrate with pSMA brush was placed under a 50:50 water/acetonitrile solution of dopamine HCl (0.053 mol/L) and TEA (0.053 mol/L) for 30 min at room temperature. The substrate was then removed, rinsed thoroughly using DI water, and dried with nitrogen.

4.3 Results and Discussion

4.3.1 Synthesis of Styrene/Maleic Anhydride Polymer Brushes

Scheme 4.1 shows the general approach for initiator immobilization on the surface and synthesis of pSMA brushes via surface-initiated polymerization. First, an asymmetric trichlorosilyl-functionalized azo initiator was attached to the hydroxylated surface of the silicon substrates. Ellipsometry measurements of the initiator modified substrates indicated the average thickness of the initiator layer was 1.6 ± 0.1 nm. Conventional free radical polymerization was employed because it is a simple and well-studied route to polymer brush surfaces. The initiator functionalized substrates were

immersed into a nitrogen purged septum-sealed reaction tubes containing degassed monomer solution. Polymerizations were carried out at 95 °C using a 54:46 mole ratio of styrene: maleic anhydride in acetonitrile as the monomer feed. Based on the reactivity ratios of these monomers, polymer brushes with an alternating copolymer structure can be expected; however, the copolymer structure is not critical for the current work. To the best of our knowledge, this is the first report of styrene/maleic anhydride polymer brushes synthesized by surface-initiated polymerization.

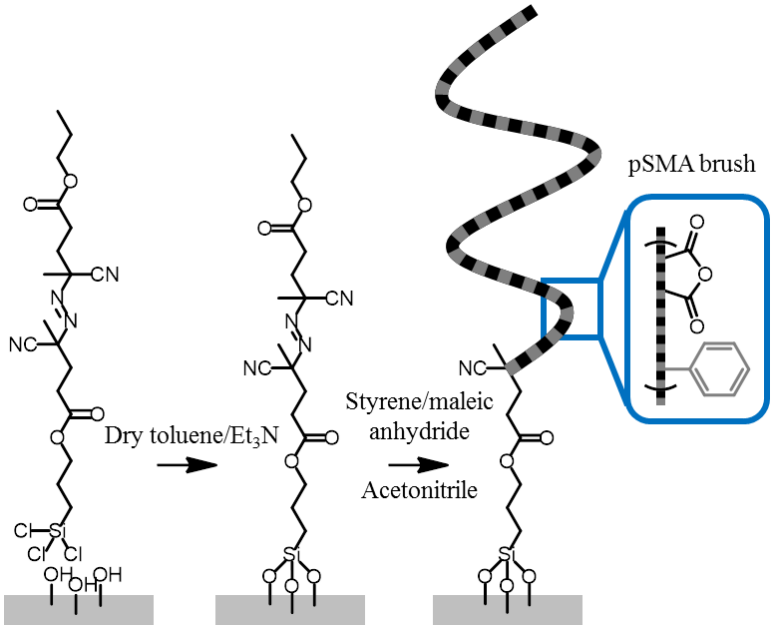

Scheme 4.1 Synthesis approach for initiator immobilization and surface-initiated radical polymerization of pSMA brush.

The polymer brush thickness can be tuned by polymerization time as shown in Figure 4.1. The brush thickness values were measured by ellipsometry. For most experiments, polymer brushes with a target thickness of 85±7 nm were synthesized unless otherwise specified. The chemical composition of the pSMA polymer brush was characterized using gATR-FTIR. Figure 4.2a shows the FTIR spectrum for pSMA with peaks at 1857 cm^{-1} and 1781 cm^{-1} attributed to the carbonyl on the five-membered ring of

the maleic anhydride.[47-48] Peaks at 1494 cm^{-1} and 1454 cm^{-1} correspond to the aromatic – C-H stretch of styrene.

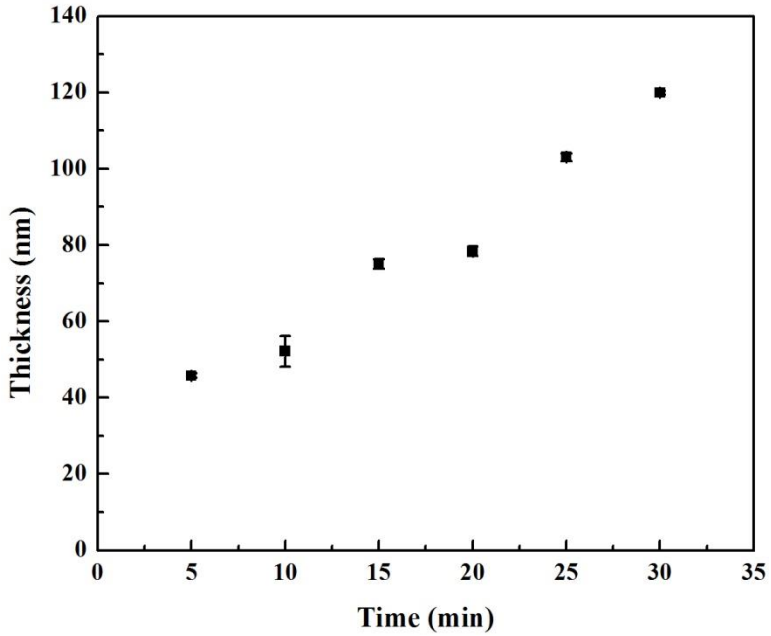

Figure 4.1 The thickness of pSMA brush versus polymerization time.

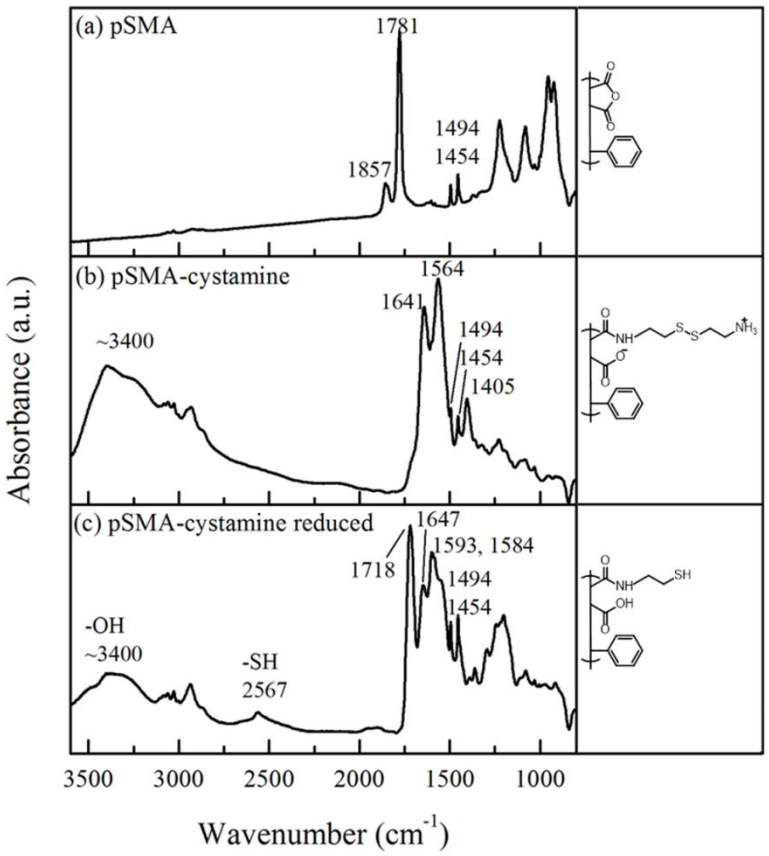

Figure 4.2 gATR-FTIR of (a) pSMA brush (b) cystamine-modified pSMA brush and (c) cystamine-modified pSMA after reduction.

4.3.2 Postpolymerization Modification (PPM) of pSMA with Cystamine Dihydrochloride

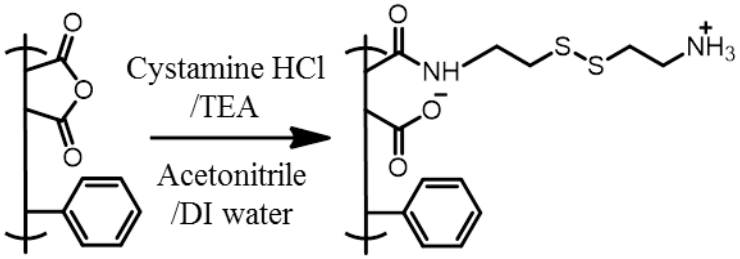

Scheme 4.2 Cystamine modification of pSMA brush under good solvent conditions.

According to Scheme 4.2, pSMA brushes were reacted with cystamine dihydrochloride in the presence of trimethylamine under good solvent conditions (acetonitrile: water, 1:1 by volume). Cystamine modification of pSMA brush yielded

amide/carboxylate salt moieties along the backbone and partially crosslinked the polymer brush. The FTIR spectrum of the cystamine-modified pSMA brush is shown in Figure 4.2b. The disappearance of the characteristic carbonyl peaks of the maleic anhydride in the IR spectrum indicates the total consumption of maleic anhydride during the PPM. The peak at 1641 cm^{-1} corresponds to amide groups. The peaks at 1564 cm^{-1} and 1405 cm^{-1} correspond to carboxylate salt moieties.

The thickness values of pSMA brush samples before and after cystamine modification were measured using ellipsometry and the results are summarized in Table 1. The modification of the pSMA brush with cystamine increases the molar mass of the repeat units and results in an increase in brush thickness. Equation 1 describes the relationship between polymer brush thickness, *T*, molecular weight of polymer repeat unit, *M*, and the mass density, ρ, of polymer brush before and after modification, [49]

$$\frac{T_2}{T_1} = \frac{M_2 \rho_1}{M_1 \rho_2} \qquad \text{Equation 1}$$

where the subscripts 1 and 2 denote the unmodified and cystamine-modified polymer brush, respectively. Assuming equivalent mass density of the polymer brush before and after postmodification, Equation 1 becomes Equation 2, where *k* represents conversion and M_{PPM} denotes the molecular weight of the modifier that reacts onto the polymer chain, respectively.

$$\frac{T_2}{T_1} = \frac{M_2}{M_1} = \frac{M_1 + kM_{PPM}}{M_1} \text{Equation 2}$$

At full conversion, (k=100%), the molecular mass of modifier, M_{PPM}, was calculated to be 135.06 g/mol, based on Equation 2. The calculated M_{PPM} is less than the molecular weight of cystamine (152.28 g/mol) which can be attributed to the cystamine

molecules that react with polymer brush by two amines. The percentage of cystamine as crosslinker, *x*, was calculated to be 12.7%, following Equation 3 in which $M_{cystamine}$ is the MW of cystamine (152.28 g/mol).

$$x = \frac{M_{cystamine} - M_{PPM}}{M_{PPM}} \quad \text{Equation 3}$$

The anhydride conversion *k* can be calculated according to Equation 4 and the results are shown in Table 1. (See Appendix for the estimation of conversion uncertainty).

$$k = \frac{M_1}{M_{PPM}}\left(\frac{T_2}{T_1} - 1\right) \quad \text{Equation 4}$$

Table 4.1

Thickness and conversion of cystamine-modified pSMA brush

Time (s)	Before PPM (nm)	After PPM (nm)	Conversion (%)
7	82.3±1.2	116.7±0.3	62.5±4.2
10	79.8±0.8	118.3±0.6	72.2±4.1
15	82.8±0.1	126.7±0.9	79.5±3.8
20	82.3±0.3	130.7±0.8	88.0±4.2
30	81.1±0.3	131.7±0.6	93.5±4.5
45	75.0±0.6	123.3±0.4	96.5±5.1
60	76.3±0.6	125.5±1.0	96.6±4.8
1200	92.7±0.9	154.7±1.6	100.0±5.7

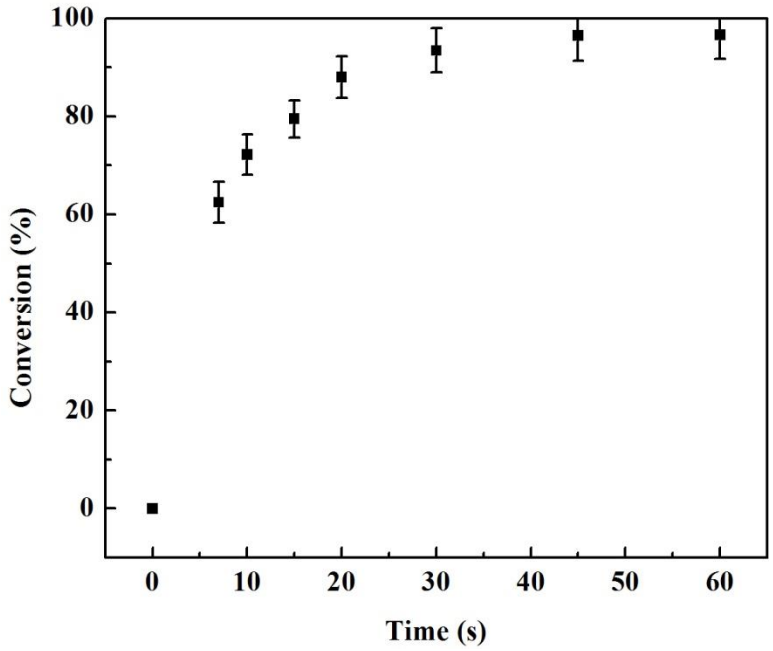

Figure 4.3 Anhydride conversion (k) versus time for the cystamine PPM of pSMA brushes (≈ 80 nm initial thickness) under good solvent conditions**.**

The intrinsic rate of the maleic anhydride-cystamine reaction was observed to be extremely fast under good solvent conditions, as shown in Figure 4.3. The anhydride conversion versus time plot for PPM of an 80 nm pSMA brush showed that 72% conversion was achieved within 10 s and near 97% conversion was reached within 60 s. The rate of the PPM reaction can be written as Equation 5 in which *t* is the reaction time, [*A*] and [*C*] represent the number of maleic anhydride units accessible to the PPM solution and cystamine concentration, respectively.

$$-\frac{d[A]}{dt} \sim [A] * [C] \text{Equation}$$

In the PPM reaction of the pSMA polymer brush, cystamine concentration in the solution is in large excess compared to the concentration of anhydride groups on the surface, so [*C*] can be assumed to be constant over time and thus the reaction rate depends only on the anhydride concentration [*A*]. As a result, the PPM of the pSMA

polymer brush under good solvent conditions should follow pseudo-first-order kinetics, as shown by Equation 6, where $[A_0]$ is the number of anhydride groups before PPM, *t* is reaction time and *S* is the apparent reaction rate constant. At a given reaction time, *t*, [*A*] can be expressed by Equation 7 where *k* is the anhydride conversion. Equation 6 can be rewritten as shown by Equation 8.

$$ln[A] = ln[A_0] - St \quad \text{Equation 6}$$

$$[A] = [A_0] * (1 - k) \quad \text{Equation 7}$$

$$\text{-}ln(1 - k) = St \text{Equation 8}$$

As shown in Figure 4.4, fitting the data (from 0 to 30 s) to a pseudo-first-order limited equation (Equation 8) yielded a plot with varying slopes, indicating that the apparent reaction rate constant decreased over time. The decrease of the apparent reaction rate constant at longer reaction time (and at higher conversion) can be attributed to additional diffusion barrier caused by PPM. As the cystamine modification adds more mass onto the polymer chains, polymer brush thickness increases. At higher conversion, cystamine molecules in solution must further diffuse into the polymer brush in order to functionalize the buried anhydride sites closest to the substrate surface and the PPM enters a 'diffusion resistance regime'.[50] The PPM of the polymer brush in the 'diffusional resistance regime' remains pseudo-first-order but proceeds at a reduced reaction rate. The reaction rate of cystamine modification of pSMA brush reduced from 0.132 s^{-1} to 0.074 s^{-1} after entering the diffusional resistance regime. Similarly, Orski *et al.* observed a polymer brush functionalization with slowed reaction rate due to diffusion limitations[51].

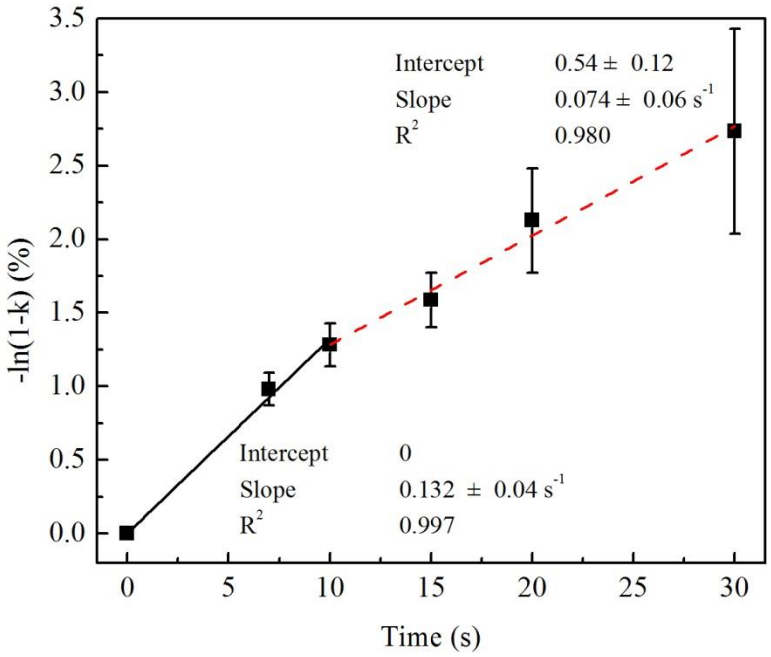

Figure 4.4 Pseudo-first-order limited plot of cystamine PPM of pSMA brush of 80 nm under good solvent conditions where k represents the anhydride conversion.

The slopes of the first and second stages are 0.132 s^{-1} and 0.074 s^{-1}, respectively.

4.3.3 Reduction of Cystamine Modification of pSMA brushes

Upon exposure the pSMA-cystamine brush in TCEP solution under a nitrogen environment, the disulfide linkage was reduced to thiol groups.(Scheme 4.3a) Figure 4.2c shows the FTIR spectrum of the reduced pSMA-cystamine brush and the peak at 2567 cm^{-1} of the –SH group confirms the formation of polyfunctional thiols along the backbone. The decrease of polymer brush thickness after cystamine reduction was mainly due to the mass loss of cystamine moieties that only reacted with the polymer brush by one amine. Assuming constant polymer brush mass density, the conversion of polymer pendent thiol was calculated as 87.2±3.2 %.

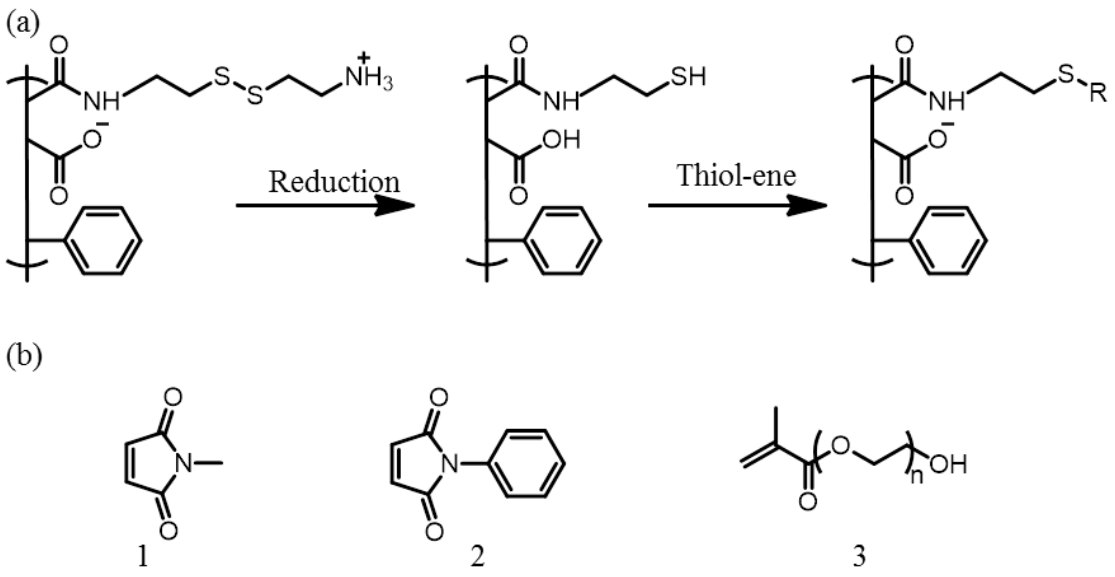

Scheme 4.3 (a) Reduction of cystamine-modified pSMA brush and subsequent thiol-ene reaction and (b) commercially available maleimides and methacrylate used for PPM: 1) *N*-methylmaleimide, 2) *N*-phenylmaleimide, 3) poly(ethylene glycol) methacrylate.

The pendent thiols exposed along the polymer brush after reduction serve as reactive handles for facile modification using various thiol-mediated reactions. Scheme 4.3 shows the approach towards sequential postmodification of the thiol groups via base-catalyzed thiol-ene reactions using a series of maleimides (*N*-methylmaleimide and *N*-phenylmaleimide) and poly(ethylene glycol) methacrylate. Specifically, the modifications were carried out using 1,8-diazabicyclo(5.4.0)undec-7-ene as the catalyst yielding a thioether as the product of the side-chain modification. Figure 4.5 shows the corresponding gATR-FTIR spectra of the thiol-ene modified polymer brush surfaces. With each modification, total disappearance of the thiol peak at 2567 cm^{-1} was observed. In Figure 4.5a, the peaks at 1774 cm^{-1} and 1695 cm^{-1} correspond to the carbonyl peaks on the characteristic five-membered ring of the maleimide. In Figure 4.5b, the peak at 1778 cm^{-1} and 1712 cm^{-1} corresponds to the carbonyl peaks on the maleimide ring. In Figure

4.5c, the peak at 1731 cm^{-1} and 1105 cm^{-1} correspond to the ester carbonyl group and the –C-O-C- linkages of PEGMA, respectively.

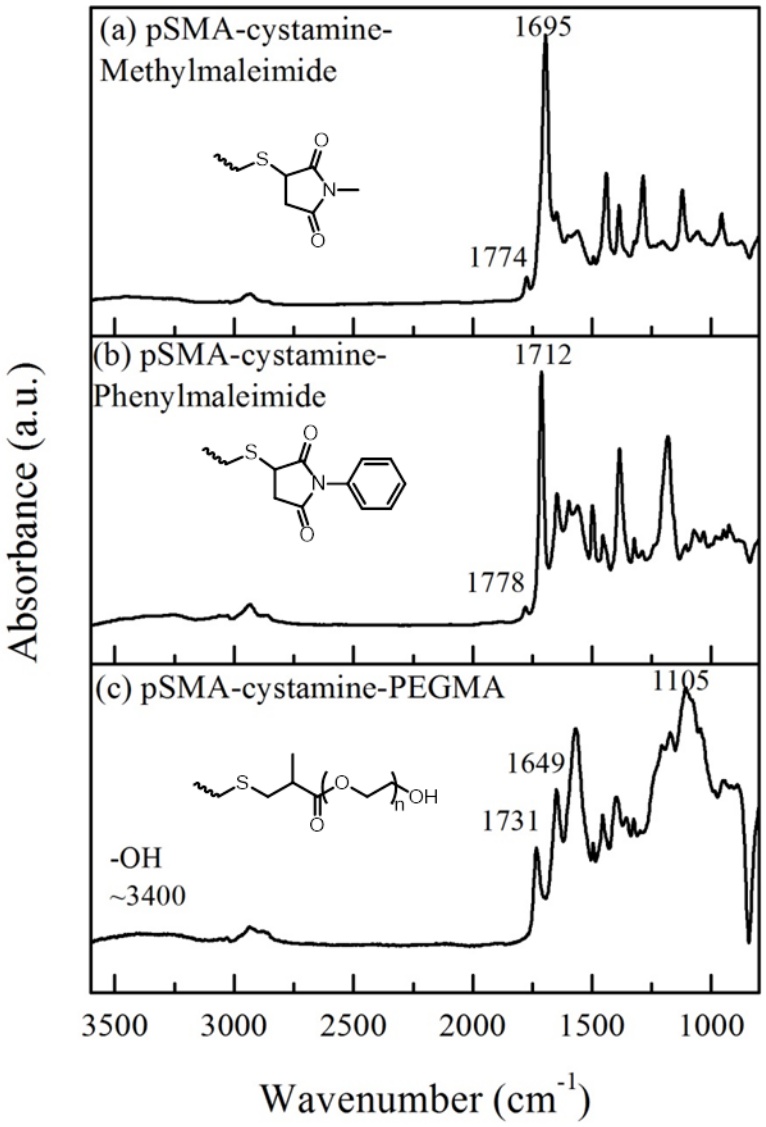

Figure 4.5 gATR-FTIR of (a) *N*-methylmaleimide, (b) *N*-phenylmaleimide, (c) poly(ethylene glycol) methacrylate modified reduced pSMA-cystamine polymer brush.

The thickness change was recorded and was used to estimate the overall conversion of each thiol-ene modification (Table 2). Modification of the pendent thiol with *N*-methylmaleimide and *N*-phenylmaleimide increased the brush thickness from 123.6 nm prior to modification to 170.9 and 190.7 nm, respectively, which indicates the

reaction approaches quantitative conversion of the thiol pendent polymer brush. The PEG-methacrylate modifier, with its large molecular weight and size, resulted in less than the quantitative conversion of the thiol pendent polymer brush due to sterically hindered penetration of the large modifier into the brush. The influence of modifier size and penetration into polymers thin film in the brush regime was well-described by Ruhe and coworkers[52]. These results illustrate cystamine modification of pSMA brushes as an efficient route to fabricate polymer brush surfaces containing polyfunctional thiol groups for subsequent thiol-ene modification.

Table 4.2

Thickness and conversion of thiol-ene modification reduced pSMA-cystamine brush

	Before PPM (nm)	After PPM (nm)	Conversion (%)
N-methylmaleimide	123.6±0.5	170.9±1.8	90.6±4.0
N-phenylmaleimide	123.6±0.5	190.7±1.2	85.3±2.2
PEG methacrylate	94.7±0.9	165.2±3.0	60.5±4.6

4.3.4 Postmodification of pSMA Brush Using Amines

As a final demonstration of the broad utility of the pSMA brush platform, we take advantage of the efficient anhydride-amine reaction as a simple and efficient route to generate functional surfaces. Scheme 4.4 shows the postmodification of pSMA brush using a number of commercially available amines. In order to achieve anhydride high conversion, amine modifications of pSMA brushes were conducted under good solvent conditions.

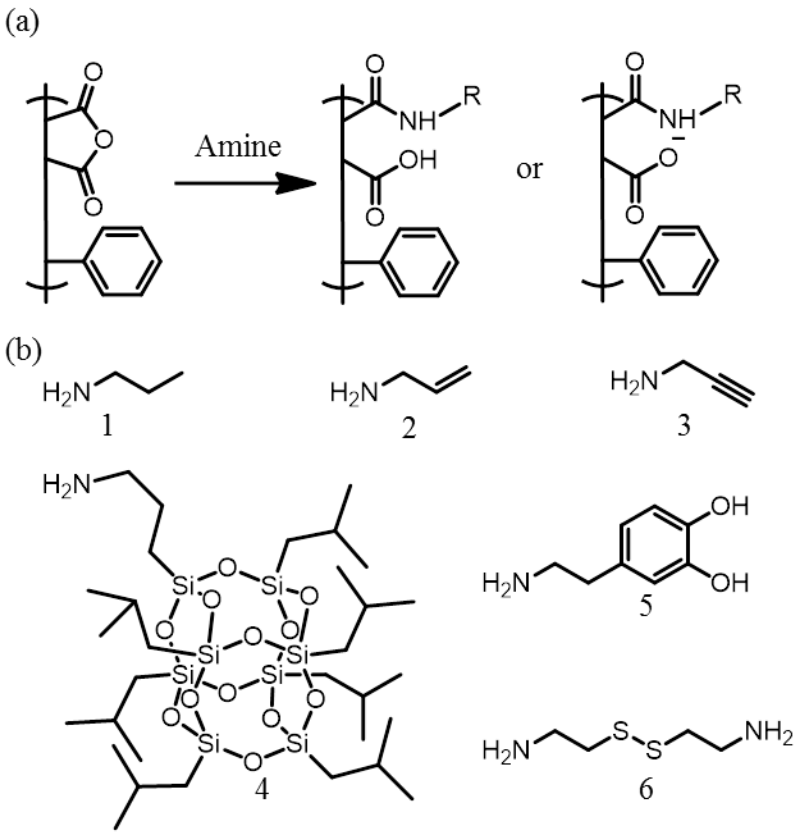

Scheme 4.4 .(a) Postmodification of pSMA brush using amines and (b) commercially available amines used for PPM: 1) propylamine, 2) allylamine, 3) propargylamine, 4) aminopropyl isobutyl POSS, 5) dopamine and 6) cystamine

Figure 4.6 shows the gATR-FTIR of the amine modified pSMA brush. In all five spectra, the anhydride peaks at 1857 cm^{-1} and 1781 cm^{-1} are no longer observed. In the spectra shown in Figure 4.6a, b, c, and e the carbonyl peaks of the carboxylic acid are observed at 1712~1716 cm^{-1}. Figure 4.6a shows the gATR-FTIR spectrum of the propylamine-modified pSMA brush with peaks at 2963 cm^{-1} and 2877 cm^{-1} correspond to the –C-H vibrations of methyl groups. Figure 4.6b shows the IR spectrum of allylamine modified pSMA brush with a peak at 919 cm^{-1} corresponds to the =C-H moiety. Figure 4.6c shows the IR spectrum of propargylamine modified pSMA brush with a characteristic peak at 2122 cm^{-1} corresponds to the ≡C-H vibration. Figure 4.6d shows

the IR spectrum of aminopropylisobutyl POSS modified pSMA brush with a very strong peak at 1103 cm^{-1} corresponds to the –Si-O- moiety that dwarfs other peaks. Figure 4.6e shows the IR spectrum of dopamine-modified pSMA brush with peaks at 1600 cm^{-1}, 1522 cm^{-1}, and 1453 cm^{-1} corresponds to the aromatic –C-H groups and a peak at 1115 cm^{-1} corresponds to the aromatic –OH group, respectively.

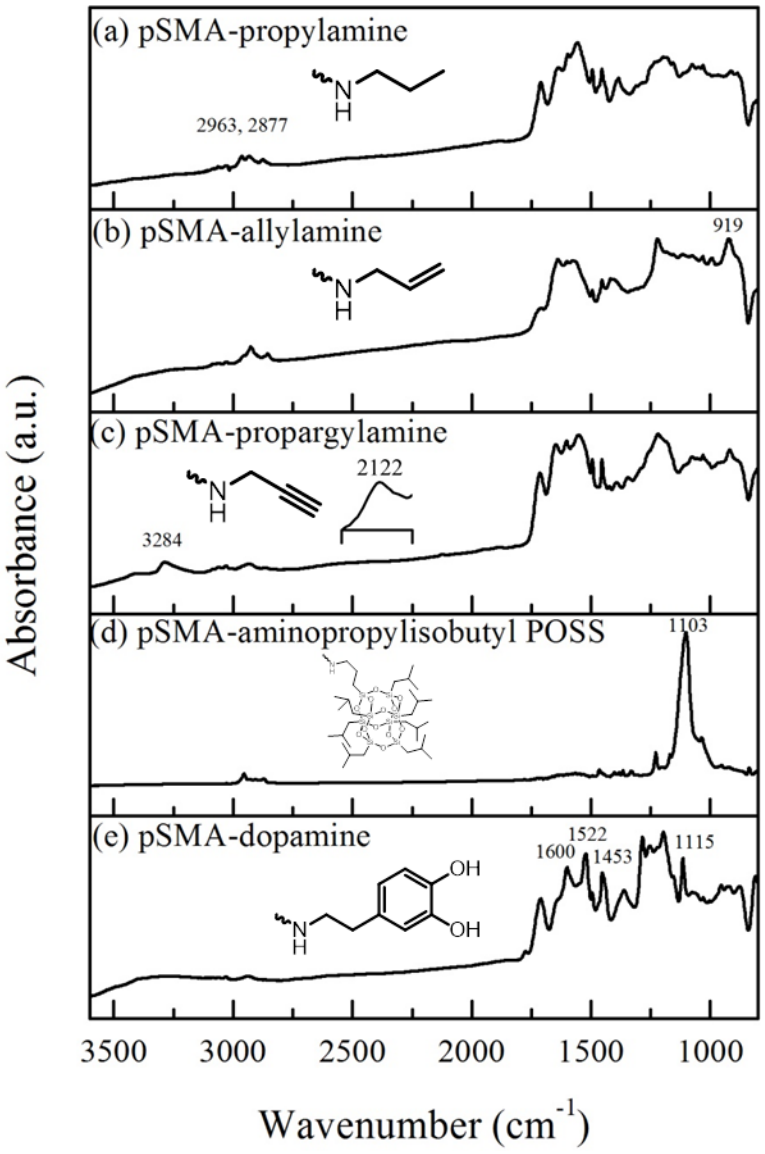

Figure 4.6 gATR-FTIR of postmodified pSMA brush by (a) propylamine, (b) allylamine, (c) propargylamine, (d) aminopropylisobutyl POSS and (e) dopamine hydrochloride

Upon addition of amines onto the polymer backbone, the brush thickness increases were measured using ellipsometry. For the amine modification reactions, all but aminopropylisobutyl POSS show high conversion (~90%). Aminopropylisobutyl POSS modified pSMA gave 62% conversion which can be attributed to the bulkiness of the POSS cage that inhibits the penetration into the polymer brush[52]. The thickness and conversion of amine modified pSMA brush samples are summarized in Table 3.

Table 4.3

Polymer brush thickness and conversion of amine modified pSMA brush

	Before PPM (nm)	After PPM (nm)	Conversion (%)
Propylamine	78.2±0.1	100.3±0.4	96.9±2.4
Allylamine	93.9±0.7	120.7±1.5	101.0±7.9
Propargylamine	78.4±0.3	99.2±0.5	97.1±3.5
Aminopropylisobutyl POSS	46.8±0.3	171.9±1.3	61.7±2.4
Dopamine	78.6±0.4	130.2±1.0	86.6±3.0

4.4 Conclusion

In this chapter, we showed that cystamine modification of pSMA brush surfaces can serve as a straightforward approach towards the fabrication of polymer brush surfaces containing pendent polyfunctional thiols for further thiol-ene modifications. Furthermore, the amine-maleic anhydride of pSMA brush was found to be very efficient so that the pSMA brush itself can be used as a modular and versatile platform for PPM with a broad range of functional amines.

4.5 References

1. Barbey, R.; Lavanant, L.; Paripovic, D.; Schüwer, N.; Sugnaux, C.; Tugulu, S.; Klok, H.-A., Polymer Brushes via Surface-Initiated Controlled Radical Polymerization: Synthesis, Characterization, Properties, and Applications. *Chemical Reviews* **2009,** *109* (11), 5437-5527.
2. Jain, P.; Baker, G. L.; Bruening, M. L., Applications of Polymer Brushes in Protein Analysis and Purification. *Annu Rev Anal Chem* **2009,** *2*, 387-408.
3. Ayres, N., Polymer brushes: Applications in biomaterials and nanotechnology. *Polym Chem-Uk* **2010,** *1* (6), 769-777.
4. Azzaroni, O., Polymer brushes here, there, and everywhere: Recent advances in their practical applications and emerging opportunities in multiple research fields. *J Polym Sci Pol Chem* **2012,** *50* (16), 3225-3258.
5. Galvin, C. J.; Genzer, J., Applications of surface-grafted macromolecules derived from post-polymerization modification reactions. *Prog Polym Sci* **2012,** *37* (7), 871-906.
6. Murata, H.; Prucker, O.; Ruhe, J., Synthesis of functionalized polymer monolayers from active ester brushes. *Macromolecules* **2007,** *40* (15), 5497-5503.
7. Orski, S. V.; Fries, K. H.; Sheppard, G. R.; Locklin, J., High-Density Scaffolding of Functional Polymer Brushes: Surface-Initiated Atom Transfer Radical Polymerization of Active Esters. *Langmuir* **2010,** *26* (3), 2136-2143.
8. Arnold, R. M.; Sheppard, G. R.; Locklin, J., Comparative Aminolysis Kinetics of Different Active Ester Polymer Brush Platforms in Postpolymerization Modification with Primary and Aromatic Amines. *Macromolecules* **2012,** *45* (13), 5444-5450.
9. Kolb, H. C.; Finn, M. G.; Sharpless, K. B., Click chemistry: Diverse chemical function from a few good reactions. *Angew Chem Int Edit* **2001,** *40* (11), 2004-+.
10. Wang, C.; Wu, J. A.; Xu, Z. K., High-Density Glycosylation of Polymer Membrane Surfaces by Click Chemistry for Carbohydrate-Protein Recognition. *Macromol Rapid Comm* **2010,** *31* (12), 1078-1082.
11. Zhang, S.; Vi, T.; Luo, K.; Koberstein, J. T., Kinetics of Polymer Interfacial Reactions: Polymer Brush Formation by Click Reactions of Alkyne End-Functional Polymers with AzideFunctional Substrates. *Macromolecules* **2016,** *49* (15), 5461-5474.
12. Lokitz, B. S.; Messman, J. M.; Hinestrosa, J. P.; Alonzo, J.; Verduzco, R.; Brown, R. H.; Osa, M.; Ankner, J. F.; Kilbey, S. M., Dilute Solution Properties and Surface Attachment of RAFT Polymerized 2-Vinyl-4,4-dimethyl Azlactone (VDMA). *Macromolecules* **2009,** *42* (22), 9018-9026.
13. Barbey, R.; Klok, H. A., Room-Temperature, Aqueous Post-Polymerization Modification of Glycidyl Methacrylate-Containing Polymer Brushes Prepared via Surface-Initiated Atom Transfer Radical Polymerization. *Langmuir* **2010,** *26* (23), 18219-18230.
14. Soto-Cantu, E.; Lokitz, B. S.; Hinestrosa, J. P.; Deodhar, C.; Messman, J. M.; Ankner, J. F.; Kilbey, S. M., Versatility of Alkyne-Modified Poly(Glycidyl Methacrylate) Layers for Click Reactions. *Langmuir* **2011,** *27* (10), 5986-5996.
15. Sun, X. L.; Stabler, C. L.; Cazalis, C. S.; Chaikof, E. L., Carbohydrate and protein immobilization onto solid surfaces by sequential Diels-Alder and azide-alkyne cycloadditions. *Bioconjugate Chem* **2006,** *17* (1), 52-57.

16. Dirlam, P. T.; Strange, G. A.; Orlicki, J. A.; Wetzel, E. D.; Costanzo, P. J., Controlling Surface Energy and Wettability with Diels-Alder Chemistry. *Langmuir* **2010,** *26* (6), 3942-3948.
17. Arumugam, S.; Popik, V. V., Patterned Surface Derivatization Using Diels-Alder Photoclick Reaction. *J Am Chem Soc* **2011,** *133* (39), 15730-15736.
18. Tasdelen, M. A., Diels-Alder "click" reactions: recent applications in polymer and material science. *Polym Chem-Uk* **2011,** *2* (10), 2133-2145.
19. Arumugam, S.; Orski, S. V.; Locklin, J.; Popik, V. V., Photoreactive Polymer Brushes for High-Density Patterned Surface Derivatization Using a Diels-Alder Photoclick Reaction. *J Am Chem Soc* **2012,** *134* (1), 179-182.
20. Pauloehrl, T.; Delaittre, G.; Winkler, V.; Welle, A.; Bruns, M.; Borner, H. G.; Greiner, A. M.; Bastmeyer, M.; Barner-Kowollik, C., Adding Spatial Control to Click Chemistry: Phototriggered Diels-Alder Surface (Bio)functionalization at Ambient Temperature. *Angew Chem Int Edit* **2012,** *51* (4), 1071-1074.
21. Gevrek, T. N.; Bilgic, T.; Klok, H. A.; Sanyal, A., Maleimide-Functionalized Thiol Reactive Copolymer Brushes: Fabrication and Post-Polymerization Modification. *Macromolecules* **2014,** *47* (22), 7842-7851.
22. Dubner, M.; Gevrek, T. N.; Sanyal, A.; Spencer, N. D.; Padeste, C., Fabrication of Thiol-Ene "Clickable" Copolymer-Brush Nanostructures on Polymeric Substrates via Extreme Ultraviolet Interference Lithography. *Acs Appl Mater Inter* **2015,** *7* (21), 11337-11345.
23. Mardyukov, A.; Li, Y.; Dickschat, A.; Schafer, A. H.; Studer, A., Chemical Modification of Polymer Brushes via Nitroxide Photoclick Trapping. *Langmuir* **2013,** *29* (21), 6369-6376.
24. Arumugam, S.; Popik, V. V., Attach, Remove, or Replace: Reversible Surface Functionalization Using Thiol-Quinone Methide Photoclick Chemistry. *J Am Chem Soc* **2012,** *134* (20), 8408-8411.
25. Jonkheijm, P.; Weinrich, D.; Koehn, M.; Engelkamp, H.; Christianen, P. C. M.; Kuhlmann, J.; Maan, J. C.; Nuesse, D.; Schroeder, H.; Wacker, R.; Breinbauer, R.; Niemeyer, C. M.; Waldmann, H., Photochemical surface patterning by the thiol-ene reaction. *Angew Chem Int Edit* **2008,** *47* (23), 4421-4424.
26. Wendeln, C.; Rinnen, S.; Schulz, C.; Arlinghaus, H. F.; Ravoo, B. J., Photochemical Microcontact Printing by Thiol-Ene and Thiol-Yne Click Chemistry. *Langmuir* **2010,** *26* (20), 15966-15971.
27. Cai, T.; Wang, R.; Neoh, K. G.; Kang, E. T., Functional poly(vinylidene fluoride) copolymer membranes via surface-initiated thiol-ene click reactions. *Polym Chem-Uk* **2011,** *2* (8), 1849-1858.
28. Madaan, N.; Terry, A.; Harb, J.; Davis, R. C.; Schlaad, H.; Linford, M. R., Thiol-Ene-Thiol Photofunctionalization of Thiolated Monolayers with Polybutadiene and Functional Thiols, Including Thiolated DNA. *J Phys Chem C* **2011,** *115* (46), 22931-22938.
29. Hensarling, R. M.; Doughty, V. A.; Chan, J. W.; Patton, D. L., "Clicking" Polymer Brushes with Thiol-yne Chemistry: Indoors and Out. *J Am Chem Soc* **2009,** *131* (41), 14673-+.

30. Wang, C.; Ren, P. F.; Huang, X. J.; Wu, J. A.; Xu, Z. K., Surface glycosylation of polymer membrane by thiol-yne click chemistry for affinity adsorption of lectin. *Chem Commun* **2011,** *47* (13), 3930-3932.
31. Hensarling, R. M.; Rahane, S. B.; LeBlanc, A. P.; Sparks, B. J.; White, E. M.; Locklin, J.; Patton, D. L., Thiol-isocyanate "click" reactions: rapid development of functional polymeric surfaces. *Polym Chem-Uk* **2011,** *2* (1), 88-90.
32. Gadwal, I.; Rao, J. Y.; Baettig, J.; Khan, A., Functionalized Molecular Bottlebrushes. *Macromolecules* **2014,** *47* (1), 35-40.
33. Rosen, B. M.; Lligadas, G.; Hahn, C.; Percec, V., Synthesis of Dendrimers Through Divergent Iterative Thio-Bromo "Click" Chemistry. *J Polym Sci Pol Chem* **2009,** *47* (15), 3931-3939.
34. Rosen, B. M.; Lligadas, G.; Hahn, C.; Percec, V., Synthesis of Dendritic Macromolecules Through Divergent Iterative Thio-Bromo "Click" Chemistry and SET-LRP. *J Polym Sci Pol Chem* **2009,** *47* (15), 3940-3948.
35. Xu, J. T.; Tao, L.; Boyer, C.; Lowe, A. B.; Davis, T. P., Combining Thio-Bromo "Click" Chemistry and RAFT Polymerization: A Powerful Tool for Preparing Functionalized Multiblock and Hyperbranched Polymers. *Macromolecules* **2010,** *43* (1), 20-24.
36. DeForest, C. A.; Anseth, K. S., Photoreversible Patterning of Biomolecules within Click-Based Hydrogels. *Angew Chem Int Edit* **2012,** *51* (8), 1816-1819.
37. Rahane, S. B.; Hensarling, R. M.; Sparks, B. J.; Stafford, C. M.; Patton, D. L., Synthesis of multifunctional polymer brush surfaces via sequential and orthogonal thiol-click reactions. *J Mater Chem* **2012,** *22* (3), 932-943.
38. Hensarling, R. M.; Patton, D. L., CHAPTER 12 Surface Engineering with Thiol-click Chemistry. In *Thiol-X Chemistries in Polymer and Materials Science*, The Royal Society of Chemistry: 2013; pp 259-285.
39. Hoyle, C. E.; Lowe, A. B.; Bowman, C. N., Thiol-click chemistry: a multifaceted toolbox for small molecule and polymer synthesis. *Chem Soc Rev* **2010,** *39* (4), 1355-1387.
40. Lowe, A. B., Thiol-ene "click" reactions and recent applications in polymer and materials synthesis. *Polym Chem-Uk* **2010,** *1* (1), 17-36.
41. Lowe, A. B., Thiol-ene "click" reactions and recent applications in polymer and materials synthesis: a first update. *Polym Chem-Uk* **2014,** *5* (17), 4820-4870.
42. Kihara, N.; Tochigi, H.; Endo, T., Synthesis and Reaction of Polymers Bearing 5-Membered Cyclic Dithiocarbonate Group. *J Polym Sci Pol Chem* **1995,** *33* (7), 1005-1010.
43. Kihara, N.; Kanno, C.; Fukutomi, T., Synthesis and properties of microgel bearing a mercapto group. *J Polym Sci Pol Chem* **1997,** *35* (8), 1443-1451.
44. Hensarling, R. M.; Hoff, E. A.; LeBlanc, A. P.; Guo, W.; Rahane, S. B.; Patton, D. L., Photocaged pendent thiol polymer brush surfaces for postpolymerization modifications via thiol-click chemistry. *Journal of Polymer Science Part A: Polymer Chemistry* **2013,** *51* (5), 1079-1090.
45. Patton, D. L.; Page, K. A.; Xu, C.; Genson, K. L.; Fasolka, M. J.; Beers, K. L., Measurement of reactivity ratios in surface-initiated radical copolymerization. *Macromolecules* **2007,** *40* (17), 6017-6020.

46. Guo, W.; Hensarling, R. M.; LeBlanc, A. L.; Hoff, E. A.; Baranek, A. D.; Patton, D. L., Rapid Synthesis of Polymer Brush Surfaces via Microwave-Assisted Surface-Initiated Radical Polymerization. *Macromol Rapid Comm* **2012,** *33* (9), 863-868.
47. Hasanzadeh, R.; Moghadam, P. N.; Samadi, N.; Asri-Rezaei, S., Removal of heavy metal ions from aqueous solution with nanochelating resins based on poly(styrene-alt-maleic anhydride). *Journal of Applied Polymer Science* **2013,** *127* (4), 2875-2883.
48. Marquardt, F.-H., The intensity of carbonyl bands in the infrared spectra of cyclic anhydrides of dicarboxylic acids. *Journal of the Chemical Society B: Physical Organic* **1966,** (0), 1242-1243.
49. Murata, H.; Prucker, O.; Ruhe, J., Synthesis of Functionalized Polymer Monolayers from Active Ester Brushes. *Macromolecules* **2007,** (40), 5497-5503.
50. Levenspiel, O., *Chemical reaction engineering*. Wiley: 1999.
51. Orski, S. V.; Sheppard, G. R.; Arumugam, S.; Arnold, R. M.; Popik, V. V.; Locklin, J., Rate Determination of Azide Click Reactions onto Alkyne Polymer Brush Scaffolds: A Comparison of Conventional and Catalyst-Free Cycloadditions for Tunable Surface Modification. *Langmuir* **2012,** *28* (41), 14693-14702.
52. Schuh, C.; Rühe, J., Penetration of Polymer Brushes by Chemical Nonidentical Free Polymers. *Macromolecules* **2011,** *44* (9), 3502-3510.

4.6 Appendix Styrene/Maleic Anhydride – An Efficient Route Toward Pendent Thiol Polymer Brush Surface and Post-Polymerization Modification Platform

Table A.3

Water contact angle measurements of pSMA before and after modification

Polymer brush	Water contact angle (degree)
pSMA	91.6±2.0
pSMA-cystamine	69.4±3.2
pSMA-cystamine reduced	65.6±3.0
pSMA-cystamine- N-methylmaleimide	63.8±1.0
pSMA-cystamine- N-phenylmaleimide	69.9±1.0
pSMA-cystamine- PEG methacrylate	36.9±1.0
Propylamine	71.9±1.3
Allylamine	71.1±1.0
Propargylamine	70.7±1.7
Aminopropylisobutyl POSS	106.2±2.2
Dopamine	72.7±2.1

Table A.4

Peak assignment of polymer brushes

Polymer Brush	Wavenumber cm^{-1}	
pSMA	1781, 1857	-C=O, maleic anhydride
	1454, 1494	-C-H, aromatic
pSMA-cystamine	1641	-C=O amide I -N-H amide II
	1564	$–COO^-$, carboxylate salt, asym
	1405	$–COO^-$, carboxylate salt, sym
	~3400	$-NH_3^+$
pSMA-cystamine reduced	1718	-C=O of –COOH
	1647	-C=O amide I -N-H, amide II
	1593, 1584	$–COO^-$, carboxylate salt, asym
	~3400	-OH
	2567	-S-H
pSMA-cystamime-methylmaleimide	1774, 1695	-C=O, maleimide
pSMA-cystamime-phenylmaleimide	1778, 1712	-C=O, maleimide
pSMA-cystamime- -PEGMA	1731	-C=O, ester
	1105	C-O-C, ether
	~3400	-O-H
pSMA-propylamine	2963, 2877	-C-H, methyl
pSMA-allylamine	919	$=CH_2$
pSMA-propargylamine	2122	-C≡C-
	3284	≡C-H
pSMA-aminopropylisobutyl POSS	1103	-Si-O-
pSMA-dopamine	1600, 1522, 1453	-C-H, aromatic
	1115	-O-H, aromatic

Uncertainty of *MPPM*

The molar mass of modifier moiety that reacts with polymer brush (M_{PPM}) at full conversion can be calculated based on Equation A1. In Equation A1 T_1 is the brush thickness before PPM, T_2 is the brush thickness after PPM, and M_1 is the molar mass of the polymer brush repeat unit, respectively.

$$M_{PPM} = M_1\left(\frac{T_2}{T_1} - 1\right) \text{Equation}$$

The uncertainty of M_{PPM} , ΔM_{PPM} can be calculated based on Equation A2.

$$\Delta M_{PPM} = \Delta\left(M_1\frac{T_2}{T_2}\right) = M_1\left(\frac{T_2}{T_1}\right)\sqrt{\left(\frac{\Delta T_2}{T_1}\right)^2 + \left(\frac{\Delta T_1}{T_2}\right)^2} \text{ Equation}$$

Uncertainty of Anhydride Conversion, k

The anhydride conversion, k can be calculated by Equation A3.

$$k = \frac{M_1}{M_{PPM}}\left(\frac{T_2}{T_1} - 1\right) \text{Equation}$$

For conversion calculations based on ΔM_{PPM}, the conversion uncertainty, Δk, can be described by Equation A4.

$$\Delta k = k * \sqrt{\left(\frac{\partial lnk}{\partial M_{PPM}}\right)^2 (\Delta M_{PPM})^2 + \left(\frac{\partial lnk}{\partial T_1}\right)^2 (\Delta T_1)^2 + \left(\frac{\partial lnk}{\partial T_2}\right)^2 (\Delta T_2)^2} \text{ Equation A4}$$

Combining Equation 4 and Equation A4, Δk can be expressed by Equation A5.

$$\Delta k = k * \sqrt{\left(\frac{\Delta M_{PPM}}{M_{PPM}}\right)^2 + \left(\frac{T_2}{T_1}\right)^2 (\frac{\Delta T_1}{T_2 - T_1})^2 + \left(\frac{\Delta T_2}{T_2 - T_1}\right)^2} \text{Equation A5}$$

For conversion calculations based on known M_{PPM} values (ΔM_{PPM} =0), the conversion uncertainty, Δk, can be described by Equation A6.

$$\Delta k = k * \sqrt{\left(\frac{\partial lnk}{\partial T_1}\right)^2 (\Delta T_1)^2 + (\frac{\partial lnk}{\partial T_2})^2 (\Delta T_2)^2} \text{Equation}$$

Combining Equation 4 and Equation A6, Δk can be expressed by Equation A7.

$$\Delta k = \frac{T_2}{T_1} * \frac{M_1}{M_{PPM}} * \sqrt{\left(\frac{\Delta T_1}{T_2}\right)^2 + \left(\frac{\Delta T_2}{T_1}\right)^2} \text{ Equation}$$

Uncertainty of –ln(1-k)

The uncertainty of –ln(1-k), Δ[–ln(1-k)],can be expressed by Equation A8.

$$\Delta[-\ln(1-k)] = \frac{\Delta k}{1-k} \text{ Equation A8}$$

CHAPTER V – BUCKLING INSTABILITIES IN POLYMER BRUSH SURFACES VIA POSTPOLYMERIZATION MODIFICATION

5.1 Introduction

Buckling instabilities are ubiquitous in soft materials and can be exploited to define the shape, morphology, and function of complex systems – as exemplified by nature in the wrinkling of skin[1] or folding of brain tissue.[2] Following nature's lead, strain-induced wrinkling of polymer thin films has emerged as a powerful bottom-up approach to engineer surfaces that exhibit complex ordered and disordered patterns at multiple length scales.[3] Recently, significant efforts have focused on exploiting this approach to create surfaces suitable for a range of applications, including advanced adhesion,[4-7] tunable wettability,[8-9] antifouling,[10-11] particle assembly,[12] stem cell growth/differentiation,[13] ultrasensitive pressure sensor,[14] stretchable electronics,[15-16] microlens arrays,[17] diffraction gratings,[18-19] microcontact printing,[20] maskless lithography,[21] open-channel microfluidics,[22] and among many others.[23-25]

Buckling instabilities in polymer films can be engineered using three primary film structures: layered, homogeneous, and gradient systems.[3, 23] In the prototypical example, surface wrinkling can occur from in-plane compression (i.e. mechanical, thermal or osmotic) of a bilayer composed of a thin, high modulus film bonded to a semi-infinite, low modulus substrate. The onset and wavelength of the wrinkles are dictated by the thickness of the top film and the film/substrate modulus ratio, whereas the wrinkle amplitude is related to applied strain. Researchers have demonstrated numerous methods to create thin film structure profiles that can buckle, including metal deposition,[18] UV/ozone oxidation,[26] photo-induced crosslinking,[27-28] and surface-grafting techniques,[29]

however, these methods have focused primarily on the fabrication of thin films with micro-scale morphologies on elastomeric substrates. Relatively few studies have focused on methods to induce buckling instabilities in ultrathin (i.e. <100 nm) polymer films attached to rigid substrates.[27, 30]

Postpolymerization modification (PPM) of polymer brushes – ultrathin assemblies of polymer chains densely grafted to a surface such that chains experience strong segmental repulsion and stretch perpendicular to the substrate – is a powerful platform for tailoring the chemical and mechanical properties of surfaces.[31] The extended chain conformation of brushes has specific implications for the PPM process, where the high osmotic pressure and reduced chain conformational entropy disfavor the penetration of reactive modifiers into the brush.[32-33] Thus, the penetration depth and the through-thickness compositional homogeneity of the brush resulting from the PPM process are ultimately dependent on i) the reaction conditions (solvent quality, reaction efficiency, and reaction time), ii) the tethered brush parameters (grafting density and thickness), and iii) the physical properties of the reactive modifier (molecular mass and steric bulk). Indeed, Klok *et al*. showed *via* neutron reflectometry[33] and XPS[34] that increases in brush thickness, grafting density, and molecular mass of the modifier result in decreased depths of penetration and increased vertical heterogeneity. Intentional manipulation of PPM parameters provides an opportunity to design brush structures with tunable crosslinking and swelling ratio that fulfill the requirements for nanoscale buckling within ultrathin films on rigid substrates but has rarely been reported.

Recently, Brooks *et al.*[35] reported the fabrication of nanoscale creases in ultrathin poly(pentafluorophenyl acrylate) (pPFPA) brushes on silicon substrates following PPM

of the pPFPA with an amine-terminated polymer under the confinement of microcontact printing (μCP). The PPM process increased the molecular weight of the brush resulting in osmotic swelling normal to the substrate surface. Confinement of the swollen brush under the stamp led to a critical in-plane stress, which was relieved via formation of creases. Brooks *et al.* demonstrated simple control over the crease morphology by varying the stamping pressure; however, the prerequisite of mechanical confinement to induce the buckling instability may limit the process to substrates with simple 2D geometries.

Herein, we report a simple PPM approach to engineer ultrathin poly(styrene-alt-maleic anhydride) (pSMA) brush surfaces with wrinkled morphologies, where the length scale of the buckled features can be tuned using PPM reaction time and conversion. PPM with a diamine modifier under poor solvent conditions for the brush limits crosslinking to the near surface region. This process yields a rigid-on-soft through-thickness brush profile that differentially swells under good solvent conditions leading to the buckling instability.

5.2 Experimental Section

5.2.1 Materials

Maleic anhydride (MA), acetonitrile, cystamine dihydrochloride, triethylamine, tris(2-carboxylethyl) phosphine hydrochloride (TCEP), propylamine, hexylamine, phosphate-buffered saline (PBS) solution and poly(styrene-maleic anhydride) polymer were purchased from Sigma-Aldrich and were used as received. Styrene (Sty) was purchased from Sigma-Aldrich and was purified by passing through an alumina column to remove inhibitor before use. Silica wafers (orientation <100>, native oxide) were

purchased from University Wafer. Plasma cleaning of silicon substrates was done on plasma cleaner from Harrick Plasma.

5.2.2 Instrumentation and Characterization

Ellipsometry measurements were carried out using a Gartner Scientific Corporation LSE ellipsometer with a 632.8 nm laser at 70° from the normal. In situ ellipsometry measurements were carried out using a home-build liquid cell with windows normal to the direction of the incident light. The in situ measurements were conducted for 60 min. Refractive indices (RI) of swollen polymer brushes were estimated using linear effective medium approximation based on the RI of dry polymer and solvent. The RI of solvent acetonitrile was 1.339. Grazing angle attenuated total reflection FTIR (gATR-FTIR) analysis was carried out using a Thermo Scientific FTIR (Nicolet 8700) equipped with a VariGATR accessory (grazing angle 65°, germanium crystal; Harrick Scientific). Spectra were collected with a resolution of 4 cm-1 by accumulating a minimum of 128 scans per sample. All spectra were collected while purging the VariGATR attachment and FTIR instrument with nitrogen along the infrared beam path to minimize the peaks corresponding to atmospheric moisture and CO_2. Spectra were analyzed and processed using Omnic software. Atomic force microscopy (AFM) was performed using a Bruker Dimension Icon instrument. AFM height images were collected in tapping mode (in air) to obtain thin film morphology. The polymer brush samples were scanned using RTESPA-300 probes (from Bruker) with a spring constant of 40 N/m. The AFM height images were analyzed using the SPIP software. The wrinkle wavelengths were obtained from the radial averaged cross-section of fast Fourier transform (FFT) of the height image. Film moduli were measured in PeakForce

Quantitative Nanomechanical Property Mapping (QNM) mode using the relative method, in which polystyrene was chosen as the reference sample. AFM lithography was performed on the same instrument with Aspire CT300-10 probe with spring constant of 40 N/m in contact mode (in air). Static water contact angles of polymer brush surfaces were measured using 6 μL water droplets on a Rame-hart goniometer. Time-of-Flight Secondary Ion Mass Spectrometry (ToF-SIMS) measurements have been performed at the Oak Ridge National Lab (ORNL) in order to characterize the spatial distribution of cystamine within the polymer brush. The experiments were conducted using ION.TOF5 mass spectrometer with Bi-ion primary gun (30 keV, 30 nA, 200 μm × 200 μm scanning region, 5 μm spot size) as the ionization source and a sputtering Ar ion-cluster gun (cluster size ~2000 ions, 5 keV, 4 nA, sputtering region 400 μm × 400 μm, spot size ~20 μm). The secondary ions were collected by a ToF detector in both positive detection modes with resolution m/Δm~2000□4000. Si+, C3H3+, H3S+ ions were used to identify carbon, sulfur and silicon component within the samples.

5.2.3 Surface-Initiated Polymerization of pSMA Brush

An azo-based trichlorosilane initiator was used and it was synthesized following literature procedures.[36-38] Silicon substrates were cleaned and functionalized with the azo-based initiator following the procedures reported in the previous chapter. An oxygen free solution containing styrene (1.0 mL, 0.91 g, 8.7 mmol), maleic anhydride (1.0 g, 10.2 mol) and anhydrous acetonitrile (10.0 mL) was prepared and was transferred into a test tube that contains an initiator modified silicon substrate under nitrogen protection. The test tube was heated at 95 °C for various times to obtain polymer brushes of different

thickness. After heating, the pSMA substrate was thoroughly rinsed with acetonitrile and dried under a flow of nitrogen.

5.2.4 PPM of pSMA Brush with Cystamine Dihydrochloride under Aqueous Conditions

Cystamine dihydrochloride (40 mg, 0.18 mmol) and triethylamine (40 μL, 29 mg, 0.29 mmol) were dissolved in 4.0 mL of DI water. A substrate with pSMA brush on the surface was placed in the cystamine solution at discrete reaction times (from 30 s to 3 h). After PPM, the polymer brush substrate was thoroughly rinsed with DI water and dried with a flow of nitrogen.

5.2.5 PPM of pSMA Brush with Cystamine Dihydrochloride in Good Solvent

Cystamine dihydrochloride (0.40 mg, 1.8 μmol) and triethylamine (0.40 μL, 0.29 mg, 2.9 μmol) were dissolved in 4.0 mL of solvent mixture that contains 50% of DI water and 50% of acetonitrile. A substrate with pSMA brush on the surface was placed in the cystamine solution for 30 s. The polymer brush substrate was thoroughly rinsed with DI water and dried with a flow of nitrogen.

5.2.6 PPM of pSMA Brush with Monofunctional Amines under Aqueous Conditions

Hexylamine (0.40 μL, 0.31 mg, 3.1μmol) was added to 4.0 mL of DI water. A substrate with pSMA brush on the surface was placed in the hexylamine solution at 30 s and 150 s. The postmodified pSMA substrates were thoroughly rinsed with DI water and dried with a flow of nitrogen. The post-modification of pSMA brush using propylamine (0.24 μL, 0.17 mg, 2.9 μmol) was carried out in 4.0 mL of DI water in the same way.

5.2.7 Reduction of Cystamine Modified pSMA Brush

A substrate with cystamine post-modified SMA brush was placed in a solution of TCEP (60 mg, 0.21 mmol) in 6 mL of acetonitrile: PBS solvent mixture (50:50 by volume) in a sealed test tube. The TCEP solution was under constant nitrogen purging for 16 h. The substrate was then taken out of the solution, rinsed with DI water and dried with a flow of nitrogen.

5.2.8 Sequential PPM of pSMA Brush

Propargylamine (40 μL, 34 mg, 0.62 mmol) was added to 4.0 mL of anhydrous acetonitrile and a substrate of cystamine post-modified pSMA brush was placed in the acetonitrile solution of propargylamine at room temperature for 1 h. The substrate was then taken out of the solution, rinsed with acetonitrile followed by drying with a flow of nitrogen.

5.3 Results and Discussion

5.3.1 Synthesis of pSMA Polymer Brush

For this work, we employed pSMA as a reactive polymer brush scaffold. As demonstrated in Chapter IV, pSMA is easily obtained from commodity monomers and is highly reactive towards amines for facile post-modification. Alternating pSMA brushes were synthesized via surface-initiated polymerization of a 54:46 Sty: MA monomer feed from silicon substrates modified with an asymmetric trichlorosilane azo-based initiator.

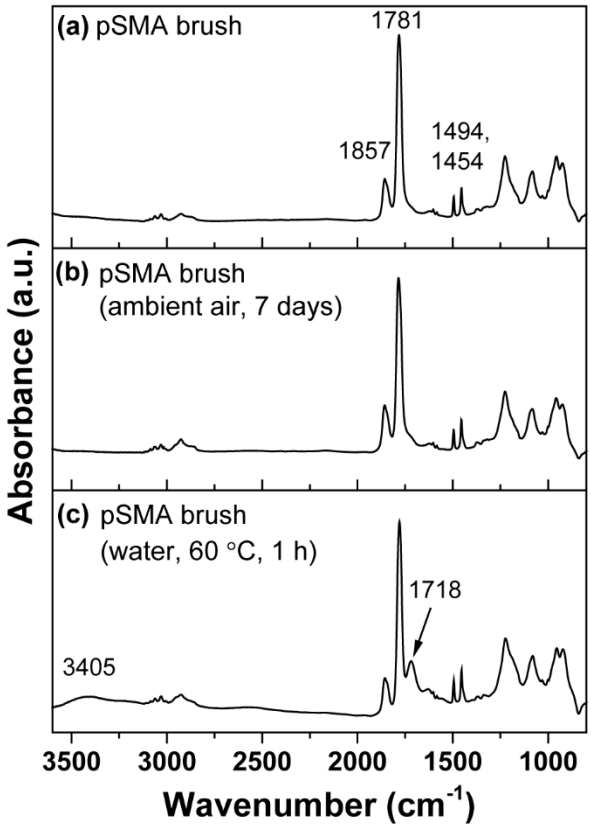

Figure 5.1 ATR-FTIR spectra for a) pSMA brush, (b) pSMA brush exposed to ambient air at room temperature for 7 days, and c) pSMA brush heated at 60 °C for 1 h in DI water.

Polymerizations were carried out at 95 °C to generate pSMA brushes with consistent thickness (≈ 80 nm). Following extraction, the surfaces displayed a typical featureless brush morphology with 6.6 nm root-mean-squared (RMS) roughness, as determined via atomic force microscopy (AFM) (See Appendix for Figure C1). The chemical composition and hydrolytic stability of the pSMA brush were measured by grazing angle attenuated total reflection Fourier transform infrared spectroscopy (FTIR). Peaks at 1781 cm^{-1} and 1857 cm^{-1} are attributed to the five-membered anhydride ring,[39-40] whereas peaks at 1454 cm^{-1} and 1494 cm^{-1} are indicative of the aromatic styrene unit. As shown in Figure 5.1, the anhydride was found to be sufficiently stable in air at room

temperature (i.e. minimal hydrolysis of the anhydride), and surprisingly stable when immersed in deionized water at 60 °C for 60 min. The hydrophobicity of the pSMA brush surfaces (92° water contact angle, Figure C1) likely contributes to the observed stability by limiting diffusion of water into the brush – an important point that we exploited for controlled PPM of the brush.

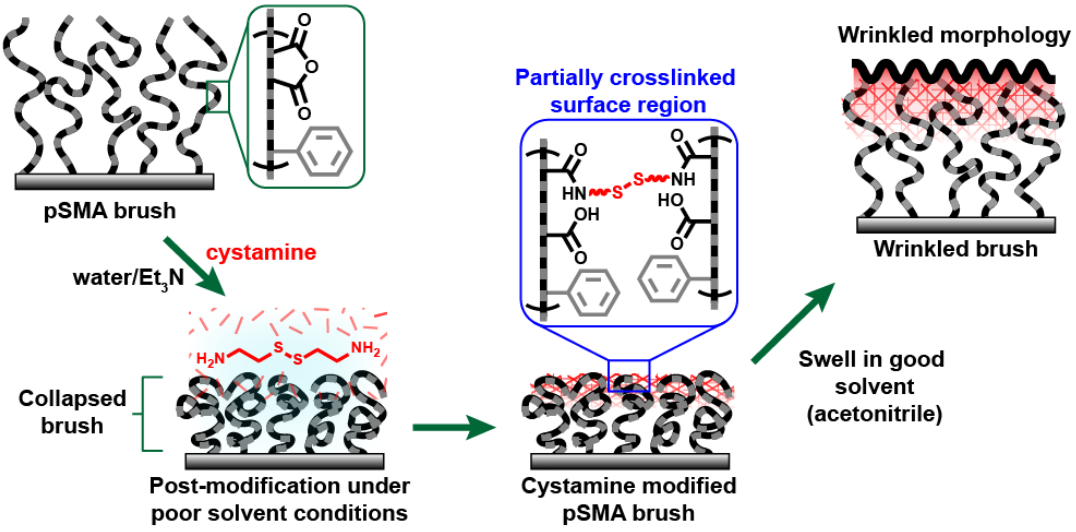

Scheme 5.1 Synthetic route to wrinkled polymer brush surfaces. PPM of pSMA brushes with cystamine under poor solvent conditions and subsequent swelling of the partially crosslinked brushes in acetonitrile.

5.3.2 Postpolymerization Modification (PPM) of pSMA with Cystamine Dihydrochloride

pSMA brushes were reacted with cystamine dihydrochloride (in the presence of trimethylamine, TEA) under aqueous conditions at discrete reaction times, according to Scheme 5.1. Cystamine serves to partially crosslink the brush via reaction between the amine and anhydride functional groups resulting in the formation of amide-acid moieties along the backbone. The molar mass of the repeat units of the polymer brush increases upon cystamine addition resulting in an overall increase in the brush thickness.[41]

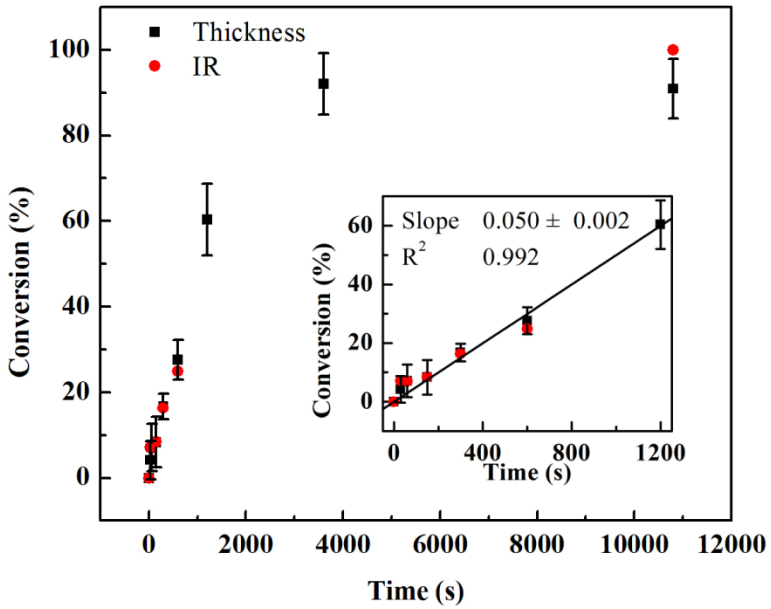

Figure 5.2 The anhydride conversion, k, versus reaction time profiles of cystamine-modified pSMA brush.

The insertion is data fitted to pseudo zero order kinetics from 0s to 1200s.

The apparent anhydride conversion of the PPM can be calculated based on the thickness increase of the polymer brush as previously described by Equation 4 in Chapter IV. The conversion can also be calculated based on the peak area of the anhydride absorption using FTIR (See Appendix for Figure C2). The anhydride conversion versus reaction time profiles of cystamine-modified pSMA brushes with an initial thickness of 80 nm is shown in Figure 5.2. As shown, conversion values from both ellipsometry and FTIR methods are in good agreement with each other. The conversion difference at very long reaction time (3h) measured using the two methods can be attributed to the hydrolysis of anhydride groups. (see Appendix for Table C1)

Notably, the overall reaction rate of the PPM under aqueous conditions is much slower compared to cystamine modification under good solvent conditions. Under aqueous conditions, the anhydride conversion achieved a plateau of ~90 % conversion at

3600s. In contrast, 93.5 % conversion was reached within 30s under good solvent conditions (see Chapter IV, Table 4.1). Under aqueous conditions, the pSMA brush exists in a collapsed state which poses a greater barrier for cystamine penetration into the brush and slows the observed rate of the PPM process. At the beginning of the PPM process, the number of accessible anhydrides to cystamine is limited by the rate of cystamine diffusion into the polymer brush. Under these conditions, the PPM reaction rate is independent of the total number of unreacted anhydride groups within the polymer brush, [*A*], thus the PPM process would be expected to follow pseudo-zero-order kinetics. (Equation 1)

$$-\frac{d[A]}{dt} \sim \mathrm{D}\ ,$$

The anhydride conversion of the 80 nm pSMA brushes under aqueous conditions is plotted in Figure 5.2 (inset) with data fitted to pseudo-zero-order conditions. The intercept of linear fit was set to zero. As shown in Figure 5.2 (inset), the kinetic model fitted the data very well from 0s to 1200s. In contrast, cystamine modification of pSMA brush under good solvent conditions follows pseudo-first-order kinetics (see Chapter IV Figure 4.4).

5.3.3 Depth Profiling of Modified pSMA Brush Using ToF-SIMS

Alswieleh and coworkers recently demonstrated the use of solvent quality to spatially control crosslinking within a brush surface; crosslinking in good solvent provided homogeneous crosslinking throughout the brush, whereas poor solvents resulted in crosslinking primarily in the surface region of the brush.[42] Similarly, in our system, poor solvent conditions are postulated to collapse the brush structure and initially limit

the cystamine crosslinking reaction to the exposed brush interface. If the amine-anhydride reaction is fast relative to diffusion of the cystamine into the brush (a good assumption under poor solvent conditions), then reaction time serves as a facile parameter to control the penetration depth of the cystamine, and consequently, the depth of the crosslinked surface region within the brush. To explore this hypothesis, ToF-SIMS analysis with argon ion cluster sputtering was employed to depth-profile the composition of the pSMA brush as a function of cystamine modification time. Additionally, the composition profiles were related to the anhydride conversion at each PPM time point. The intensity of the carbon-containing ($C_3H_3^+$) and sulfur-containing secondary ions (H_3S^+) characteristic of the pSMA brush backbone and cystamine modifier, respectively, were recorded as a function of the sputtering time and compared with the Si^+ ions originating from the underlying silicon substrate.[43] The obtained composition versus sputter time profiles, as shown in Figure 5.3, give a qualitative estimation of the depth profile relative to the concentration of the cystamine in the polymer brush. The full modification depth of cystamine was determined using the ratio of carbon and sulfur ion intensities. The polymer brush/substrate interface was determined using the intersection of the $C_3H_3^+$ and Si^+ profiles.[44]

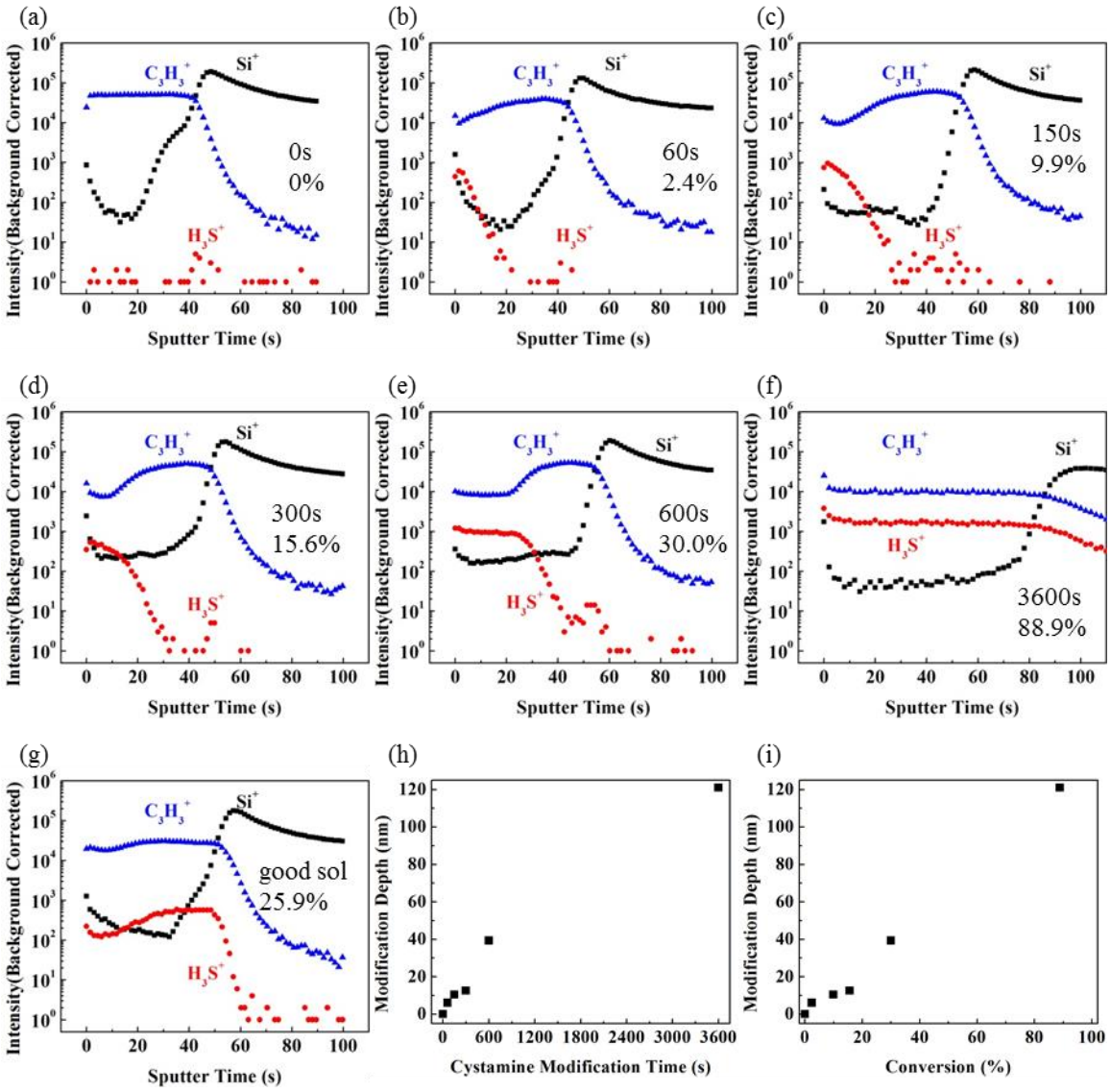

Figure 5.3 Secondary ion intensity – sputtering time profiles of unmodified and cystamine modified pSMA brush samples.

(a) an 80 nm unmodified pSMA brush, cystamine-modified pSMA under aqueous conditions for (b) 60s, (c) 150s, (d) 300s, (e) 600s, and (f) 3600s. (g) Cystamine modified pSMA brush under good solvent conditions. Anhydride conversion values are shown for each PPM time point. (h) Fully modification depth versus cystamine modification time plot. (i) Fully modification depth versus conversion plot.

Figure 5.3a displays the ion profiles of an unmodified pSMA brush. A homogenous $C_3H_3^+$ intensity was observed for the full thickness of the pSMA brush. The noise level H_3S^+ intensity indicates the absence of sulfur within the brush, as expected

without cystamine modification. The ToF-SIMS profiles of cystamine-modified pSMA brushes under an aqueous condition with reaction times of 60s, 150s, 300s, and 600s are shown in Figure 5.3b-e, respectively. As shown, H_3S^+ ions are primarily observed at the polymer/air interface at short reactions times with intensities that quickly decay to noise level with increasing sputter time. The H_3S^+ profiles progressively show a deeper penetration of cystamine with increasing PPM time. Conversion of the sputter time axis to cystamine modification depth (using knowledge of total brush thickness and sputter rate) shows that PPM for 60s, 150s, 300s, and 600s under poor solvent conditions yields cystamine modification depths of 6.0, 10.4, 12.5, and 39.3 nm, respectively (Figure 5.3h). With extended cystamine modification time (3600s, Figure 3f), the H_3S^+ profiles exhibit a high ion intensity that is homogeneous over the full thickness of the pSMA polymer brush – results that indicate the modification reaction eventually penetrates the full thickness of the brush (e.g. full 120 nm of the modified brush thickness contains cystamine). To illustrate the importance of poor solvent conditions on the ability to tailor the depth profile, Figure 5.3g shows the ToF-SIMS profile for a pSMA brush modified with a very low concentration cystamine solution (0.45 mmol/L) for 30s under good solvent conditions. The H_3S^+ profile shows a homogeneous distribution of cystamine over the full brush thickness, despite having a much shorter cystamine modification time. PPM under good solvent conditions swells the brush and reduces the disparity in the timescales between amine-anhydride reaction time and the time required for diffusion of the modifier into the brush resulting in a more homogeneous modified brush profile. Figure 5.3h and 5.3i show the full modification depth versus modification time and conversion, respectively. The results showed linear relationships between the

modification penetration depth with reaction time and anhydride conversion. Collectively, these ToF-SIMS results confirm the hypothesis that PPM reaction time under poor solvent conditions enables control over the depth of the crosslinked surface region within the brush.

5.3.4 Buckling Instability in Cystamine Modified pSMA Brush Surfaces

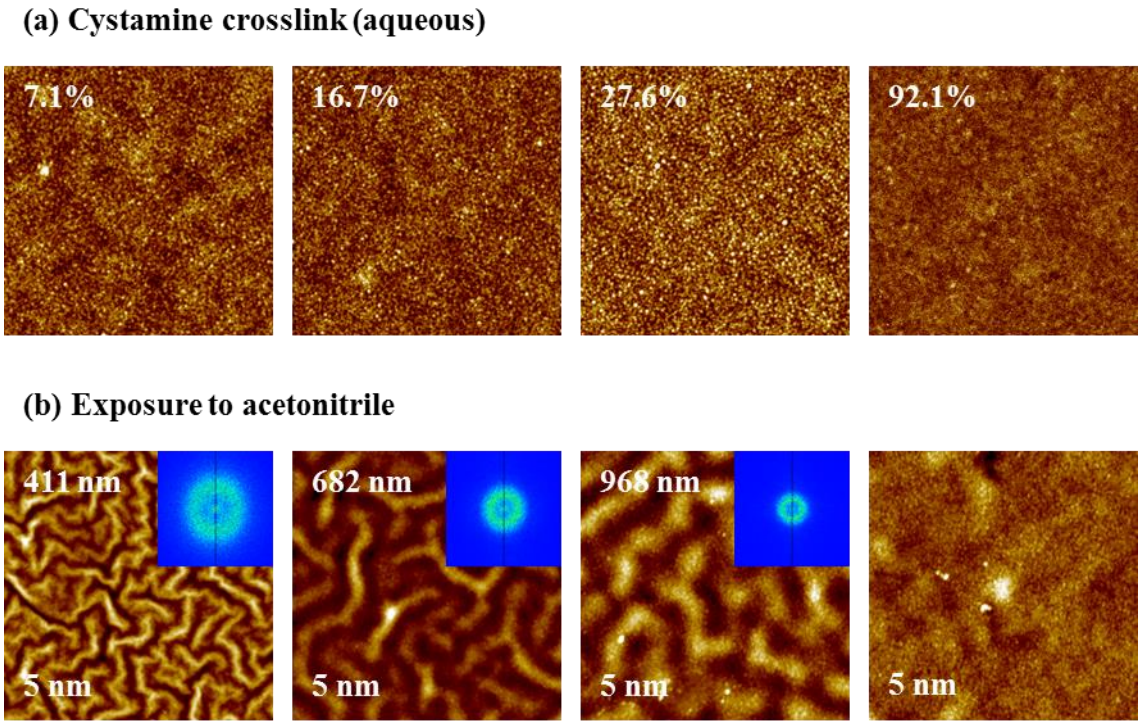

Figure 5.4 AFM height images and corresponding 2D fast Fourier transform (FFT) spectra of cystamine-modified pSMA brushes (~80 nm initial thickness) following reaction with cystamine and subsequent exposure to good solvent (acetonitrile) conditions.

Next, pSMA brushes postmodified with cystamine under poor solvent conditions were immersed in a good solvent (acetonitrile) for 60 min to induce swelling, as shown in Scheme 5.1. We postulate that exposure of the selectively crosslinked brushes to a good solvent will generate a swelling mismatch between the lateral and perpendicular directions, and consequently a compressive stress at the interface of the crosslinked and

non-crosslinked regions of the brush, creating an opportunity for swelling instabilities to rise. Prior to swelling, the postmodified samples exhibited a typical featureless brush morphology (RMS roughness: 6.6 nm) that was unchanged in comparison to the unmodified pSMA brush morphology using AFM (Figure 5.4a). Figure 5.4b shows the brush morphologies after swelling in acetonitrile for 60 min. The brush wrinkling patterns that developed as a result of exposure to good solvent show a clear dependence on the anhydride conversion, transitioning from random labyrinth with low conversion (7.1 %) to lamellar-like morphologies at intermediate conversion (17%), and further to connected peanut-like morphologies at higher conversion (27%). In general, wrinkles were not observed in polymer brush samples modified with cystamine under poor solvent conditions with anhydride conversions > 40 %.

To understand how swelling of the partially crosslinked polymer brush leads to surface wrinkling, we determined the swelling ratio (SR) of the cystamine-modified pSMA brushes as a function of anhydride conversion. *In situ*, ellipsometric thickness measurements were conducted on a single angle/wavelength ellipsometry using a home-made liquid cell. The thickness of swollen brush was calculated using a multilayer model consisting of Si, SiO_2, initiator, and a homogeneous swollen polymer. The refractive index (RI) of the swollen polymer layer was estimated using a linear effective medium approximation of the dry pSMA brush and solvent.[45] The swelling ratio was calculated as the thickness ratio of swollen polymer over that of the dry polymer. Exposure of the modified brushes to good solvent resulted in an increase in thickness as a result of polymer chain extension. The presence of crosslinks within the film, while generating the compressive stress needed for surface buckling, inhibits the segmental rearrangement

of the brush and reduces the swelling ratio. Figure 5.5 shows the relationship between swelling ratio and conversion for the cystamine-modified pSMA brushes. The swelling ratio of an unmodified pSMA brush was ~2.1. At anhydride conversions < 20%, an increase in the swelling ratio was observed that can be attributed to the solvent compatibility contribution of carboxylic acid functional groups formed upon reaction of the maleic anhydride with cystamine. Samples with anhydride conversions >30% displayed lower swelling ratio due to the inhibition of swelling by the cystamine crosslinks.[46] The critical swelling ratio, below which the osmotic stress is insufficient to induce surface buckling, was found to be ~1.75 (~40% anhydride conversion) – a critical value that is consistent with other reports from literature.[47]

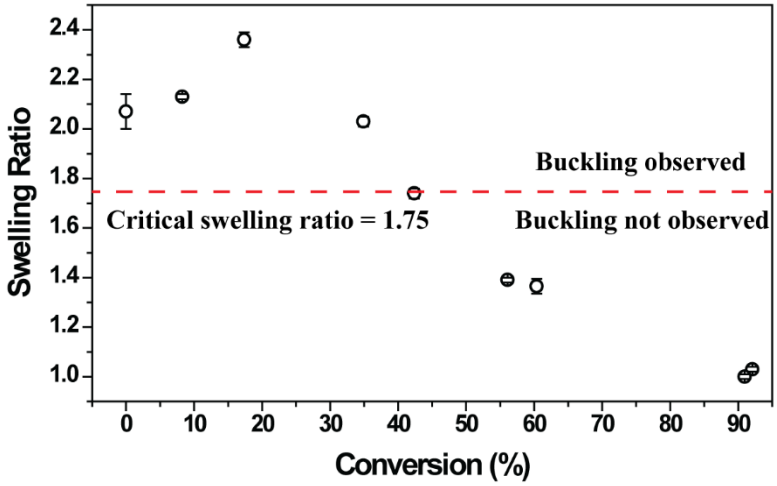

Figure 5.5 Swelling ratio versus anhydride conversion for pSMA brushes postmodified with cystamine. The horizontal red line represents the critical swelling ratio.

The distribution of crosslinks within the pSMA brush also affects the swelling ratio. A pSMA brush modified by cystamine under good solvent conditions with 17% anhydride conversion resulted in a low swelling ratio (1.48) and no wrinkles were observed after swelling in acetonitrile (see Appendix for Figure C3). Notably, the swelling ratio for a brush sample with similar conversion but modified in aqueous

condition was 2.4. As indicated by the previous ToF-SIMS discussion, pSMA brushes postmodified under aqueous conditions exhibit a selectively crosslinked composition profile. Postmodification under good solvent conditions yields crosslinks homogeneously distributed throughout the thickness of the brush. Following acetonitrile swelling, the more homogeneously crosslinked polymer brush swelled much less than the selectively crosslinked brush. Thus, the swelling ratio was below the critical value for the onset of the buckling instability and the compressive stress was insufficient to induce surface wrinkling.

5.3.5 The Dependence of Wrinkle Wavelength on Conversion

The wavelength λ of wrinkling surfaces is governed by a factor f(H) associated with film thickness and the relative stiffness of the upper layer and the bottom layer (B/K), as shown in Equation 2,

$$\lambda \sim f(H) * \left(\frac{B}{K}\right)^{e} \quad \text{Equation 2}$$

in which B is the bending stiffness of the skin, K is the stiffness of the underlying foundation and the exponent, e, can be 1/3 or 1/4 depending on the different models.[1]

The wavelength of the wrinkle morphologies can be measured by taking the radial average of the AFM 2D Fast Fourier Transform (FFT) spectra (Figure 5.4b, inset) in which the circular shape of FFT is indicative of 2D isotropic oriented wrinkles and the size of the rings scales inversely with the periodicity in the morphological feature.

A bilayer model of a rigid-on-soft modulus distribution profiles is used to describe the wrinkle wavelength. Consider a rigid-on-soft model that contains a rigid upper layer and an infinite underlying foundation, the wrinkle wavelength λ scales proportionally with the thickness of the upper rigid layer h, as shown in Equation 3,

$$\lambda = 2\pi h \left(\frac{(1 - v_f^2)E_s}{3(1 - v_s^2)E_f} \right)^{1/3}$$ Equation

where v_s, E_s and v_f, E_f are the Poisson's ratios and elastic moduli of the skin and foundation materials, respectively.[3]

Based on the results of modification depth obtained by SIMS measurement, it can be assumed that the upper layer thickness, h, is approximately proportional to conversion, *k*. As a result, wrinkle wavelength λ is expected to be proportional to conversion, k, as shown by Equation 4.

$$\lambda \sim h \sim k$$

The λ – k plots of cystamine-modified pSMA brushes are shown in Figure 5.6. Also displayed are the linear fitted lines. The wrinkle wavelength λ scales linearly with the conversion *k*. The fact that the fitted intercept was not zero is due to the finite thickness of polymer brush.

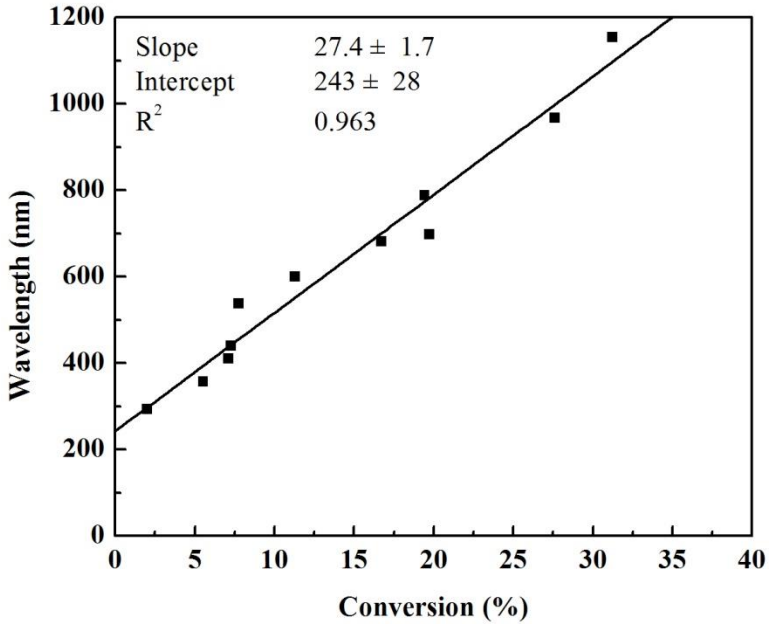

Figure 5.6 Wrinkle wavelength – conversion plot.

5.3.6 Tuning Wrinkle Wavelength by Adjusting Solvent Quality

Given a certain film thickness, wrinkle wavelength depends on the stiffness ratio of the hard top layer and the soft foundation, as shown by Equation 2.[1] Swelling of the polymer brush not only generates osmotic stress within the film but also reduces the film modulus.[48] The more a polymer brush swells the smaller its modulus is expected to be. Given equivalent solvent conditions, the bottom layer of unmodified pSMA brush swells more than the upper layer which is near quantitatively modified by cystamine. Thus, the modulus of the non-crosslinked region decreases far more than that of the crosslinked regions upon swelling. While it is challenging to measure the polymer brush modulus under swollen state, one would expect the polymer brush swelled under better solvent quality to display greater stiffness ratio. Thus it is possible to tune the wrinkle wavelength by adjusting the relative stiffness of the crosslinked/non-crosslinked regions via solvent quality.

Modified pSMA brushes at equivalent conversions (7.8%) were swelled in water/acetonitrile mixtures with different acetonitrile solution for 60 min. The AFM images and FFT spectra in Figure 5.7 show that wrinkle wavelength increases with increasing acetonitrile percentage in the swelling solution. Solutions with a higher acetonitrile component exhibit better solvent quality thus increasing the stiffness ratio and the wrinkle wavelength.

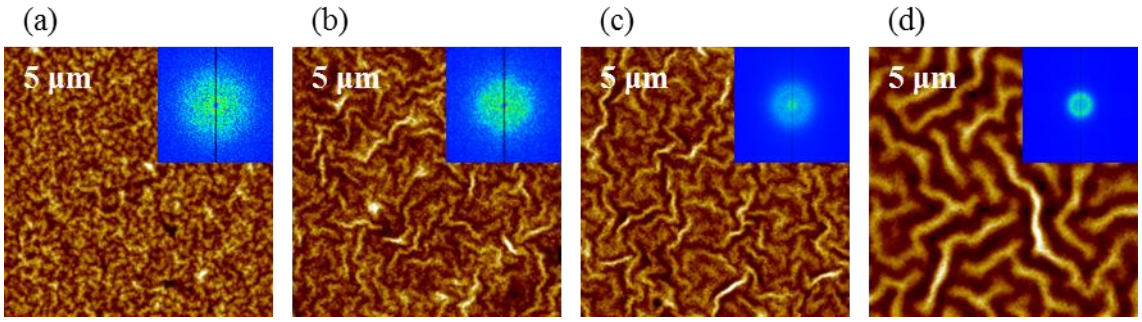

Figure 5.7 AFM height images of modified pSMA brushes with 7.8% conversion swelled in water/acetonitrile medium with increasing acetonitrile content.

(a) 30% of acetonitrile (λ=208 nm), (b) 50% of acetonitrile(λ=272 nm), (c) 70% of acetonitrile (λ=333 nm) and (d) 100% of acetonitrile for 60 min (λ=538 nm). Insets are the FFT of the AFM images.

5.3.7 Evolution of the Wrinkling Process

After understanding the influence of crosslinks and solvent quality on the wrinkle formation, we further studied the evolution of wrinkles by swelling cystamine-modified pSMA brush samples (7% conversion) in acetonitrile for various times. Upon swelling, the osmotic stress was immediately generated and triggered the out of plane deformation of the flat surface. As shown in Figure 5.8a, discernable wrinkling features were observed within remarkably short swelling time (1 min) with peak-to-valley height differences (amplitude) of ~20 nm. Following 5 min of swelling, the surface displayed a well-defined wrinkle morphology with peak-to-peak amplitude increased to ~35 nm (Figure 5.8b). Longer swelling times allow full development of surface buckling where the amplitude increased at a slower pace. The reduced amplitude growth rate is due to relaxation of compressive stress via out-of-plane deformation.[49] The AFM images of 15 min and 60 min swelled samples (Figure 5.8c, d) showing similar morphology and peak-to-peak amplitude (~45 nm) indicates that the surface reached an equilibrium state. Notably, samples of different swelling times displayed essentially equivalent wrinkle

wavelength as shown by the FFT insertions (Figure 5.8, insertion) as the wrinkle periodicity is ultimately governed by the thickness and mechanical parameters (i.e. stiffness ratio) of the film under swelling condition and is thus independent of the swelling time.[49]

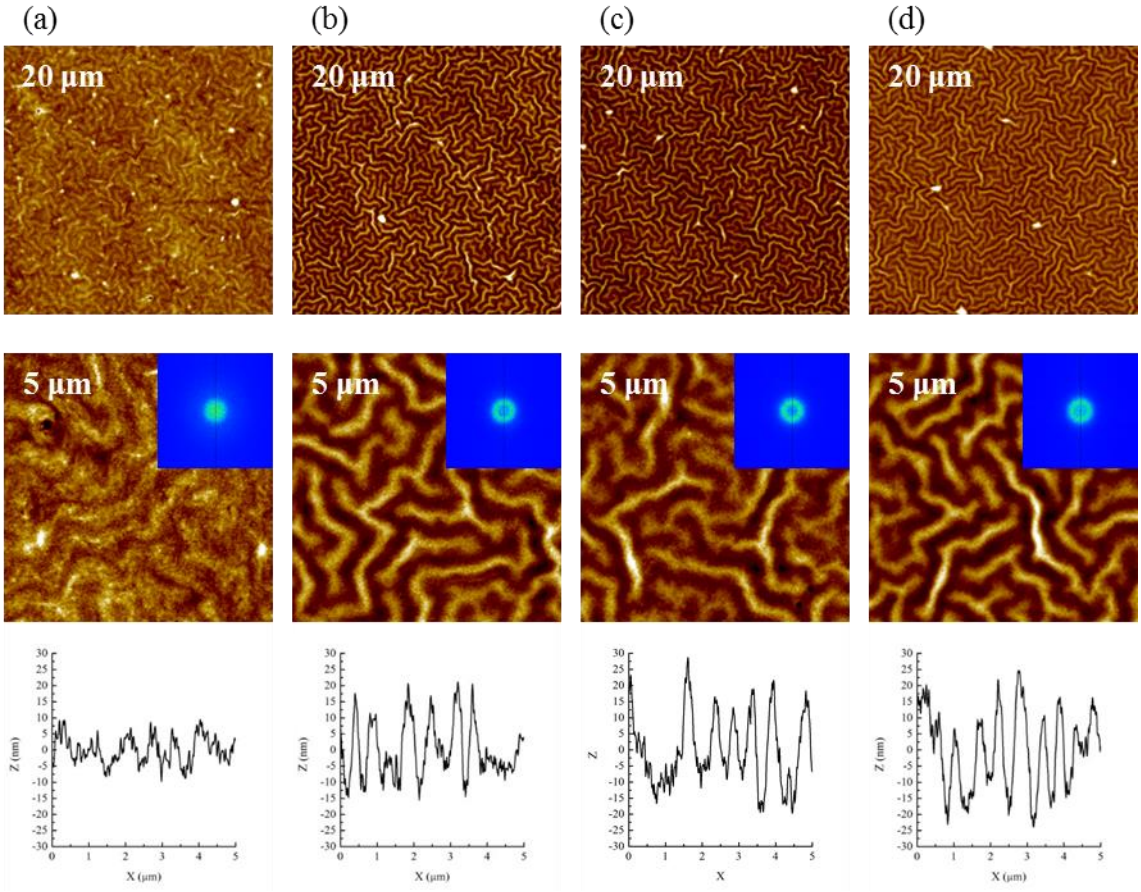

Figure 5.8 AFM height images (20 µm × 20 µm and 5 µm × 5 µm) and representative cross sections along the X direction of cystamine-modified pSMA polymer brush samples with 7.8% conversion swelled in acetonitrile for different times.

(a) 1 min (λ=556 nm), (b) 5 min (λ=556 nm), (c) 15 min (λ=556 nm) and (d) 60min (λ=538 nm). Insertions are the FFT of the AFM images.

5.3.8 Thermal Stability of Cystamine Modified Surfaces

The thermal stability of cystamine-modified surfaces before and after swelling was demonstrated by placing samples in an oven above the glass transition temperature

for pSMA (e.g. 145°C overnight). Prior to acetonitrile swelling, the cystamine-modified pSMA brush remained featureless after annealing at 145°C overnight. Following acetonitrile swelling and wrinkle formation, the sample was annealed at 145°C overnight. The AFM images showed essentially same buckling morphology. (See Appendix for Figure C4) The results suggest that without swelling, heating alone does not buckle the surface, and once wrinkled, the surface is thermodynamically stable.

5.3.9 Monofunctional Amine Modified pSMA Brush

The importance of employing cystamine as a crosslinker to facilitate the wrinkling morphology was illustrated through several control experiments. First, pSMA brushes were modified with two monofunctional amines (e.g. propylamine and hexylamine) under aqueous conditions. The reactivity of propylamine and hexylamine was much higher than that of cystamine dihydrochloride. As a result, the monofunctional amine solutions with lower concentrations were used in order to target the anhydride conversion of pSMA within a range (2.7% to 24.2%) over which pSMA brush postmodified with cystamine showed wrinkled morphologies. Despite the similar chain length of cystamine and hexylamine, using monofunctional amines as post-modifiers did not lead to the formation of wrinkles regardless of PPM reaction time.(See Appendix for Figure C5). Upon exposure to good solvent, pSMA brushes modified with primary amines undergo osmotic swelling but lack the crosslinks necessary to generate the compressive stress required for buckling.

5.3.10 Reduction of Cystamine Modified Polymer Brush

The second control experiment exploits the reversible nature of the disulfide linkage in the cystamine crosslinker. Figure 5.9a shows a featureless AFM image of a

cystamine-modified pSMA brush surface before acetonitrile swelling. Figure 5.9b shows a buckling morphology occurred on the surface after swelling the sample in acetonitrile. Subjecting the wrinkled pSMA brush to reducing conditions (tris(2-carboxyethyl) phosphine (TCEP) in phosphate buffer) resulted in the release of the wrinkles, as evidenced by the formation of a featureless brush morphology shown in Figure 5.9c. This result again highlights the role of crosslinking on the buckling of polymer brush surfaces in our system. Furthermore, the wrinkling-to-featureless morphological transition points to an opportunity to engineer brush surfaces with dynamic buckling behavior, where wrinkle formation and release are dictated via an external stimulus.

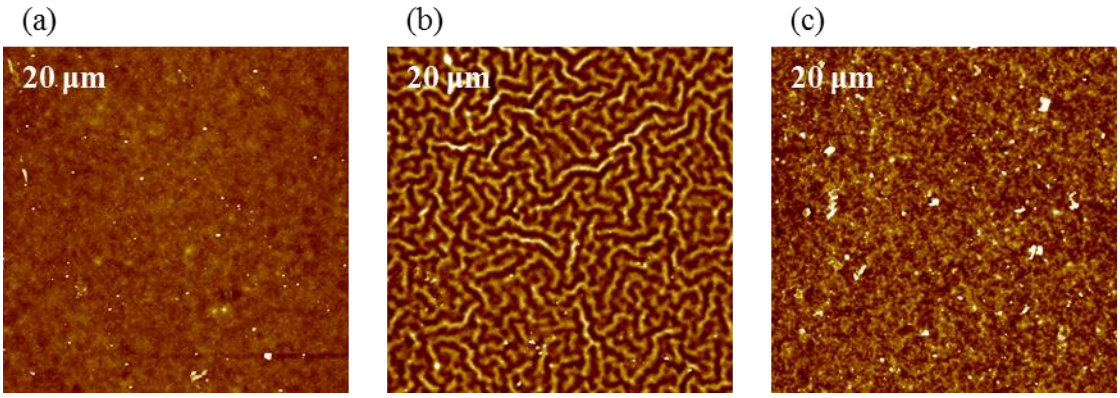

Figure 5.9 AFM height images of pSMA brushes (a) partially crosslinked with cystamine, (b) exposed to acetonitrile to induce wrinkling, and (c) subjected to reducing condition (TCEP in phosphate buffer solution) to cleave the disulfide linkage.

5.3.11 Alignment of wrinkles via AFM lithography

The orientation of wrinkled surfaces, if well aligned, have the applications as microlens arrays,[17] diffraction gratings[18-19], and open-channel microfluidics.[22] While the surface buckling instability is caused by the applied compressive stress within the film, the orientation of wrinkles is governed by the direction of the primary compressive stress. The primary compressive stress can be tuned either by applying an external uniaxial

strain on elastomeric foundations or by the uniaxial release of compressive stress (Scheme 5.2).[24, 50]

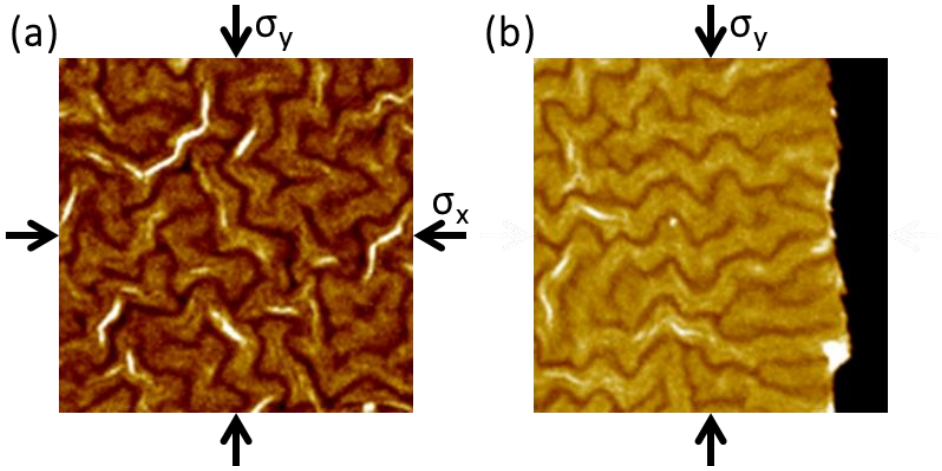

Scheme 5.2 Schematic illustration of (a) isotropic stress-induced wrinkles with random orientation and (b) aligned wrinkle induced by a uniaxial stress along the Y direction.

In our study, AFM lithography was used to pattern polymer brush surfaces in order to align the wrinkled topographic features. As shown in Figure 5.10a-c (upper images), the surfaces without patterning show isotropic wrinkling morphologies. The surfaces with patterning on the right end of the image displayed aligned wrinkles near the boundary (Figure 5.10a-c, center images). The cross sections along the X direction (perpendicular to the edge) of the corresponding samples are also shown (Figure 5.10a-c, bottom images) and the abrupt height changes at the right end of the height profiles confirmed the total removal of film material from the surface. The edges displayed sharp transitions in terms of thickness and the narrow peaks over the edge were due to the crowding out effect of the AFM scratching process.

Notably, the wrinkles near the boundary were well aligned and were perpendicular to the edge in all three images (Figure 5.10a-c, center images). Near the

boundary, the compressive stress in the direction perpendicular to the edge was released due to the discontinuity of the densely grafted polymer brush through the edge. Upon swelling, the surface only experiences the stress parallel to the edge (primary stress) resulting in aligned wrinkles in the transverse direction of the edge. Moving away from the edge to the polymer side, the alignment of the wrinkles persists over a finite distance beyond which the wrinkle gradually transits from ordered to random as the in-plane compressive stress changed from uniaxial to isotropic. The length over which the wrinkle is aligned is referred to as the persistence length, ζ.

The upper images of Figure 5.10a-c display the AFM images of wrinkled polymer brush surfaces with different wrinkle wavelength. The center images of Figure 5.10a-c show the AFM images of wrinkled polymer brush surfaces with different persistent length. The observation that samples with larger wrinkle wavelength have larger persistence length is consistent with the theoretical description of $\zeta - \lambda$ relation, as shown in Equation 14 where Σ is the strain applied to the rigid upper layer from the osmotic stress upon swelling. E_s and E_f are the modulus of the top and the bottom layer, respectively. The v_s is the Poisson's ratio of the upper rigid layer.[51-52]

$$\zeta \approx \lambda \left(\frac{1}{2\Sigma^{1/2}} + 2 \left(\frac{1}{4(1-v_s^2)} \frac{E_s}{E_f} \right)^{1/3} \right)$$

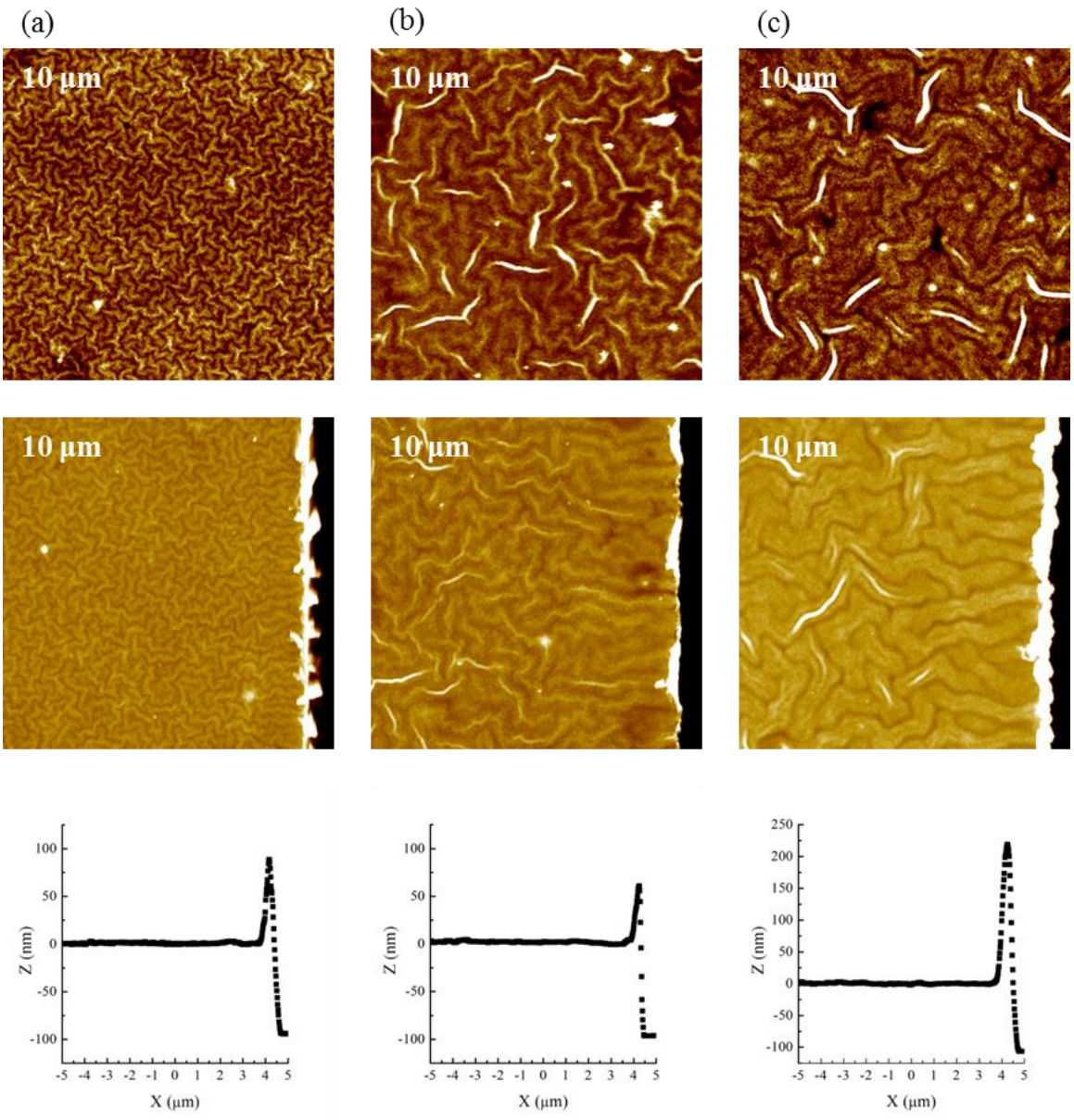

Figure 5.10 AFM height images of unpatterned (upper), patterned cystamine modified pSMA brush (unmodified thickness ~ 97 nm) after swelling (center) and corresponding cross section profiles along the X direction (bottom) at (a) 4.1 %, (b) 9.6 % and (c) 16.1% conversion.

As a demonstration of the ability to fabricate surfaces with complex morphology, a wrinkled surface of cystamine-modified pSMA brush was patterned with orthogonal edges. (See Appendix for Figure C6) The resulting surface displayed two wrinkle orientations that were perpendicular to each other.

5.3.12 Long-Range Control of Wrinkle Alignment via Periodic Patterns

While the AFM lithography patterned surfaces demonstrated the creation of aligned wrinkles, the range of wrinkle alignment is limit by the persistence length. Periodically patterning of the surface is an efficient approach to allow long range control of wrinkle orientation. Utilizing AFM lithography, pSMA brush surfaces modified with cystamine at various conversions were patterned with periodic stripes in order to guide the wrinkle direction. The periodicity of the pattern was 10 μm and the polymer brush material between the stripes was totally removed from the substrates to allow the uniaxial release of the compressive tension. As shown in Figure 5.11a, when the persistence length was far smaller than the distance between stripes, the aligned wrinkle that stemmed from the edges gradually converged to randomly oriented morphology at the center of two stripes. With longer wrinkle wavelength and persistence length, as is shown in Figure 5.11b and 5.11c, the ordered domains grew from the sides and merged with one another at the center thus achieving long-range order of wrinkle arrangement that covers a large area.

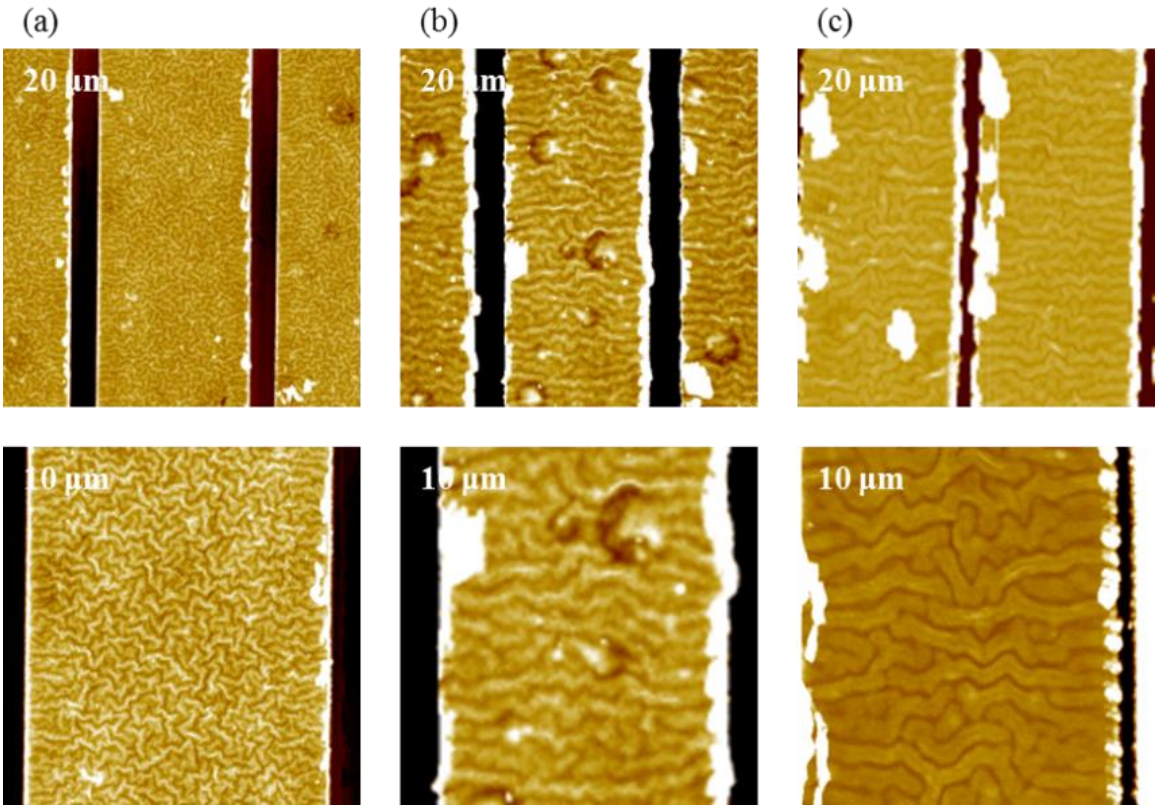

Figure 5.11 AFM height images of periodically patterned cystamine-modified pSMA brush (original thickness ~97 nm) of (a) 4.1 %, (b) 9.6 % and (c) 16.1 % conversion after swelling with the pattern periodicity of 10 µm.

5.3.13 Tuning Wrinkle Alignment via Scratch Depth and Gradient

In this section, how the scratch depth and cross section profile affect the wrinkle alignment was studied. AFM lithography was used to pattern the surfaces in such a way that the surfaces were scratched at different depths and polymer brush material within scratches was only partially removed from the substrate. Within each stripe, there was only one sharp edge with abrupt thickness change while the other side exhibited a gradual change of thickness through the edge. Figure 5.12 shows the 20 µm and 10 µm AFM height images of patterned wrinkle surfaces (original thickness 96 nm, conversion 21.7 %) and the cross section profiles of the scratches along the X direction. The pattern

periodicity is 10 μm and the stripe width is ~2 μm. The cross-section profile in Figure 5.12a shows that the depth of scratch on the right side of the groove is 35 nm and the left side exhibited a depth gradient. The AFM image in Figure 5.12a showed that the wrinkle on the right side of the groove (the one with drastic thickness change) was aligned in the transverse direction of the edge with shorter persistence length compared to the patterned surfaces in which the polymeric materials within the stripes was totally removed. Decreasing the depth of scratch, as shown in Figure 5.12b and 5.12c, reduced the degree of alignment and the persistence length and, eventually, yields isotropic wrinkles.

The trend observed is consistent with Equation 14. While removal of the polymeric material of the upper layer allows releasing of compressive stress and wrinkle alignment, the remaining polymer within the groove results in larger strain (Σ in Equation 14) applied to the neighboring surface from osmotic stress upon swelling. Further decreasing the scratch depth increases Σ and reduces the persistence length. On the left sides of the stripes where the edges exhibited a gradual thickness transition the wrinkles are isotropic presumably because the continuous thickness change over the edge prevents the compressive stress along the X direction from being sufficiently released. The findings point to the possibility of using the scratch depth and shape to tune the alignment of wrinkling surfaces.

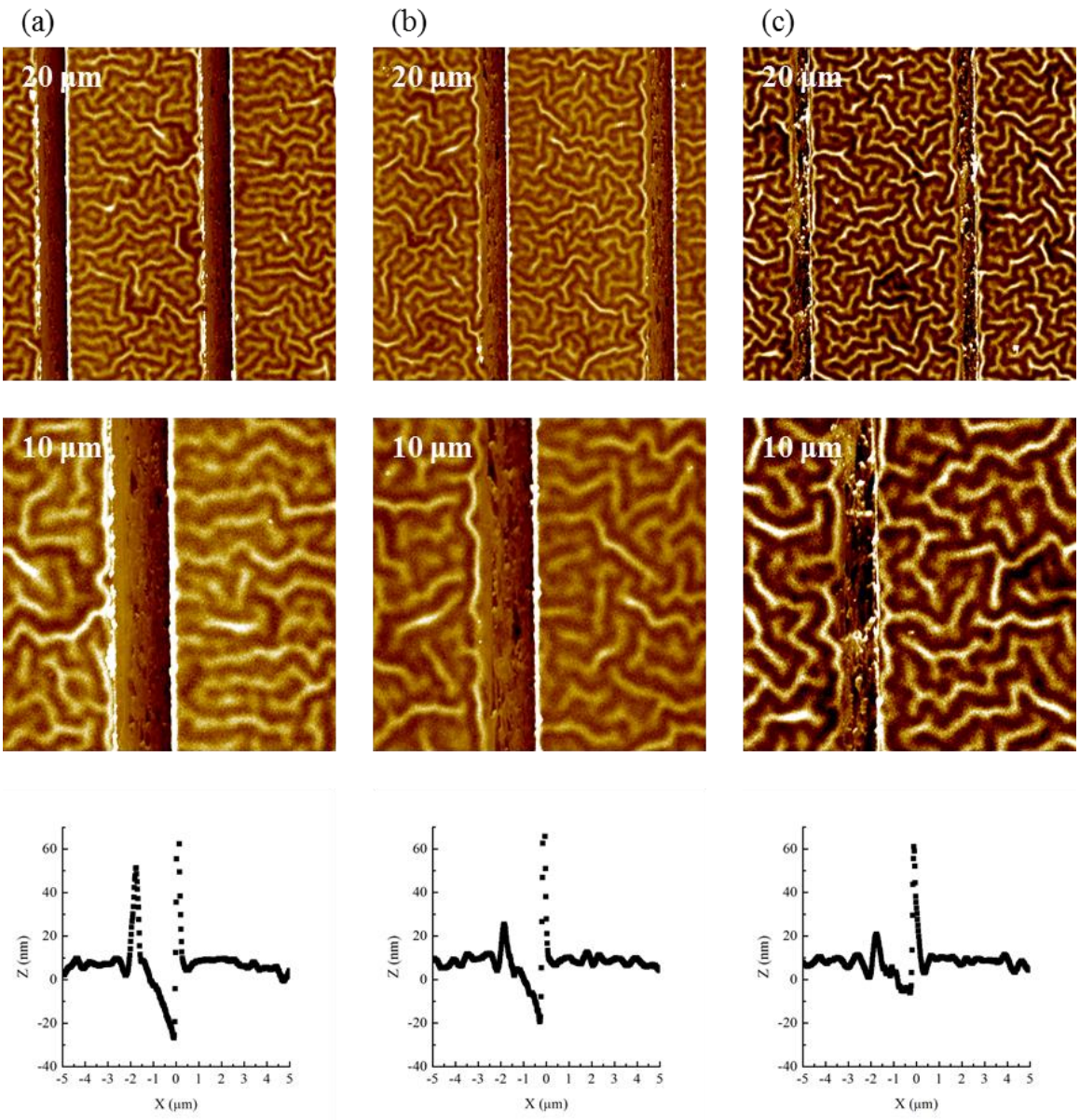

Figure 5.12 AFM height images of wrinkled cystamine-modified pSMA brush surfaces patterned with various depth of scratch: (a) 35 nm, (b) 20 nm and (c) 10nm along with corresponding cross-section profiles in the X direction.

5.3.14 Sequential PPM of pSMA Brush

Exerting control over brush wrinkle morphology simply using PPM reaction time and conditions motivated us to investigate routes to tailor the brush morphology while endowing the surface with additional chemical functionality. Following the initial

cystamine modification using short reaction times, wrinkled pSMA brushes have a significant fraction of residual anhydride functionality that can be addressed using sequential postmodification reactions.

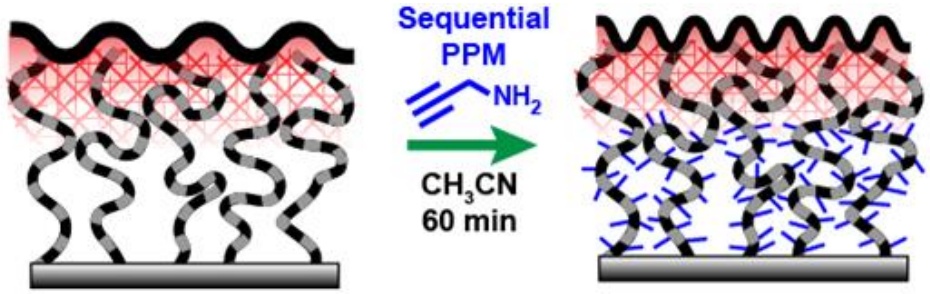

Scheme 5.3 Synthetic route for sequential postmodification reactions on pSMA brushes. Wrinkled brushes are sequentially modified with propargylamine in acetonitrile for 60 min.

To demonstrate this capability, wrinkled pSMA brushes were subjected to a second postmodification reaction using propargylamine in acetonitrile for 60 min (Scheme 5.3). These conditions re-swell the wrinkled brush, fully convert the remaining anhydrides to the amide-acids and provide alkyne moieties pendent to the polymer backbone (See Appendix for Figure C7, carbon-carbon triple bond stretch 2125 cm^{-1}). Figure 5.13 shows the AFM morphologies for sequentially modified pSMA brush. A significant decrease in wavelength (1154 nm to 517 nm, Figure 5.13) upon sequential modification with propargylamine, was observed. The propargylamine backfilling reaction added more mass onto the polymer brush and increased segmental repulsion between grafted chains and further stretched the underlying layer. Sequential modification with propargylamine increases the modulus of the underlying layer, thus reducing the modulus ratio between the sequentially modified regions (i.e. pSMA fully

modified with propargylamine exhibits a dry modulus of ≈2.5 GPa, Figure C8). The second step modification of the partially crosslinked brush also swells the partially crosslinked polymer brush due to an increase in osmotic pressure which would be expected to increase the compressive stress exerted on the crosslinked surface region of the brush that ultimately leads to the evolution of buckling morphology.

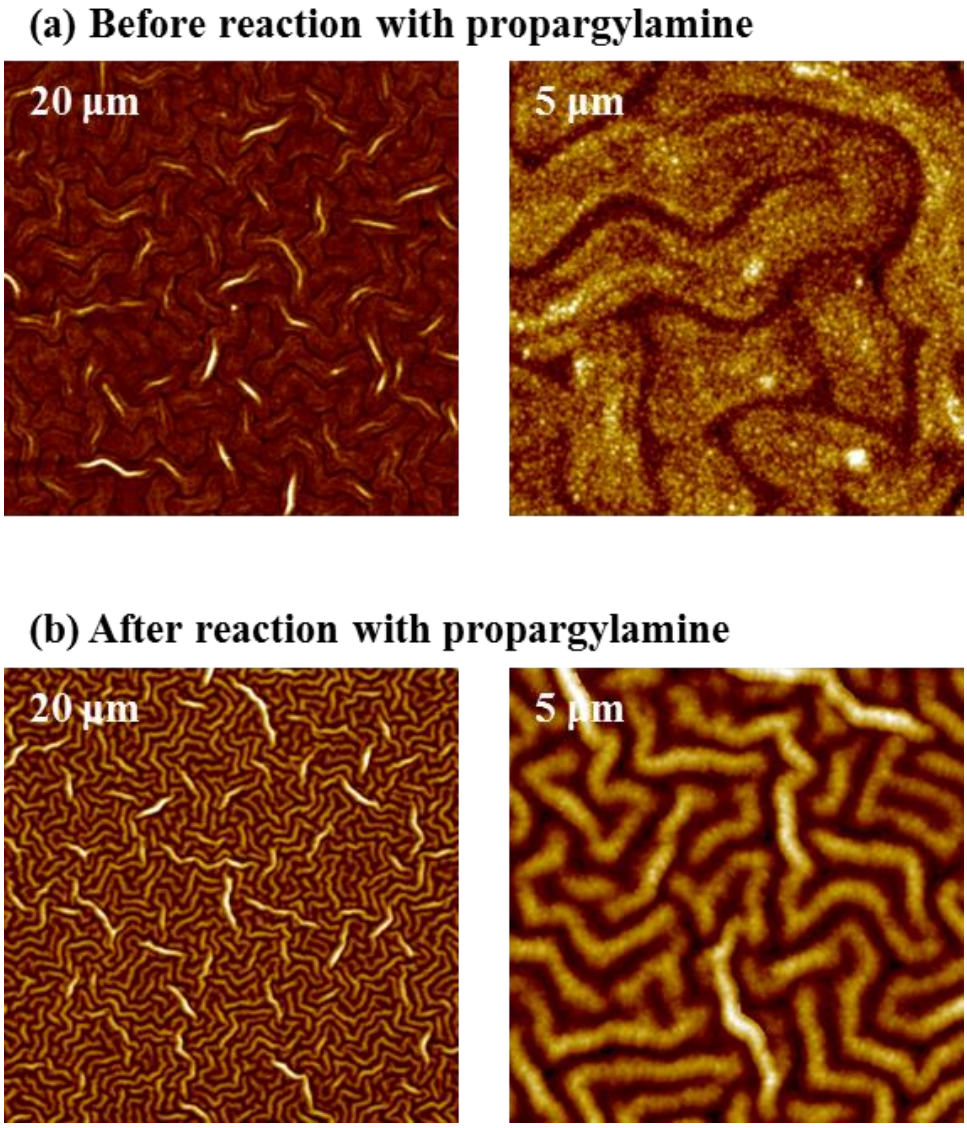

Figure 5.13 Evolution of pSMA brush morphology (31.1% conversion) (a) before and (b) after sequential reaction with propargylamine.

5.4 Conclusion

In summary, we demonstrated a simple postpolymerization modification approach to engineer ultrathin polymer brush surfaces with tunable wrinkled and morphologies. Postmodification of pSMA brushes under poor solvent conditions enabled crosslinking under a collapsed state, where reaction time was postulated to dictate the ultimate thickness and profile of the crosslinked surface region. Exposure of the partially crosslinked brushes to good solvent conditions swells the polymer brush and generates an anisotropic osmotic pressure. Swelling ratio was found to increase with decreasing crosslinking conversion. At low conversion, the high compressive stress within highly swelled polymer brush give rise to the buckling instability on the surface. The brush morphology can be tailored from nanoscale labyrinth-like wrinkles to microscale lamellar-like wrinkles simply by tuning the conversion, while wrinkle wavelength scales linearly with conversion. We anticipate our work will provide new routes to engineer ultrathin brush surfaces with complex functionality and morphology for a variety of applications.

5.5 Acknowledgements

The acquisition of the AFM instrumentation used in this work was enabled via partial funding from the Office of Naval Research (Award N00014-07-1-1057). The ToF-SIMS measurements were supported by a Rapid Access User Proposal for the Center for Nanophase Materials at Oak Ridge National Lab. We thank Dr. Olga Ovchinnikova, Dr. Anton Ievlev, and Dr. Bradley Lokitz for assistance with the ToF-SIMS measurements and data analysis.

5.6 References

1. Cerda, E.; Mahadevan, L., Geometry and physics of wrinkling. *Phys Rev Lett* **2003,** *90* (7), 074302.
2. Tallinen, T.; Chung, J. Y.; Rousseau, F.; Girard, N.; Lefèvre, J.; Mahadevan, L., On the growth and form of cortical convolutions. *Nature Physics* **2016,** *12* (6), 588-593.
3. Genzer, J.; Groenewold, J., Soft matter with hard skin: From skin wrinkles to templating and material characterization. *Soft Matter* **2006,** *2* (4), 310-323.
4. Chan, E. P.; Smith, E. J.; Hayward, R. C.; Crosby, A. J., Surface wrinkles for smart adhesion. *Adv Mater* **2008,** *20* (4), 711-+.
5. Davis, C. S.; Crosby, A. J., Mechanics of wrinkled surface adhesion. *Soft Matter* **2011,** *7* (11), 5373-5381.
6. Davis, C. S.; Martina, D.; Creton, C.; Lindner, A.; Crosby, A. J., Enhanced Adhesion of Elastic Materials to Small-Scale Wrinkles. *Langmuir* **2012,** *28* (42), 14899-14908.
7. Jeong, H. E.; Kwak, M. K.; Suh, K. Y., Stretchable, Adhesion-Tunable Dry Adhesive by Surface Wrinkling. *Langmuir* **2010,** *26* (4), 2223-2226.
8. Li, Y. Y.; Dai, S. X.; John, J.; Carter, K. R., Superhydrophobic Surfaces from Hierarchically Structured Wrinkled Polymers. *Acs Appl Mater Inter* **2013,** *5* (21), 11066-11073.
9. Zhang, Z. Q.; Zhang, T.; Zhang, Y. W.; Kim, K. S.; Gao, H. J., Strain-Controlled Switching of Hierarchically Wrinkled Surfaces between Superhydrophobicity and Superhydrophilicity. *Langmuir* **2012,** *28* (5), 2753-2760.
10. Efimenko, K.; Finlay, J.; Callow, M. E.; Callow, J. A.; Genzer, J., Development, and Testing of Hierarchically Wrinkled Coatings for Marine Antifouling. *Acs Appl Mater Inter* **2009,** *1* (5), 1031-1040.
11. Hoipkemeier-Wilson, L.; Schumacher, J. F.; Carman, M. L.; Gibson, A. L.; Feinberg, A. W.; Callow, M. E.; Finlay, J. A.; Callow, J. A.; Brennan, A. B., Antifouling Potential of Lubricious, Micro-engineered, PDMS Elastomers against Zoospores of the Green Fouling Alga Ulva (Enteromorpha). *Biofouling* **2004,** *20* (1), 53-63.
12. Muller, M.; Karg, M.; Fortini, A.; Hellweg, T.; Fery, A., Wrinkle-assisted linear assembly of hard-core/soft-shell particles: impact of the soft shell on the local structure. *Nanoscale* **2012,** *4* (7), 2491-2499.
13. Guvendiren, M.; Burdick, J. A., The control of stem cell morphology and differentiation by hydrogel surface wrinkles. *Biomaterials* **2010,** *31* (25), 6511-6518.
14. Gao, N.; Zhang, X.; Liao, S.; Jia, H.; Wang, Y., Polymer Swelling Induced Conductive Wrinkles for an Ultrasensitive Pressure Sensor. *ACS Macro Letters* **2016**, 823-827.
15. Wagner, S.; Lacour, S. P.; Jones, J.; Hsu, P. H. I.; Sturm, J. C.; Li, T.; Suo, Z. G., Electronic skin: architecture and components. *Physica E* **2004,** *25* (2-3), 326-334.
16. Khang, D. Y.; Jiang, H. Q.; Huang, Y.; Rogers, J. A., A stretchable form of single-crystal silicon for high-performance electronics on rubber substrates. *Science* **2006,** *311* (5758), 208-212.
17. Chan, E. P.; Crosby, A. J., Fabricating microlens arrays by surface wrinkling. *Adv Mater* **2006,** *18* (24), 3238-+.

18. Bowden, N.; Brittain, S.; Evans, A. G.; Hutchinson, J. W.; Whitesides, G. M., Spontaneous formation of ordered structures in thin films of metals supported on an elastomeric polymer. *Nature* **1998,** *393* (6681), 146-149.
19. Harrison, C.; Stafford, C. M.; Zhang, W.; Karim, A., Sinusoidal phase grating created by a tunably buckled surface. *Applied Physics Letters* **2004,** *85* (18), 4016-4018.
20. Meitl, M. A.; Zhu, Z. T.; Kumar, V.; Lee, K. J.; Feng, X.; Huang, Y. Y.; Adesida, I.; Nuzzo, R. G.; Rogers, J. A., Transfer printing by kinetic control of adhesion to an elastomeric stamp. *Nat Mater* **2006,** *5* (1), 33-38.
21. Pretzl, M.; Schweikart, A.; Hanske, C.; Chiche, A.; Zettl, U.; Horn, A.; Boker, A.; Fery, A., A Lithography-Free Pathway for Chemical Microstructuring of Macromolecules from Aqueous Solution Based on Wrinkling. *Langmuir* **2008,** *24* (22), 12748-12753.
22. Khare, K.; Zhou, J. H.; Yang, S., Tunable Open-Channel Microfluidics on Soft Poly(dimethylsiloxane) (PDMS) Substrates with Sinusoidal Grooves. *Langmuir* **2009,** *25* (21), 12794-12799.
23. Rodríguez-Hernández, J., Wrinkled interfaces: Taking advantage of surface instabilities to pattern polymer surfaces. *Progress in Polymer Science* **2015,** *42*, 1-41.
24. Yang, S.; Khare, K.; Lin, P.-C., Harnessing Surface Wrinkle Patterns in Soft Matter. *Advanced Functional Materials* **2010,** *20* (16), 2550-2564.
25. Chen, D.; Yoon, J.; Chandra, D.; Crosby, A. J.; Hayward, R. C., Stimuli-responsive buckling mechanics of polymer films. *Journal of Polymer Science Part B: Polymer Physics* **2014,** *52* (22), 1441-1461.
26. Bowden, N.; Huck, W. T. S.; Paul, K. E.; Whitesides, G. M., The controlled formation of ordered, sinusoidal structures by plasma oxidation of an elastomeric polymer. *Applied Physics Letters* **1999,** *75* (17), 2557.
27. Chandra, D.; Crosby, A. J., Self-wrinkling of UV-cured polymer films. *Adv Mater* **2011,** *23* (30), 3441-5.
28. Guvendiren, M.; Burdick, J. A.; Yang, S., Solvent induced transition from wrinkles to creases in thin film gels with depth-wise crosslinking gradients. *Soft Matter* **2010,** *6* (22), 5795.
29. Huang, H.; Chung, J. Y.; Nolte, A. J.; Stafford, C. M., Characterizing Polymer Brushes via Surface Wrinkling. *Chem. Mater* **2007,** (19), 6555–6560.
30. Singamaneni, S.; McConney, M. E.; Tsukruk, V. V., Spontaneous self-folding in confined ultrathin polymer gels. *Adv Mater* **2010,** *22* (11), 1263-8.
31. Arnold, R. M.; Patton, D. L.; Popik, V. V.; Locklin, J., A dynamic duo: pairing click chemistry and postpolymerization modification to design complex surfaces. *Acc Chem Res* **2014,** *47* (10), 2999-3008.
32. Schuh, C.; Rühe, J. r., Penetration of Polymer Brushes by Chemical Nonidentical Free Polymers. *Macromolecules* **2011,** *44* (9), 3502-3510.
33. Schüwer, N.; Geue, T.; Hinestrosa, J. P.; Klok, H.-A., Neutron Reflectivity Study on the Postpolymerization Modification of Poly(2-hydroxyethyl methacrylate) Brushes. *Macromolecules* **2011,** *44* (17), 6868-6874.
34. Barbey, R.; Laporte, V.; Alnabulsi, S.; Klok, H.-A., Postpolymerization Modification of Poly(glycidyl methacrylate) Brushes: An XPS Depth-Profiling Study. *Macromolecules* **2013,** *46* (15), 6151-6158.

35. Brooks, K.; Razavi, M. J.; Wang, X.; Locklin, J., Nanoscale Surface Creasing Induced by Post-polymerization Modificatio. *ACS Nano* **2015,** *9* (11), 10961–10969.
36. Patton, D. L.; Page, K. A.; Xu, C.; Genson, K. L.; Fasolka, M. J.; Beers, K. L., Measurement of Reactivity Ratios in Surface-Initiated Radical Copolymerization†. *Macromolecules* **2007,** *40* (17), 6017-6020.
37. Patton, D. L.; Page, K. A.; Hoff, E. A.; Fasolka, M. J.; Beers, K. L., A robust and high-throughput measurement platform for monomer reactivity ratios from surface-initiated polymerization. *Polym. Chem.* **2012,** *3* (5), 1174-1181.
38. Guo, W.; Hensarling, R. M.; LeBlanc, A. L.; Hoff, E. A.; Baranek, A. D.; Patton, D. L., Rapid Synthesis of Polymer Brush Surfaces via Microwave-Assisted Surface-Initiated Radical Polymerization. *Macromol Rapid Comm* **2012,** *33* (9), 863-868.
39. Marquardt, F.-H., The intensity of carbonyl bands in the infrared spectra of cyclic anhydrides of dicarboxylic acids. *Journal of the Chemical Society B: Physical Organic* **1966,** (0), 1242-1243.
40. Hasanzadeh, R.; Moghadam, P. N.; Samadi, N.; Asri-Rezaei, S., Removal of heavy-metal ions from aqueous solution with nanochelating resins based on poly(styrene-alt-maleic anhydride). *Journal of Applied Polymer Science* **2013,** *127* (4), 2875-2883.
41. Murata, H.; Prucker, O.; Ruhe, J., Synthesis of Functionalized Polymer Monolayers from Active Ester Brushes. *Macromolecules* **2007,** (40), 5497-5503.
42. Alswieleh, A. M.; Cheng, N.; Leggett, G. J.; Armes, S. P., Spatial control over cross-linking dictates the pH-responsive behavior of poly(2-(tert-butylamino)ethyl methacrylate) brushes. *Langmuir* **2014,** *30* (5), 1391-400.
43. Cyriac, J.; Pradeep, T.; Kang, H.; Souda, R.; Cooks, R. G., Low-Energy Ionic Collisions at Molecular Solids. *Chem Rev* **2012,** *112* (10), 5356-5411.
44. Navarro, M.; Benetti, E. M.; Zapotoczny, S.; Planell, J. A.; Vancso, G. J., Buried, covalently attached RGD peptide motifs in poly(methacrylic acid) brush layers: The effect of brush structure on cell adhesion. *Langmuir* **2008,** *24* (19), 10996-11002.
45. Edmondson, S.; Nguyen, N. T.; Lewis, A. L.; Armes, S. P., Co-nonsolvency effects for surface-initiated poly(2-(methacryloyloxy)ethyl phosphorylcholine) brushes in alcohol/water mixtures. *Langmuir* **2010,** *26* (10), 7216-26.
46. Toomey, R.; Freidank, D.; Ruhe, J., Swelling behavior of thin, surface-attached polymer networks. *Macromolecules* **2004,** *37* (3), 882-887.
47. Han, Q.; Li, C.; Guan, Y.; Zhu, X. X.; Zhang, Y., Swelling-induced surface instability of a hydrogen-bonded LBL film and its self-healing. *Polymer* **2014,** *55* (9), 2197-2204.
48. LeMieux, M. C.; Peleshanko, S.; Anderson, K. D.; Tsukruk, V. V., Adaptive Nanomechanical Response of Stratified Polymer Brush Structures. *Langmuir* **2007,** *23* (1), 265-273.
49. Huang, R., A Kinetics Approach to Surface Wrinkling of Elastic Thin Films. In *Mechanical Self-Assembly: Science and Applications*, Chen, X., Ed. Springer New York: New York, NY, 2013; pp 69-109.
50. Huck, W. T. S.; Bowden, N.; Onck, P.; Pardoen, T.; Hutchinson, J. W.; Whitesides, G. M., Ordering of spontaneously formed buckles on planar surfaces. *Langmuir* **2000,** *16* (7), 3497-3501.

51. Groenewold, J., Wrinkling of plates coupled with soft elastic media. *Physica A* **2001,** *298* (1-2), 32-45.
52. Chan, E. P.; Crosby, A. J., Wrinkling Polymers for Surface Structure Controle and Functionality. In *Polymer Thin Films,* Tsui, O. K. C.; Russell, T. P., Eds. World Scientific: 2008; pp 141-162.

5.7 Appendix Buckling Instabilities in Polymer Brush Surfaces Via Postpolymerization Modification

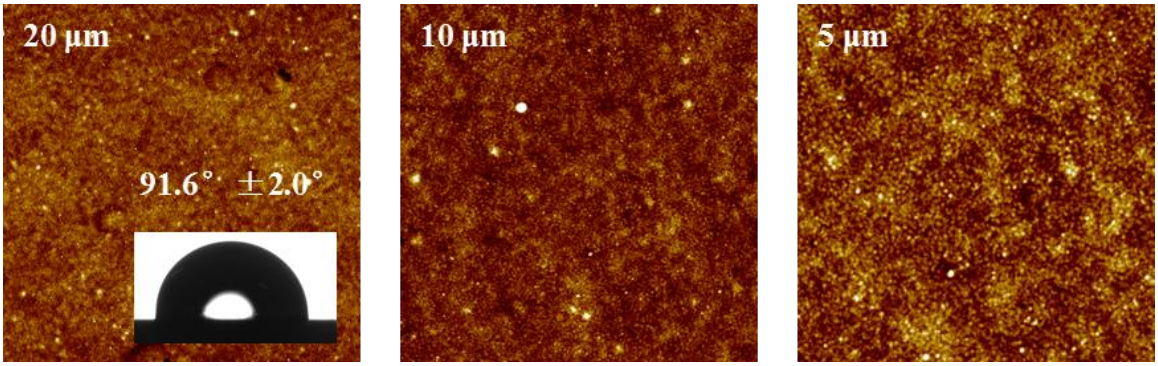

Figure A.6 AFM height images of a typical unmodified pSMA brush surface. Inset image shows the static water contact angle of the unmodified pSMA brush

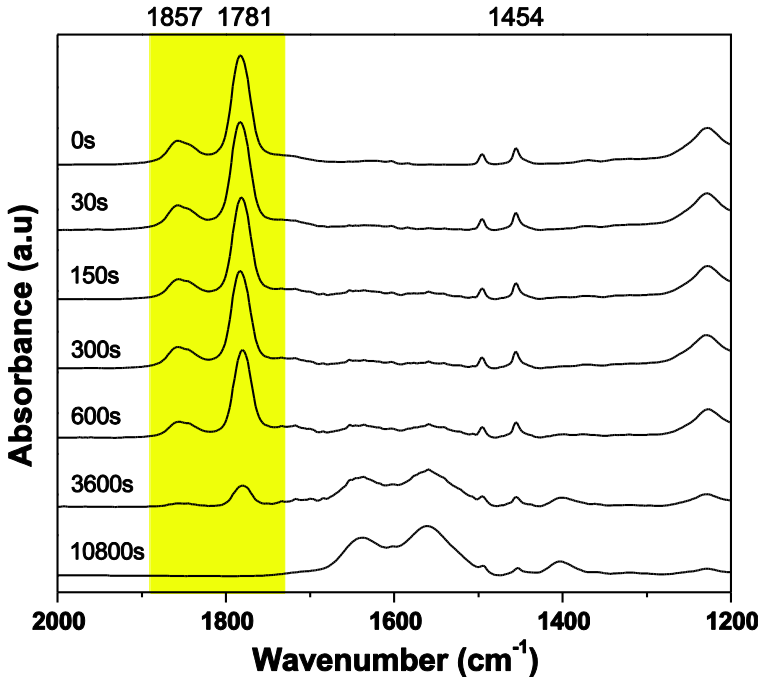

Figure A.7 ATR-FTIR spectra of pSMA brushes (≈ 80 nm initial thickness) post-modified with cystamine aqueous solution at discrete reaction times.

The conversion of the amidation reaction of maleic anhydride at discrete times was calculated using the peak area values of the anhydride peak at 1781 cm^{-1} (aromatic peak at 1454 cm^{-1} used as reference).

Table A.5

Brush thickness and conversion following postmodification with cystamine

Time (s)	Conversion (%)	
	IR	Ellipsometry
60	7.0	7.1±4.5
150	8.6	8.3±5.9
300	16.6	16.7±3.0
600	25.3	27.6±4.6
1200	NA	60.3±8.3
3600	NA	92.1±7.2
10800	100	91.0±7.9

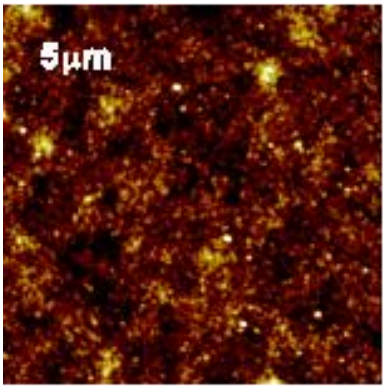

Figure A.8 AFM height image of a pSMA brush surface modified with cystamine under a good solvent condition with 17% conversion followed with swelling in acetonitrile.

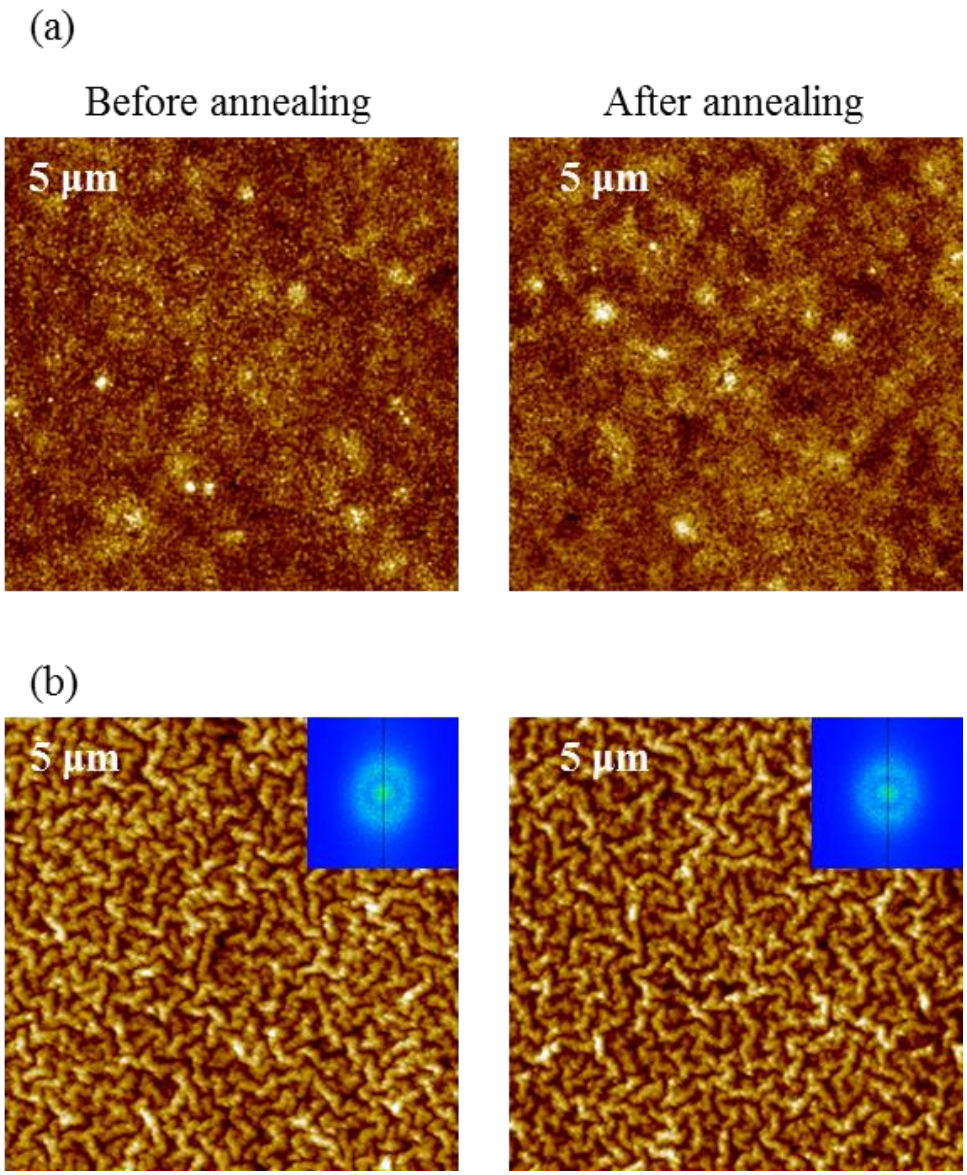

Figure A.9 AFM height images cystamine-modified pSMA brushes of (a) before swelling (b) after swelling, prior and after annealing at 145°C overnight

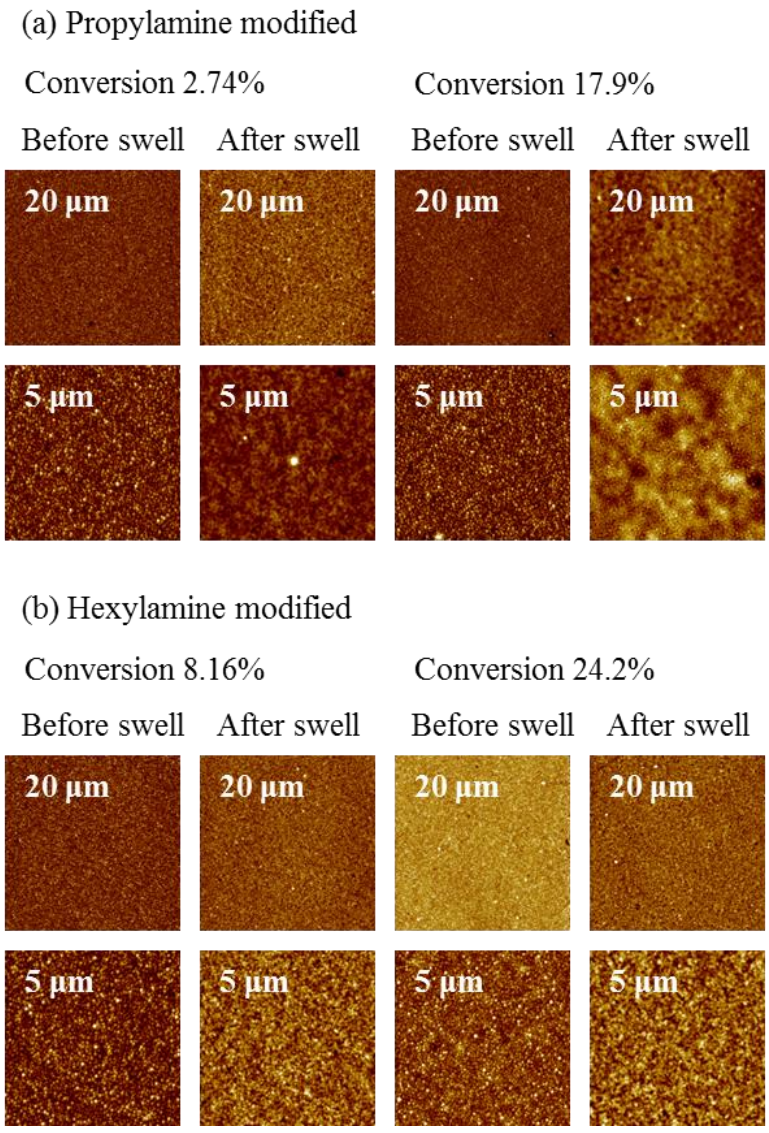

Figure A.10 AFM images of pSMA brushes postmodified with monofunctional amines.

using identical reaction conditions as used for cystamine: (a) hexylamine and (b) propylamine. As shown, wrinkles were not observed after swelling in acetonitrile.

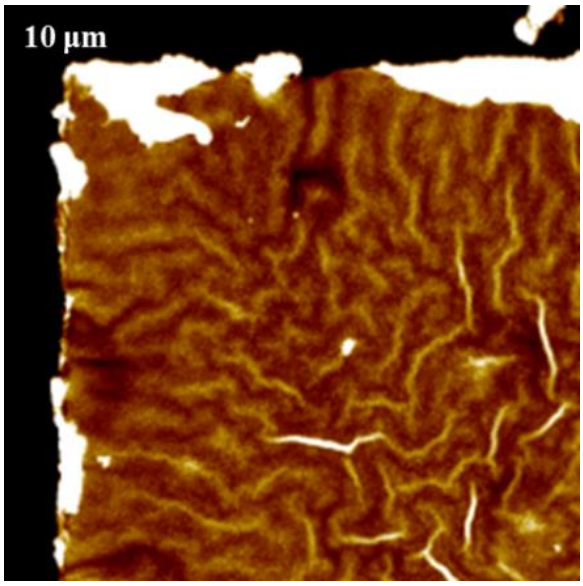

Figure A.11 AFM height image of a wrinkling surface of pSMA brush modified with cystamine and patterned with orthogonal scratches.

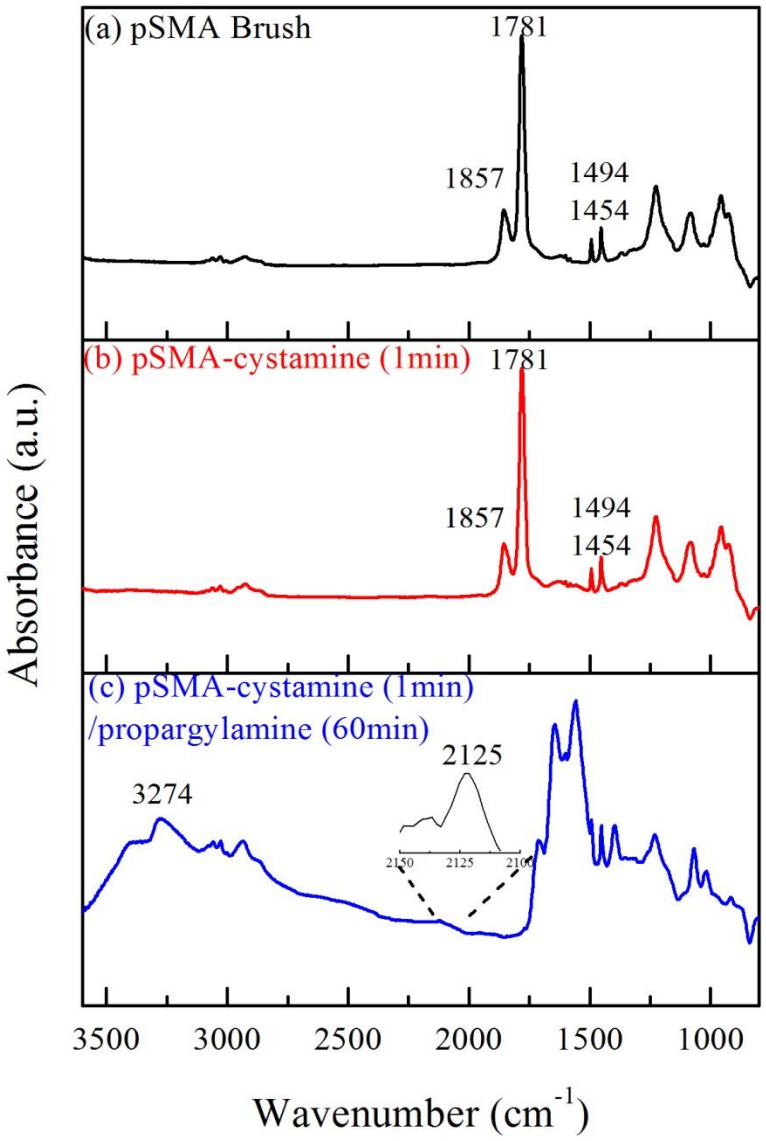

Figure A.12 ATR-FTIR: a) pSMA brush b) pSMA brush in cystamine aqueous solution for 1 min (≈ 7 % anhydride conversion) (c) cystamine-modified pSMA brush after backfilling of propargylamine (PA) in acetonitrile for 60 min.

Peaks at 2122 cm^{-1} and 3274 cm^{-1} indicate the incorporation of the alkyne functional group.

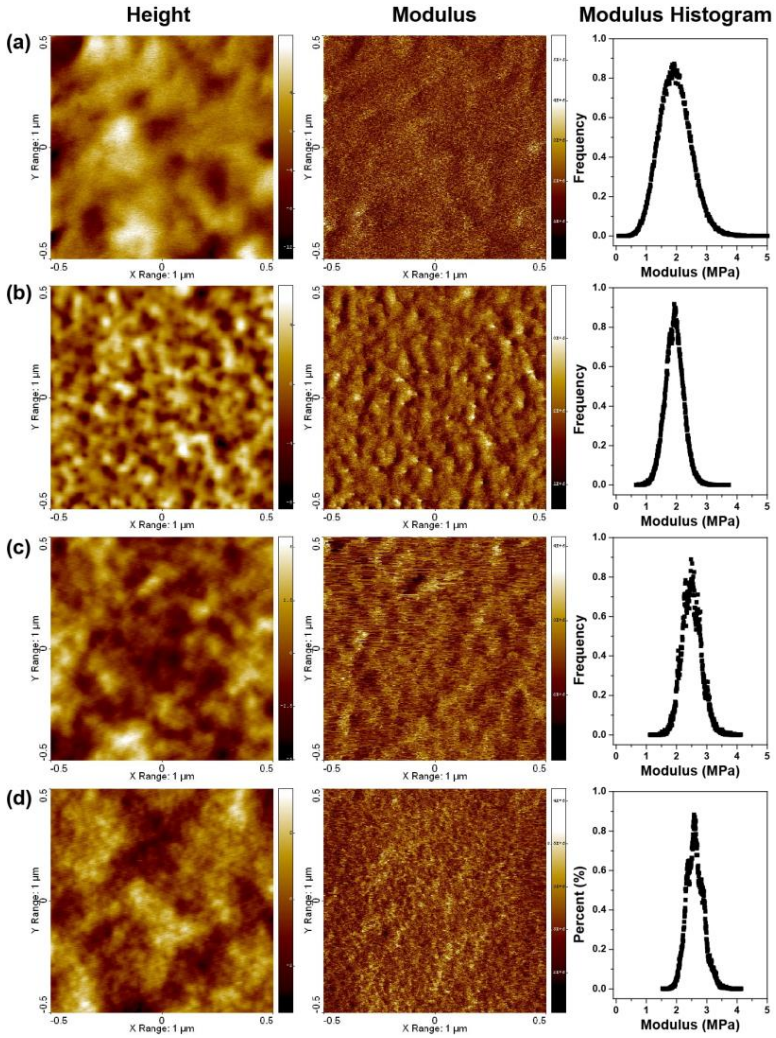

Figure A.13 Height, modulus, and modulus image histograms for (a) pSMA (melt pressed film), (b) pSMA brush, (c) pSMA brush modified with cystamine, and (d) pSMA brush modified with propargylamine.

Images were obtained using PeakForce Quantitative Nanomechanical Mapping (Bruker Dimension Icon).

Table A.6

Molecular weight of monomers and cystamine.

Compound	MW (g/mol)
Styrene	104.15
Maleic anhydride	98.06
Styrene-Maleic anhydride	202.21
Cystamine	152.28
Cystamine as crosslinker	77.14
Propargylamine	55.08

Table A.7

IR absorption peaks of pSMA and postmodified brushes

Wavenumber (cm^{-1})	Peak Assignment
1857, 1781	C=O, cyclic five-membered ring anhydride
1494, 1454	aromatic
3405	O-H, carboxylic acid
1718	C=O, carboxylic acid
3400	N-H, amine
1641	C=O, amide
1564	asym C=O, carboxylic salt
1405	sym C=O, carboxylic salt
2567	S-H, thiol
1718	C=O, carboxylic acid
3274	≡C-H, yne
2125	C≡C, yne

CHAPTER VI - CONCLUSION AND FUTURE WORKS

6.1 Conclusion

The research presented in this dissertation is focused on the fabrication of polymer brush surfaces with complex functionality and architectures via postpolymerization modification – specifically with a better understanding of the balance of the effectiveness of PPM and parameters that govern the diffusion of reactive moieties into near-surface regions. In Chapter I, a general introduction was provided overviewing the properties, synthesis, and characterization of ultrathin polymer brush on surfaces, the postpolymerization modification of polymer brush in an effort to the fabrication of functional soft surfaces, the effectiveness of PPM, and buckling instability of thin films.

In Chapter II, microwave-assisted surface-initiated polymerization (μW-SIP) was developed and employed to demonstrate the synthesis of polymer brushes on silicon and quartz substrates. The μW-SIP approach shows significant enhancements in polymer brush thickness at reduced reaction times and monomer concentration.

In Chapter III, the postpolymerization modification of a poly(2-isocyanatoethyl methacrylate) (pNCOMA) brush surfaces with two deuterated thiols of different sizes was studied and the depth profiles of the distribution of deuterated thiourethane alkyl moieties within the polymer brush were drawn using neutron reflectometry analysis. By applying a sequential PPM strategy, polymer brush with pseudo-block copolymer architectures was synthesized.

In Chapter IV, a poly(styrene-alt-maleic anhydride) (pSMA) copolymer brush was synthesized in an effort to fabricate polymer brush surface containing pendent polyfunctional thiols for further thiol-ene modifications via a two-step modification.

Furthermore, the pSMA brush itself was found to be a stable and versatile platform for amine modifications.

In Chapter V, a straightforward PPM approach, utilizing the knowledge gained in Chapter III and IV, to engineer ultrathin polymer brush surfaces with tunable wrinkled and creased morphologies was demonstrated by creating a modulus mismatch between the top layer and bottom of the polymer brush via selectively crosslinking of the outer layer of pSMA brushes by balancing the rate of PPM and reactive molecule diffusion.

6.2 Future Works

The knowledge gained in this dissertation has broadened the scope of the approach of surface-initiated polymerization and postpolymerization modification in terms of polymer surface engineering. The following recommendations are suggested to advance the work reported in this dissertation:

1) The observed enhancement effect of microwave assisted surface-initiated polymerization in Chapter II has great potential in reduce the cost and improve the efficiency of the synthesis of polymer brushes. It would be beneficial that this approach be applied to polymer brush synthesized on non-flat surfaces, i.e. nanoparticles, nanotubes, graphenes etc and to postpolymerization modifications that requires heating.

2) The preliminary findings of heterogeneity of postmodified pNCOMA brush in Chapter III point to further investigation of the influence of parameters such as solvent quality, grafting density on the PPM process.

3) The results in Chapter IV suggest that cystamine-modified pSMA brush has huge potential as polymer brush platform for postpolymerization modification that contains polymer chain pendent polyfunctional thiols that can be further exploited by a

plethora of thiol ‘click’ reactions including photo- and base-catalyzed thiol-ene, thiol-yne, and thiol-bromo reactions. Cystamine modified polymer brush provides a straightforward route towards pendent protected thiol polymer brush which often requires more complicated synthesis of either monomer or postmodifier with protecting groups.

4) The buckling instability of cystamine-modified pSMA surfaces demonstrated the fabrication of nanoscale wrinkled surface on rigid substrates without physical compression or other external applied confinement by selectively crosslinking of the polymer brush. Current research (not included in this dissertation) already showed that other crosslinkers such as aliphatic diamine modified pSMA would show similar buckling instabilities and the same approach shall be applicable to polymer brushes with different chemistries. The effect of crosslinker (size, architecture, and reactivity), polymer brush properties (grafting density, copolymer) on the buckling behavior is yet to be studied. The modulus change of polymer brush upon swelling and sequential modification has not been thoroughly understood due to the difficulty of *in-situ* measurement of polymer brush under swelling state.